



BIPOLAR PHASING OF ABRUPT CLIMATE CHANGE DURING THE LAST GLACIAL PERIOD

MASTER'S THESIS

Written by Anna Maria Klüssendorf
December 20th 2022

Supervised by
Anders Svensson

UNIVERSITY OF COPENHAGEN

NIELS BOHR INSTITUTE, SECTION FOR THE PHYSICS OF ICE, CLIMATE AND EARTH

Abstract

The Last Glacial Period is characterised by a strong climate variability, where millennial-scale warming events identified in paleoclimatic data from the Greenland ice sheet have interrupted the cold glacial climate. These abrupt climate changes are a typical example for pre-historic tipping points in the climate system with global consequences. Presumably initiated in the North Atlantic region, atmospheric and oceanic inter-hemispherical coupling result in fingerprints of the Northern Hemisphere warming events to modulate the temperature in Antarctica. According to the bipolar seesaw hypothesis, the hemispheres are in distinct antiphase, with Antarctic temperature decreases lagging Greenland abrupt warming. Despite being related to oscillations in the strength of the Atlantic Meridional Ocean Circulation, the physical mechanisms underlying the climate fluctuations, however, are not yet fully understood. With progressive modern climate change, the need for a comprehensive understanding of the processes behind abrupt changes has increased in order to drive climate models predicting possible tipping points. As one main feature of the pre-historic temperature fluctuations, this study approaches the bipolar phasing between Antarctica and Greenland over stadial-interstadial transitions. For this purpose, the onsets of 33 Greenland interstadials associated with Dansgaard-Oeschger (DO) events during the entire last glacial are defined in the NGRIP stable oxygen isotope record. This enables the determination of the Antarctic response time relative to Greenland temperature rises. Based on bipolar volcanic synchronisation, the Antarctic average response time is reduced compared to previous studies. Investigating the climate across different groups of DO events classified by the time of occurrence and size, possible processes provoking the abrupt changes are assessed. The climate interpretation is further extended by a comparison between the ice core records and temperature profiles provided by a global climate model simulating DO events under distinct CO₂ forcing. This suggests a tight connection between abrupt temperature rises and rapid sea ice retreat in the North Atlantic and Northern Seas. Therefore, this work discusses the potential for future abrupt climate changes as experienced during the last ice age under ongoing anthropogenic climate change.

Acknowledgements

First and foremost, I would like to thank my supervisor Anders Svensson for always having an open door and finding time to give academic advice and to support me in my work. My thanks also go to Guido Vettoretti for sharing his knowledge about the utilised climate model and ideas on possible interpretations. Special thanks go to Johannes Lohmann for talking me through statistics, but especially for conveying a keen interest in the project. I would officially like to thank PICE for providing me with personal office space, and my fellow students for creating a great atmosphere; in particular, Anna, who made the last and long days of work more enjoyable. Much is owed to Lide and Jon for all their academic and emotional support and strong encouragement. Lastly, thankful thoughts go to Emma for always radiating positive energy and for sharing chocolate-rich coffee breaks, good laughs, and honest thoughts.

Contents

Acronyms	III
List of Figures	IV
List of Tables	V
1 Introduction	1
2 Scientific Background	5
2.1 Ice Sheet Dynamics	5
2.1.1 Densification	5
2.1.2 Ice Flow and Layer Thinning	6
2.2 Ice Cores and Palaeoclimatology	7
2.2.1 Stable Isotope Records	8
2.2.1.1 Isotopic Fractionation	8
2.2.1.2 Temperature Dependency of $\delta^{18}\text{O}$	9
2.2.2 Ice Core Dating Methods	11
2.2.2.1 Annual Layer Counting	11
2.2.2.2 Glaciological Modelling and Orbital Tuning	13
2.2.3 Synchronisation of Ice Cores	13
2.2.3.1 Greenhouse Gas Synchronisation	14
2.2.3.2 Cosmogenic Isotope Synchronisation	15
2.2.3.3 Bipolar Volcanic Synchronisation	15
2.2.3.4 Ice Core Chronologies	17
3 Data and Methods	18
3.1 Ice Core Records	18
3.2 Abrupt Climate Change Simulations	20
3.3 Defining the Onsets of Dansgaard-Oeschger Events	22
3.4 Determining the Bipolar Phasing	23
3.5 Uncertainty Evaluation	26
4 Results and Discussion	29
4.1 Stadial-Interstadial Transitions	29
4.2 Climate Across Dansgaard-Oeschger Events	33
4.3 Bipolar Phasing	36

4.4	Towards an Understanding of the Mechanisms Behind Dansgaard-Oeschger Events	38
4.4.1	Comparing Classes of DO Events	39
4.4.2	Modelling Abrupt Climate Change	42
4.4.3	Major Volcanic Eruptions as Potential Trigger of DO Events	45
4.5	Potential for Future Abrupt Climate Change	47
5	Conclusion and Outlook	49
6	Bibliography	51
A	Ice Core Data Resolution	65
B	Stadial-Interstadial Transitions	66
C	Amplitude of DO Events	68
D	Uncertainty Estimations	70
E	Climate Across DO Events	74
F	Bipolar Phasing Estimates	88
G	Class Comparison of DO Events	92
H	Simulated Bipolar Phasing	96
I	Code and Data Availability	100

Acronyms

ACC Antarctic Circumpolar Current.

AICC2012 Antarctic Ice Core Chronology 2012.

AIM Antarctic Isotope Maximum/Maxima.

AMOC Atlantic Meridional Overturning Circulation.

b2k before 2000 CE.

BP Before Present (before 1950 CE).

CCSM4 Community Climate System Model Version 4.

CFA Continuous Flow Analysis.

DF Dome F.

DO Dansgaard-Oeschger (Event).

GICC05 Greenland Ice Core Chronology 2005.

IPCC Intergovernmental Panel on Climate Change.

ITCZ Intertropical Convergence Zone.

ka Thousand years.

MCE Maximum Counting Error.

RCP Representative Concentration Pathway.

SMOW Standard Mean Ocean Water.

TAL Talos Dome.

YD-PB Younger Dryas-Preboreal transition.

List of Figures

1.1	Climate During the Last Glacial Period	2
1.2	The Bipolar Seesaw	3
2.1	Idealised Cross Section of an Ice Sheet with Perfectly Horizontal Bedrock	6
2.2	Rayleigh Distillation	10
2.3	Seasonal Isotope signal	12
2.4	Schematic Illustration of (Bipolar) Volcanic Synchronisation	16
3.1	Map of Greenland and Antarctica	19
3.2	Simulated Temperature Under a CO ₂ Forcing of 210 ppm	21
3.3	Defining Onsets of Dansgaard-Oeschger Events	22
3.4	Determining the Bipolar Phasing.	24
4.1	Temporal Delay of Midpoint Compared to the Onset of Dansgaard-Oeschger Events	29
4.2	Deviation of Determined Transitions Between Different Studies.	31
4.3	Ages of the Abrupt Climate Transitions Determined in Different Studies	32
4.4	Interhemispherical Climate Signal Across Dansgaard-Oeschger Events	34
4.5	Average Interhemispherical Climate Signal Across Greenland Abrupt Warming Transitions	36
4.6	Bipolar Phasing During the Entire Last Glacial Period and its Early Half	38
4.7	Stadial-Interstadial Transitions for Different Classes of Dansgaard-Oeschger Events	40
4.8	Variation in $\delta^{18}\text{O}$ Across Dansgaard-Oeschger Transitions	42
4.9	Bipolar Phasing During a Background CO ₂ Concentration of 210 ppm	43
4.10	Bipolar Volcanic Eruptions During the Last Glacial Period	46
A.1	Ice Core Data Resolution	65
B.1	Average Greenland Temporal Difference Between Midpoint of Stadial-Interstadial Transition and Initiation and Termination of Interstadials	66
B.2	Climate Signal During the Last Glacial Period	67
C.1	Determining the Amplitude of a Single Dansgaard-Oeschger event	68
C.2	Amplitude of All Stadial-Interstadial Transitions in the Individual Ice Cores	69
D.1	Antarctic Response Time Depending on Smoothing the Data for Individual Dansgaard- Oeschger Events	70
D.2	Bipolar Phasing Between Greenland and Antarctica	71

D.3	Uncertainty of Bipolar Volcanic Synchronisation	72
D.4	Determining the Uncertainty on the Antarctic Breakpoint	72
E.1	Interhemispherical Climate signal Across Dansgaard-Oeschger Events	87
F.1	Bipolar Phasing during the Second Half of the Last Ice Age	88
F.2	Bipolar Phasing for Minor Dansgaard-Oeschger Events	89
F.3	Bipolar Phasing for Major Dansgaard-Oeschger Events	90
F.4	Bipolar Phasing Excluding EDML and Dome F	91
G.4	Comparing Dansgaard-Oeschger events of different classes	95
H.1	Atmospheric CO ₂ Concentration Between 15 ka and 65 ka b2k	96
H.4	Bipolar Phasing for Simulated Dansgaard-Oeschger Events	99

List of Tables

3.1	Ice Core Characteristics	19
3.2	Dansgaard-Oeschger Event Classification	25
3.3	Uncertainty Estimates	28
4.1	Onsets of the Dansgaard-Oeschger Events	30
D.1	Uncertainty on the Breakpoints	73
E.1	Timing of Dansgaard-Oeschger Event Onsets	74

1. Introduction

In the past few decades, climate change has become a prominent topic in scientific research as well as in society. It is beyond dispute that human-induced alterations to the climate system have exceeded natural variability. Since the year 2000, the observed global temperature rise can very likely exclusively be attributed to human-induced warming, accounting for natural influences from solar and volcanic activity. Anthropogenic greenhouse gas emissions from predominantly fossil fuel combustion, deforestation, and agricultural practices have led to a global temperature increase of about 0.8-1.2°C respective to pre-industrial levels, where the rate of warming has more than doubled (on average 0.18°C per decade) in the last 50 years (NOAA National Centers for Environmental Information (2022)). Due to important climate feedbacks, the poles are particularly vulnerable to temperature rises and are currently experiencing a temperature gradient about twice as high as the rest of the world (e.g. Ballinger et al. (2021); Stuecker et al. (2018); Masson-Delmotte et al. (2006)). Both the sea ice and the ice caps at the poles retreat, further amplifying atmospheric temperature increases, and continental glaciers around the world are melting. As a consequence, the global mean sea level is rising, and the oceans are freshening in return leading to a change in large-scale ocean circulations. This has impacts on the Earth's climate system with the potential of driving the system across a tipping point with unknown global consequences.

During the last glacial period, covering more than hundred thousand years before the onset of the current climate period, the Holocene at 11.7 thousand years before 2000 CE (ka b2k), the temperatures are believed to have been up to 6°C colder and the global mean sea level around 120 m lower at the Last Glacial Maximum (around 21 ka b2k) than during pre-industrial conditions (Tierney et al. (2020)). However, this period was characterised by a highly fluctuating climate, where the cold glacial climate was interrupted by millennial-scale milder periods. Within a few decades or shorter, the local temperatures in North Greenland abruptly rose by five to 16°C (Steffensen et al. (2008); Rasmussen et al. (2014); Kindler et al. (2014)) subsequently decreasing more gradually back to full glacial conditions. The full circle of the transition into a warm interstadial and back into the cold stadial are referred to as Dansgaard-Oeschger (DO) events. The climatic variations have been most pronounced in the North Atlantic, as can be seen from Greenland ice cores, unveiling the characteristics of the stadials and interstadials. Here, stable water isotopes used as a proxy for temperature, reveal the abrupt changes of several degrees. Figure 1.1 presents the $\delta^{18}\text{O}$ record of the NGRIP ice core, showing 25 main DO events, where some of them comprise several interstadials during the last glacial period.

In addition to distinct temperature increases, Greenland interstadials experienced about twice the amount of snow accumulation (Alley et al. (1993); Cuffey and Clow (1997)) in correspondence to warmer temperatures. The increase in precipitation is owed to the atmospheric saturated water vapour pressure scaling positively with higher air temperatures (Robin (1977); Wallace and Hobbs (2006)), and a reduction in sea ice cover decreasing the distance to the

moisture source. The stadials, on the contrary, are marked by a cold and dry climate with stronger winds driven by a higher temperature gradient between high and low latitudes (Rasmussen et al. (2014)). Generally, this reveals that the impact of DO events extends beyond the North Atlantic and the signal even might propagate across hemispheres. In fact, expressions of the Northern Hemisphere DO events are found in ice cores drilled in Antarctica, designated as Antarctic Isotope Maxima (AIM) (Figure 1.1). Based on previous bipolar synchronisation, Antarctic ice cores exhibit gradual millennial-scale warming and cooling periods temporarily offset to each of the Greenland transitions, emphasising a strong interhemispheric coupling of ocean and atmosphere (Pedro et al. (2018); Buizert et al. (2015); Stocker and Johnsen (2003)).

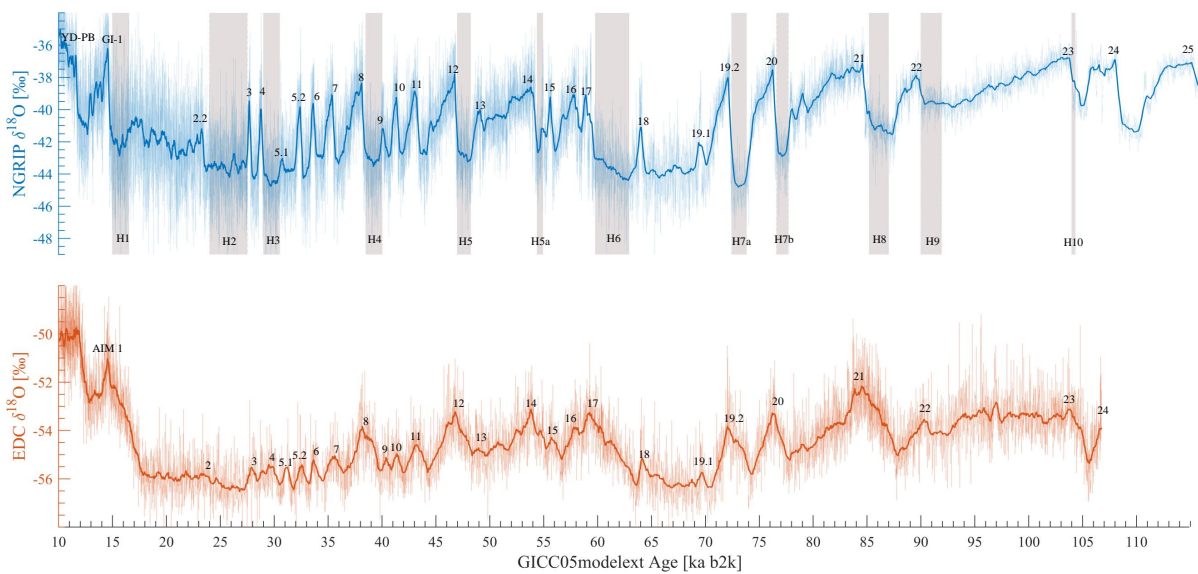


Figure 1.1 | Climate during the Last Glacial Period. Stable oxygen isotope records from NGRIP, Greenland revealing more than 25 distinct abrupt warming events numbered as Greenland Interstadials (GIs) with their corresponding Southern Hemisphere counterparts visible as Antarctic Isotope Maxima (AIM) in the EDC $\delta^{18}\text{O}$ profile. Grey vertical bars mark the approximate temporal positions of Heinrich events detected in North Atlantic sediment cores (Heinrich (1988); Rasmussen et al. (2003); Rashid et al. (2003)).

Even though DO events are one of the best-studied rapid climate fluctuations, a comprehensive explanation of their cause has not yet been provided. Supported by the antiphase behaviour between Greenland and Antarctica, the most important component behind the dynamics is thought to be the Atlantic Meridional Overturning Circulation (AMOC), driving the inter-hemispherical heat distribution. The concept is based on the instability of the thermohaline circulation expressed in a simple box model described by Stommel more than half a century ago (Stommel (1961)). During phases of strong overturning, more heat is transported from the Equator towards the north, warming the ocean around Greenland, while a weaker circulation reduces the meridional heat transport resulting in lower temperatures in the North Atlantic.

In the Southern Hemisphere, a weakening of the overturning results in warmer temperatures as the heat transport towards the north is reduced and the energy is predominantly stored in the Southern Ocean, and vice versa during periods of strong overturning. Owing to the high heat capacity of the (Southern) Ocean and the ocean circulation occurring on longer timescales, this so-called bipolar seesaw results in the Southern Hemisphere temporally lagging Northern Hemisphere climate changes (Stocker and Johnsen (2003)). Further, this causes the temperature to change less abruptly than during Greenland warming transitions. Figure 1.2 demonstrates the temperature change of the heat reservoir induced by the bistability of the AMOC.

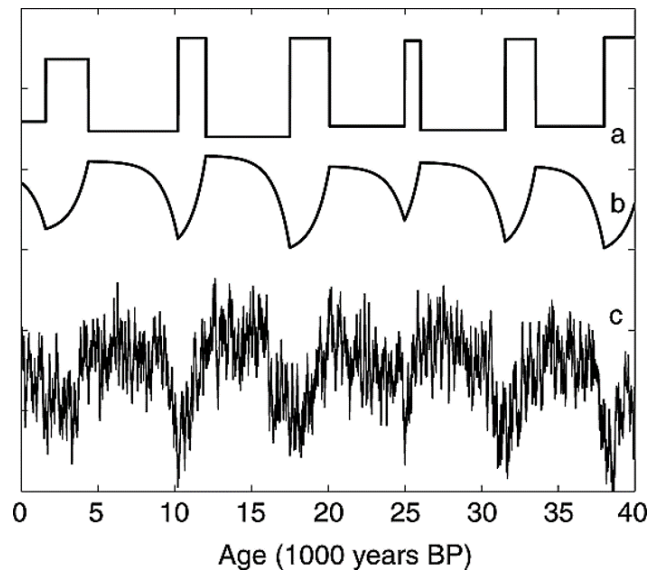


Figure 1.2 | The bipolar seesaw. Synthetic palaeoclimatic time series to mimic the bipolar seesaw. Signal a reveals the on-off changes in the AMOC, where the system spends approximately 2000 years in the on-state, and 5000 years in off-state. Curve b represents the simulated temperature of the heat reservoir, increasing nearly logarithmically when the AMOC is shut off, and decaying exponentially after the AMOC is reactivated. Curve c depicts red noise of half the variance, which is added to the temperature of the heat reservoir. Figure adapted from Stocker and Johnsen (2003).

Freshwater perturbation is the most invoked trigger of overturning circulation variations by modulating the density, which is the main driver of deep ocean circulation. Based on this, the key factor behind the oscillations is thought to be changes in the sea ice cover of the Arctic Ocean, which is closely coupled to the AMOC and regulates the heat exchange between ocean and atmosphere (e.g. Vettoretti et al. (2022)).

Potential mechanisms behind the AMOC oscillations include among others solar and orbital forcing (Braun et al. (2008)) driving natural climate variability in the Earth's history such as glacial-interglacial changes. However, the frequency of DO events is not consistent with any solar cycle. Alternative hypotheses related to DO oscillations refer shifts in the Southern Hemisphere westerly winds (Buizert et al. (2018)) as well as volcanic short-term cooling influence on the ocean (Lohmann and Svensson (2022)). However, the oscillating AMOC remains the

predominant driver as it can capture most of the spatial patterns observed during these rapid climate changes. Since the 1960s, the theory has evolved, now considering a complete shutoff of the AMOC as an additional state to the previous simple bistability dynamic between weak and strong circulation (e.g. Rahmstorf (2002), Sarinthein et al. (1994), Clark and Mix (2002)).

A shutoff of the AMOC is said to be responsible for colder anomalies occurring during several stadial periods. From distinct layers of coarse-grained material in marine sediment cores, several so-called Heinrich Events have been identified (Figure 1.1). The layers were matched with carbon-rich sediments in Eastern Canada, and could therefore be concluded to originate from ice-rafted debris most likely from the Laurentide ice sheet, indicating enhanced iceberg discharge carrying the eroded material as far as to the Portuguese coast. The fact, that the icebergs were able to travel this far before melting, points towards a southward-expanded cold-water pool as well as larger ice mass stored in the Northern Hemisphere ice sheets (Bond et al. (1992); Heinrich (1988)). Since their frequency does not agree with the reoccurring stadials, Heinrich Events can not simply be linked to DO events. However, the mechanisms behind the dynamics might be similar, as being related to freshwater influx to the North Atlantic, consequently altering the thermohaline circulation. In return, the behaviour of the DO events succeeding a Heinrich event might be influenced by the exceptionally strong cooling during this period.

Understanding the physical mechanisms and how they have controlled the Earth's prehistorical climate variability is crucial to simulate future climate changes. Even though the rapid changes during the last glacial period have been naturally driven and were triggered by mechanisms different from anthropogenic climate change, the rapidity and magnitude of the temperature swings is comparable to prognoses of ongoing modern climate change (Jansen et al. (2020)). According to the IPCC, with global warming of $> 2^{\circ}\text{C}$ small alterations in the climate system can exceed a critical threshold resulting in abrupt and/or irreversible changes with catastrophic consequences (Arias et al. (2021)). These tipping points are suspected to exist in processes related to the Greenland and West Antarctica Ice Sheet (WAIS), the AMOC, as well as permafrost thawing, the Amazon rainforest, and the El Niño-Southern Oscillation (Lenton et al. (2019)). DO events are an example of prehistoric tipping points well represented in palaeoclimate archives (Ditlevsen (2017)), setting the motivation for this study.

Modelling the well-dated past and comparing the results to data collected from the ice core records, is an important tool to predict the outcome of the current alteration of the planet's coupled climate system. An important process in the global system is the interplay between the Northern and the Southern Hemisphere. Particularly, how Antarctica responded to the transitioning climate mostly pronounced in the North Atlantic. This project, therefore, focuses on the bipolar phasing between the Antarctic climate respective to Northern Hemisphere DO events. The phasing determination is based on volcanic synchronisation, utilising volcanic marker horizons existing in both Greenlandic and Antarctic ice cores to link individual timescales and establish a common chronology for the different ice cores of both hemispheres. Comparing local temperatures simulated by a global climate model reconstructing DO events to ice core data, this work further addresses possible mechanisms behind the abrupt events in order to contribute to an assessment of the potential for abrupt climate change in the future.

2. Scientific Background

2.1 Ice Sheet Dynamics

Over the course of the Eocene and Oligocene around 40 million years ago, when the Drake's Passage opened, Antarctica was isolated from other continental mass. Completely surrounded by the ocean and a strong circumpolar current, the local temperatures drastically decreased allowing glaciation of the continent (Vincze et al. (2021); Zachos (2007)). Ice sheets modulate the global climate system predominantly through feedback mechanisms by changing the Earth's albedo, reflecting solar energy and perturbing atmospheric circulation, among others. This further promoted extensive global cooling which finally resulted in the formation of the Greenland Ice Sheet (Thiede et al. (2011); Thomas (2008)). The extent of the Northern and Southern Hemisphere ice sheets significantly varied under glacial-interglacial oscillations driven by changes in the incoming solar radiation, which in return is regulated by the Earth's orbit around the Sun. In particular, the eccentricity of the orbit, and the obliquity and precession of the rotation axis determine the distance between Earth and Sun and thereby the insolation. These periodic parameters are thought to drive the occurrence and termination of global ice ages, where the eccentricity has the dominating influence on this cycle (Milankovitch (1941)). However, local short-term variations such as Northern Hemisphere DO events during the Last Glacial Period do not coincide with either of the frequencies of the orbital parameters.

2.1.1 Densification

An ice sheet forms when the climatic conditions favour the snow accumulation to exceed the amount ablated from the ice mass through for example surface melting or calving at the margins. In the accumulation zone, in the centre of the ice sheet, over time newly deposited snow buries previously accumulated masses, increasing the pressure and finally compressing older snow layers to ice. New accumulated snow on the surface of an ice sheet has a density of about $50\text{-}70\text{ kg m}^{-3}$. Under favourable conditions, i.e. when the temperatures are cold enough for the snow not to be melted, it is gradually compressed by the overlying weight. Recrystallisation, rearrangement, and growth of grains, the porous material reaches an intermediate state, where the pores are still in contact with the atmosphere. Sintering, i.e. plastic and elastic deformation at the interface between the grains, finally results in a sealing of the pores Herron and Langway (1980). This way, all air bubbles are locked up in the ice, containing information on the atmosphere composition at the close-off time (e.g. Blunier et al. (1998); Blunier and Brook (2001)). Compressing the air bubbles, the density increases to a maximum of 917 kg m^{-3} , the density of pure glacial ice (Shumskiy (1960)). Thus, at about 150 m depth, added weight at the surface will result in layer thinning rather than further densification.

2.1.2 Ice Flow and Layer Thinning

When the density of pure glacial ice is reached, the ice will deform under the applied stress of the overlying ice masses added in the accumulation zone. With a general ice flow downward and towards the margins the layers gradually thin in the vertical direction and elongate laterally. The thinning rate is therefore strongly dependent on the ice flow, which is most commonly described by the Dansgaard-Johnsen model determining the vertical velocity as a function of depth (Dansgaard and Johnsen (1969)). Related to deformation in pure shear, the incompressibility of ice requires continuity of the system, i.e. conservation of mass, and thus, simply relates the two-dimensional velocity components at any point in the ice sheet, namely compression and extension of the ice (Cuffey and Paterson (1994b)). Here, the horizontal flow is said to be uniform from the surface to a certain depth, where the velocity results from the surface mass balance. At greater depth, the velocity decreases linearly towards the bedrock as visualised in Figure 2.1. The flow is further idealised by assuming a perfectly horizontal bedrock and a constant mean annual accumulation rate Dahl-Jensen et al. (1993). Based on the continuity equation, integration of the horizontal flow over depth yields the vertical velocity profile of the ice, which in turn, gives a depth-age relationship depending on the accumulation rate and total ice thickness when integrated (Nye (1963); Dahl-Jensen et al. (1993)) and describes the thinning rate profile with depth.

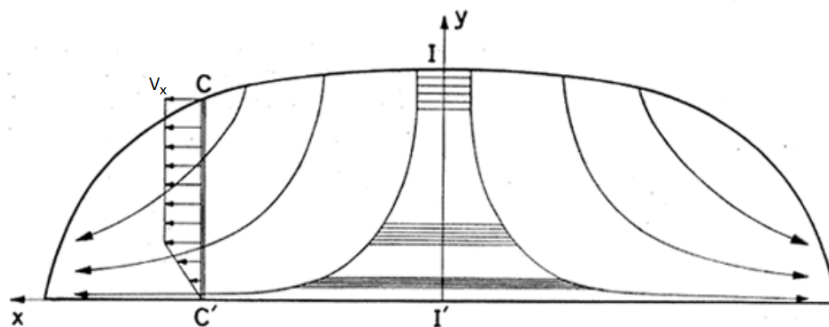


Figure 2.1 | Idealised cross section of an ice sheet with perfectly horizontal bedrock. Thick arrows indicate the main flow through the ice sheet described by the horizontal velocity component, V_x (horizontal arrows), and the accumulation rate at an arbitrary location, $C - C'$. Horizontal lines around the ice divide, $I - I'$, represent annual layers undergoing horizontal thinning. Figure adapted from Dansgaard et al. (1969).

In reality, the flow often is disturbed by uneven bedrock topography. Moreover, the accumulation rate strongly depends on the atmospheric temperatures as anticipated by the Clausius-Clapeyron relation (Wallace and Hobbs (2006)) and the geographical position, as for instance elevation and distance to moisture source, and can therefore not be considered uniform. Close to the ice divide, I , where the ice flows in opposing directions, the horizontal flow velocity is negligibly low. Consequently, the flow disturbance of the layers is minimal since the ice on the horizontal plane originates from approximately the same location near the divide. Therefore, an ice core record is ideally constructed from ice close to the ice divide.

2.2 Ice Cores and Palaeoclimatology

In palaeoclimatology, past climatic conditions often are reconstructed by analysing ice cores for physical characteristics related to another variable, which can not be measured directly, known as climate proxies. These proxies comprise an isotopic composition of, among others, oxygen and carbon from ice or sediment core records, and chemical impurities. Atmospheric reconstructions, on the other hand, can be directly extracted from gas concentration measurements of ancient atmosphere enclosed in the ice.

The air sealed during the firn-ice transition (Section 2.1.1) preserves information about past atmospheric composition, such as greenhouse gas concentrations. Due to the proximate distance to terrestrial sources, the Greenlandic ice cores show a strong methane (CH_4) signal. Antarctic ice cores, however, reveal reliable data about the carbon dioxide (CO_2) concentration due to the surrounding Southern Ocean storing vast amounts of carbon, which is released to the atmosphere as CO_2 during periods with a low atmospheric partial pressure of CO_2 .

Moreover, airborne impurities transported to the ice sheet accumulate in the stratigraphy as wet or dry deposition. Insoluble particles, such as terrestrial dust, are seen as indicators of an arid climate since fewer particles are washed out by precipitation when transported through the atmosphere during these periods. Enhanced dust levels further suggest a lower sea level exposing larger terrestrial areas being a source of dust as well as higher intrahemispheric temperature variations characterised by stronger wind intensity. Thus, higher dust concentrations in the ice core are indicative of a colder climate and give information about the atmospheric circulation when analysing its mineral composition for source determination (Ruth et al. (2003)).

Increased storminess further enhances the seawater aerosolisation, which can be seen in the elevated ionic particle levels, as for instance sea salt (Fischer et al. (2007)). This, again, points to generally lower temperatures rather than periods with smaller sea ice cover giving rise to aerosolisation from wave action at the open sea-air interface, as might be expected.

Biogenic signals can be used as a proxy for continental ice extension since larger areas covered with ice suppress biological emissions from vegetation and soil respiration as well as decomposition and reduce large-scale (mainly boreal) forest fires visible as short-term signals in the ice core record (Kreutz (2007)).

Another continental signal is attributable to explosive volcanic eruptions, releasing acids and fragmented lava into the atmosphere. While tephra deposits are rare, the conductivity of the ice is affected by the sulphate and occasionally fluorides (Langway et al. (1988)). Greenland ice cores are mostly impacted by Icelandic and Alaskan volcanoes, whereas Antarctica receives the strongest signals from Southern Hemisphere eruptions. However, if the eruption is large enough to eject particles into the stratosphere the signal can be distributed across hemispheres (e.g. Lin et al. (2022)). Volcanic evidence in combination with other climate proxies can this way describe the impact of large eruptions on the global climate system. They are further an important tool to date and synchronise ice cores as they can be utilised as marker horizons in the ice cores.

One of the most essential proxies for prehistoric climate conditions is the isotopic composition of the ice. More precisely, stable isotopes of the water molecule can be utilised as a temperature proxy revealing both seasonal and perennial temperature variations. They, further, indicate the moisture source composition and thereby can avail to reconstruct sea ice extent and atmospheric

circulation patterns.

In this work, volcanic signals and oxygen isotope composition, will play a dominant role and are therefore discussed in more detail in Section 2.2.1 and Section 2.2.3.3, respectively. Rapid temperature variations seen in the isotope data characterise DO events in the Greenland ice cores and corresponding isotope maxima are revealed in the Antarctic ice cores. To study the influence of these Northern Hemisphere events on the Southern Hemisphere, bipolar eruptions are used to synchronise ice cores from Greenland and Antarctica as elucidated in Section 2.2.3.3.

2.2.1 Stable Isotope Records

Atoms from the same chemical species have an identical number of protons and electrons, but the number of neutrons in the nucleus can vary. Consequently, these so-called isotopes of the element have different atomic masses. This, in return, results in different physical and chemical properties (Sharp (2017)). The isotopes belonging to the water molecule are ^1_1H (99.984 %) and deuterium (D), ^2_1H (0.016 %) for hydrogen, and three stable oxygen isotopes, $^{16}_8\text{O}$ (99.76 %), $^{17}_8\text{O}$ (0.04 %), and $^{18}_8\text{O}$ (0.2 %) (Bradley (2014)). The most abundant molecules consisting of these isotopes are H_2^{16}O , H_2^{18}O , and HDO.

2.2.1.1 Isotopic Fractionation

In the three states of water, solid (ice), liquid (water), and gaseous state (vapour), the proportions of the isotopic molecules deviates due to isotopic fractionation mainly occurring during phase change. The relative abundance of the rare, usually heavier isotope compared to the more common isotopes is expressed by the rate, R , in Equation 2.1.

$$R = \frac{N_h}{N_l} \quad (2.1)$$

Here, N_h and N_l denote the number of isotopically heavier and lighter atoms, respectively. During phase change, the relative abundance of the isotopes changes on account of their mass distinction having an influence on the mobility of the atoms. For a molecule, mass, m , and velocity, v , are inversely related as can be seen from the expression for kinetic energy, E_{Kin} , in Equation 2.2.

$$E_{Kin} = \frac{1}{2}m\bar{v}^2 = \frac{1}{2}fkT \quad (2.2)$$

The mobility of the molecule is described by the degrees of freedom, f , k is the Boltzmann constant, and T refers to the temperature. In order to obtain the equal amount of energy isotopologues of higher mass, hence, have lower velocity than their lighter counterpart at the same temperature. This reduces diffusion and the collision frequency and thereby the possibility of reaction. Consequently, heavier molecules tend to evaporate less rapidly and conversely, condensate more easily. The effect of atomic mass differences is further visible in terms of their bond energy, which is increased for isotopically heavier molecules. Thus, for the heavier molecules, a slightly higher energy input is required to overcome the higher bond strength.

Considering evaporation, the higher average translational velocity of the lighter favours the diffusion at the boundary between liquid and gaseous water, leaving the reservoir enriched in heavier molecules. The difference in vapour pressure, i.e. the tendency to change into a gaseous state, between the lighter and the heavier isotope in equilibrium is described by the fractionation factor, α in Equation 2.3.

$$\alpha = \frac{R_c}{R_v}, \quad (2.3)$$

with the subscript c and v denoting the isotopic ratio of the condensate and vapour, respectively. Due to the general low abundance of the heavier isotopes, R is given by a small number. Therefore, the isotopic composition is mostly quantified by comparing the isotopic ratio to a standard rate, R_{std} , and determining its deviation to unity. This normalised ratio is referred to as the δ -value presented in Equation 2.4.

$$\delta = \frac{R}{R_{std}} - 1 \quad (2.4)$$

According to this expression, the δ value of a standard is defined to be zero. As a ratio, the value is unitless, but owing to its small magnitude often given in permille. The δ -notation usually specifies the isotopologues by the heavier isotope. In climate studies, often $\delta^{18}\text{O}$ values are represented by comparing the isotopic composition of the sample to Standard Mean Ocean Water (SMOW) used as standard, as defined in Equation 2.5.

$$\delta^{18}\text{O} = \left(\frac{\frac{^{18}\text{O}}{^{16}\text{O}}_{\text{sample}}}{\frac{^{18}\text{O}}{^{16}\text{O}}_{\text{SMOW}}} - 1 \right) \cdot 10^3 \text{ [‰]} \quad (2.5)$$

2.2.1.2 Temperature Dependency of $\delta^{18}\text{O}$

The isotopic composition of oxygen and hydrogen is highly dependent on temperature. Generally, isotope effects are less significant at higher temperatures, caused by atoms occupying higher energy levels, which diminishes the difference in binding energies of different isotopologues. The atmospheric vapour pressure decreases with temperature leading to condensation when humid air masses cool (Wallace and Hobbs (2006)). Due to the tendency of heavier isotopes to condensate preferably, the condensate is enriched in ^{18}O , while the vapour progressively is depleted in heavier isotopes with increasing degree of condensation. This results in the δ value of both the vapour and the subsequent condensate becoming more negative by a rate defined by the fractionation factor, α . When the condensation occurs under so-called Rayleigh conditions, i.e. when no back exchange with the reservoir takes place after the separation, fractionation can cause a strong depletion in the heavier isotopes of the water vapour when travelling through the atmosphere. This isotopic fractionation process is illustrated in Figure 2.2.

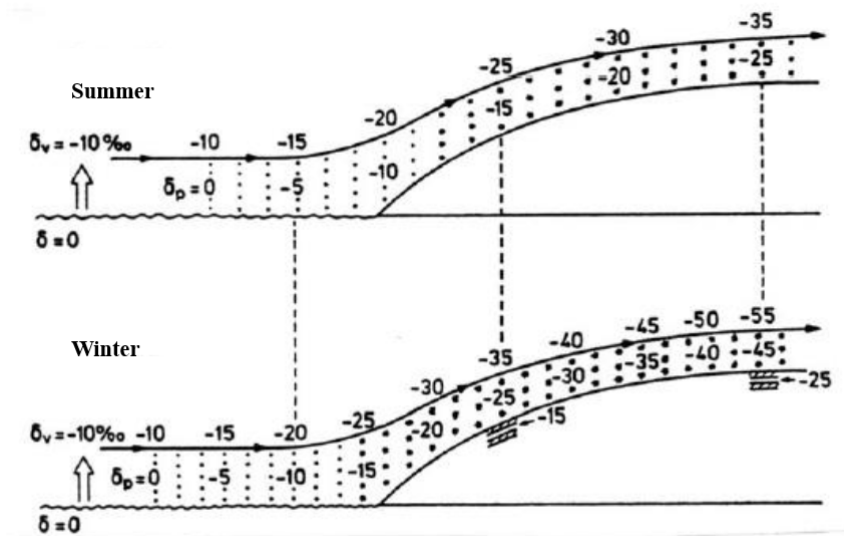


Figure 2.2 | Rayleigh distillation. Simplified illustration of oxygen isotope fractionation during evaporation from the moisture source ($\delta = 0$) and subsequent condensation due to cooling as the air is transported towards higher latitudes or ascends higher altitudes over an ice sheet. With the heavy components precipitating faster the δ -value decreases towards higher latitudes/altitudes. The upper panel shows summer conditions. The lower panel presents winter conditions, where generally lower temperatures result in a stronger depletion of the heavy components and thus, lower δ -values compared to summer. This results in distinct annual layers in the ice cores. Figure adapted from Dansgaard et al. (1973).

The reconstruction of palaeoclimate avails the temperature dependency and uses isotopes as a temperature proxy. In ice cores, more negative $\delta^{18}\text{O}$ values measured by isotope ratio mass spectrometry, reveal colder climate conditions at the time of precipitation because the air masses arriving at the ice sheet have experienced a higher amount of condensation and thus, are depleted in the heavier isotopes. Accordingly, warmer climate conditions are evidenced by less negative $\delta^{18}\text{O}$ due a higher abundance of isotopically lighter molecules.

However, the interpretation of the stable oxygen isotope record in an ice core related to absolute temperature is not always straightforward, but rather complicated by their correlation to meteorological conditions. Hence, general temporal and spatial variations have to be accounted for when drawing comparative conclusions about palaeoclimatic fluctuations at different locations. The $\delta^{18}\text{O}$ -value is namely affected by the elevation of the drilling site, which governs local temperatures as defined by the lapse rate. Further, both transport mechanisms and distance to the moisture source influence the isotopic composition, as more precipitation events can occur the larger the distance to the originating reservoir, which results in a lower $\delta^{18}\text{O}$ -value. Furthermore, the isotopic composition of the moisture source sets the initial conditions. This, in return, is modulated by glacial growth and retreat during glacials and interglacials, respectively. Being depleted in the heavy isotopes, the $\delta^{18}\text{O}$ value of the ocean water decreases when glacial meltwater returns to the ocean. During glacials, on the contrary, the ocean $\delta^{18}\text{O}$ is higher as the heavy isotopes precipitate earlier, while the isotopically lighter molecules are stored in the ice sheets (Cuffey and Paterson (1994a)).

Empirically, a general, linear relationship between oxygen isotopes and temperature has been determined, which, however, needs to be tuned for different ice cores to account for the site-specific variations. With a change of $0.62 \text{‰}/^\circ\text{C}$ representing fractionation during moist-adiabatic cooling of air masses as predominantly experienced in Greenland at higher altitude and taking into account the isotopic latitude effect ($\sim 1 \text{‰}/^\circ\text{C}$), among others, the relationship found for NGRIP can be expressed as in Equation 2.6 (Dansgaard et al. (1973)).

$$\delta^{18}\text{O} = 0.62T - 15.25 \text{ [‰]} \quad (2.6)$$

This relationship would imply DO temperature amplitudes of approximately 7°C . However, this spatial gradient is not uniformly applicable throughout Earth's history. Nevertheless, $\delta^{18}\text{O}$ is a robust proxy for palaeoclimatic reconstructions, especially when quantifying relative climate fluctuations rather than absolute temperatures. In this way, the Northern Hemisphere ice cores reveal a distinct signal of the rapid temperature increases during the last glacial period (see Figure 1.1). In the same way as oxygen isotopes the hydrogen isotopic composition, δD , represents local temperatures. The differences between the records, accounting for the relative mass difference of factor 8, store additional information about the moisture source temperatures rather than the air temperature at the time of precipitation. This second-order parameter referred to as Deuterium excess, $d = \delta\text{D} - 8\delta^{18}\text{O}$ (Dansgaard (1964)), is, therefore, an important supplementary proxy for reconstructing palaeoclimatic environments.

2.2.2 Ice Core Dating Methods

The interpretation of a climate signal obtained from ice core measurements requires an accurate and precise ice core chronology. More precisely, the climate record corresponding to a certain depth segment of the ice core needs to be assigned to a specific age in order to describe the Earth's climate history. The currently longest continuous ice core record comprises a high-resolution deuterium profile from the Antarctic EPICA Dome C ice core extending more than 800 ka back in time (Jouzel et al. (2007)). Greenland ice cores, on the other hand, cover the prehistorical glacial period in some cases reaching back into the Eemian interglacial period (Dahl-Jensen et al. (2013)). A chronology for a single ice core can be compiled by applying different techniques including the use of well-dated reference markers, annual layer counting based on stable isotopes and impurity seasonality, glaciological modelling of the ice flow and deformation, and orbital tuning.

2.2.2.1 Annual Layer Counting

The upper part of an ice core reveals a visible annual signal, as seasonal refrozen surface or melt layers distinctly separate winter and summer layers. The signal is, however, weakened after the snow and firn layers have been compressed to ice. Here, the isotopic composition of the ice reveals a distinct annual cycle.

2. Scientific Background

Since the stable hydrogen and oxygen isotopes are closely related to the local temperature at the time of precipitation, the isotope records depict a seasonal variance (Figure 2.3). Due to lower air temperatures and following more condensation, the water is depleted in heavier isotopes during winter, while higher air temperatures and a consequently increased water vapour pressure favour evaporation, resulting in an enrichment of isotopically heavier water molecules (see Section 2.2.1). According to the isotope ratio and the definition of the δ -value in Equation 2.1 and Equation 2.5, $\delta^{18}\text{O}$ is lower in winter than in the summertime.

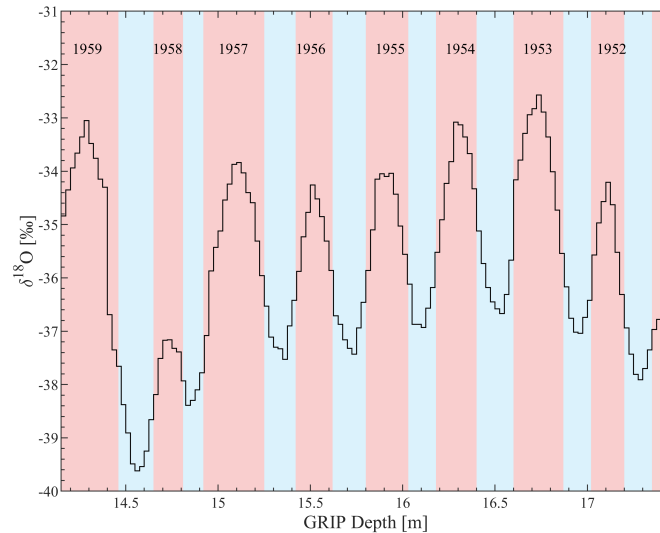


Figure 2.3 | Seasonal isotope signal. Stable oxygen isotope record ($\delta^{18}\text{O}$) of the upper part of the GRIP ice core in central Greenland showing a distinct seasonality. Warm summer layers and cold winter layers are indicated by red and blue shading, respectively. One year extends approximately from a minimum in $\delta^{18}\text{O}$ to the next minimum.

The isotope signal is, however, strongly attenuated by the compression of the ice with depth. Before the sealing of the porous material, molecular diffusion along the pressure gradient results in the water vapour moving into open pores. As pressure is controlled by the temperature gradient, vapour from warmer snow will diffuse towards colder areas in the firn disturbing the isotope-related temperature signal. The diffusion length is directly linked to the diffusion rate and has therefore shown to completely erase the isotope profile in layers thinner than 15-20 cm (Kahle et al. (2018)). Deeper in the ice, when the pores are occluded, the diffusion depends on the glacial flow and the diffusivity of solid ice. Higher temperatures, occurring for instance closer to the bedrock due to geothermal heat flux, and the chemistry of the isotopologues can enhance diffusion. The original record can be reconstituted by mathematically correcting for diffusion. However, this is only possible at high accumulation sites.

At sites with low annual accumulation, the glaciochemical record achieved from a Continuous Flow Analysis (CFA) can preserve an annual signal longer back in time. Impurities, enclosed in the ice matrix and thereby unaffected by diffusion, may contribute to annual layer counting when experiencing seasonality. Greenland dust, mostly indicated by calcium (Ca^{2+}), shows a maximum during spring, whereas sodium (Na^{2+}) used as a proxy for sea salt peaks during winter

as a result of higher storminess (Capron et al. (2021)). Ammonium (NH_4^+) increases in summer perhaps owed to enhanced soil and vegetation emissions (Kellerhals et al. (2010)).

In order to avoid misinterpretation, multiple records are analysed separately for annual signals. In a short-term period with constant climate conditions, the annual layer thickness is expected to be rather uniform. Therefore, when counting annual peaks, a year not clearly pronounced in the profile can be recorded if it agrees with the periodicity of the annual signal. These uncertain layers are counted as 0.5 ± 0.5 years and give rise to an uncertainty of $0.5N$ for N uncertain years on the age determination, referred to as the maximum counting error (MCE). Uncertainties directly arising from the CFA measurements or handling of the ice core (e.g. removing contaminated segments) are neglectable compared to the MCE. This way multi-proxy layer counting can establish a chronology also at low-accumulation sites (Rasmussen et al. (2014)).

2.2.2.2 Glaciological Modelling and Orbital Tuning

Flow-based thinning of the annual layers as well as surface melt and basal flow over uneven bedrock undulation can disturb the stratigraphy and complicate the development of an ice core chronology. When annual layers are difficult to identify, glaciological modelling can be used to establish a time scale. Accounting for the surface and basal mass balance, i.e. accumulation rate, sublimation, and surface as well as basal melt, a depth-age relationship can be determined (Dansgaard and Johnsen (1969)) (see Section 2.1.2). More sophisticated models also include physical properties of the ice itself; for instance the ice crystal structure, impurity concentrations, and temperature (Ritz et al. (2001)).

Additionally, palaeoclimatic records can be dated by so-called orbital tuning (Bazin et al. (2015); Bender (2002)) under the assumption of the Northern Hemisphere summer insolation driving long-term fluctuations governed by the Earth's orbital parameters (Milankovitch (1941)). Isotope measurements of atmospheric oxygen trapped in the ice, for example, have revealed a coherence with insolation variations lagging the precession cycle by 5-6 ka (Bender et al. (1994)). However, poorly constrained linking between orbital forcing and ice core records implies large uncertainties of thousands of years (Bazin et al. (2013)).

Often multiple techniques are combined to create an individual and precise ice core chronology. The chronology can further be complemented by integrating diverse palaeoenvironmental records from for example marine sediment cores or dendrochronology studies (e.g. Rasmussen et al. (2014); Hoek et al. (2008)). However, in order to interpret regional differences or similarities, or describe the coupling of the two hemispheres by the climate system, records from different ice cores have to be synchronised.

2.2.3 Synchronisation of Ice Cores

Exploiting the observed differences in the individual ice core records to understand past climate dynamics, the ice cores are cross-dated to transfer the individual chronologies to a common multi-core timescale. First, the synchronisation of ice cores within Greenland and Antarctica, respectively, is performed by identifying layers of exactly the same age in at least two different

ice cores. Most commonly, distinct layers with volcanic signatures, meaning higher electrical conductivity signals compared to the mean or even tephra deposits (Rasmussen et al. (2013)), detected in two or more profiles are used as reference horizons for stratigraphic linking. Linearly interpolation between these matchpoints creates a common chronology framework, essential for direct comparison of climate records. Analysing the interhemispherical coupling can be achieved by identifying striking bipolar marker horizons or global signals in Greenland and Antarctic ice cores. Synchronous global events can be visible in well-mixed greenhouse gas profiles such as carbon dioxide (CO₂) and methane (CH₄) (e.g. Blunier et al. (1998); Buizert et al. (2015)), cosmogenic isotope records (Raisbeck et al. (2006); Steinhilber et al. (2010)), and extensive volcanic eruptions (Sigl et al. (2015); Svensson et al. (2013); Svensson et al. (2020)).

2.2.3.1 Greenhouse Gas Synchronisation

The global greenhouse gas concentrations (e.g. CO₂ and CH₄) have changed in accordance with climate variations in the past. Since CO₂ and CH₄ are relatively well-mixed and long-lived gases, large-scale concentration changes can be observed approximately synchronous in both hemispheres (Stauffer et al. (1998)). During the process of densification, air bubbles get sealed in the ice preserving the atmospheric composition at this time (see Section 2.1.1). In a CFA, the gas bubbles can be extracted and the concentrations of the components determined. This enables correlating ice core chronologies and linking climate and environmental changes globally. Due to Antarctica being surrounded by oceans, the gas record reveals a strong CO₂ signal as a result of carbon sink dynamics of the ocean. Being a well-mixed gas, the CO₂ is rather uniform around the globe. However, Greenland is largely influenced by terrestrial carbon sources caused by its proximity to land masses distorting the atmospheric reconstruction. In contact with the air in the ice, organic carbon can oxidise affecting the total CO₂ concentration measurable in the ice. Therefore, mostly CH₄ records are used to synchronise ice cores with a precision of a few hundred years (Blunier and Schwander (2000)). The largest uncertainty and challenge when synchronising ice core records from gas profiles arise from the age difference between the trapped air bubbles and the surrounding ice. The full close-off occurs at roughly 80 m where, depending on accumulation rate, surface temperature, and to a minor extent on ice flow, the ice already has achieved a certain age while the air is still in contact with the atmosphere (Section 2.1.1). The age difference between the enclosed gas and the surrounding ice denoted Δage , therefore, highly varies between drilling sites in a range of a few hundred to a few thousand years with Δage increasing with decreasing temperature and consequently lower accumulation rate (Blunier and Schwander (2000); Buizert (2021)).

Firn densification models and measurements of the temperature-depending oxygen-isotope gradient (Severinghaus and Brook (1999)) can be used to quantify the age difference. This requires a precise understanding of the physical firn processes, accumulation rate and temperature conditions at this time and thus, the determined values are often fraught with uncertainties in the order of a few hundred years (Blunier and Brook (2001)). Consequently, defining the absolute timing of a particular climate event is rather uncertain. Nevertheless, an internal comparison can be forwarded by the methane data series. After linking the gas records from different ice cores the other profiles (e.g. $\delta^{18}\text{O}$) can be aligned.

2.2.3.2 Cosmogenic Isotope Synchronisation

In the upper atmosphere, high-speed interactions between cosmic ray particles and atomic nuclei lead to the production of cosmogenic isotopes. The production rate is determined by the solar activity and the strength of the magnetic field, in return, reacting to the strength of the solar winds to shield the Earth from cosmogenic particles. More precisely, higher solar activity increases the strength of the magnetic field and consequently lowers the production of cosmogenic isotopes. Therefore, cosmogenic isotope records can be used to relate past climate signals to solar activity. Interactions of cosmogenic rays with nitrogen and oxygen in the atmosphere produce radioactive carbon-14 (^{14}C) and beryllium-10 (^{10}Be) isotopes. In the lower atmosphere, ^{14}C oxidises to $^{14}\text{CO}_2$ (Lal and Peters (1967)), whereas ^{10}Be gets attached to aerosols and washes out with precipitation after an average residence time in the stratosphere of one to two years (McHargue and Damon (1991)). While the latter is attributable to the production rate alone, ^{14}C is affected by the carbon cycle. In ice cores, significant in-situ production requires sufficient biogenic material for the abundance of ^{14}C to be adequately detectable. On the contrary, ^{10}Be show measurable concentrations and thus, can be used to date the ice based on its radioactive decay rate.

Due to its short lifetime in the atmosphere, larger variations in the ^{10}Be content are recorded synchronously over the globe enabling the synchronisation of Greenlandic and Antarctic ice cores. Prominent geomagnetic excursions such as the Laschamp Event at around 41 ka b2k doubling the production rate of ^{10}Be (Raisbeck et al. (2006)) are important matchpoints for bipolar ice core synchronisation. However, similar significant events are rare in recent Earth history focusing on shorter timescales, such as the Last Glacial Period. Advantageously, compared to greenhouse gas matching, ^{10}Be is captured in the ice matrix itself and thus, no age difference between the atmosphere in the air bubbles and the ice needs to be accounted for. Nevertheless, despite a proven independence of the ^{10}Be production rate on $\delta^{18}\text{O}$ (Muscheler et al. (2000)), the radionuclide data are marked by climate-induced influences on the transport and deposition of ^{10}Be . As bound to aerosols, the accumulation rate can interfere with the total radioisotope deposition (Fischer et al. (2007)). Further, sampling ^{10}Be is highly ice-expensive and the record is often impeded by a noisy signal, and, therefore, high-resolution data series are difficult to accomplish (Raisbeck et al. (2006)).

2.2.3.3 Bipolar Volcanic Synchronisation

Well-dated volcanic eruptions traceable in an ice core record provide information about the total age of the ice at the time of the eruption. This is especially possible when the chemical composition of the ash can be traced back to its origin. Elevated acidity levels, mainly due to sulphuric acid indicated in the electric conductivity record, and sometimes even layers of ash particles or tephra can be used to synchronise ice cores by identifying distinct marker horizons in two or more ice cores in order to align the records (Svensson et al. (2020)). When the eruption is strong enough to eject sulphuric acids and solid particles into the stratosphere, the signal can be detected in ice cores of both hemispheres and the sulphate deposition ascribed to approximately the same year in the different ice core records (Lin et al. (2022); Svensson et al. (2020)).

Combining ice core volcanic proxies and annual layer counting, bipolar ice cores can be synchronised enabling the interpretation of climate variations and how the hemispheres are coupled through the atmosphere-ocean system. This is particularly relevant when studying the bipolar phasing of climate oscillations like the DO events imprinted in the Greenland isotope record with a corresponding Antarctic counterpart, the AIM. For this, the onset of the DO event is defined in at least one Greenlandic ice core from which the annual layers are counted up to a certain marker horizon, i.e. a sequence of bipolar volcanic eruptions. After linking the Greenland ice core, their profiles can be matched with an ice core from Antarctica revealing the same sequence of volcanic events by identifying the point in the data set with the same number of years from the volcanic fingerprint, as exemplified in Figure 2.4.

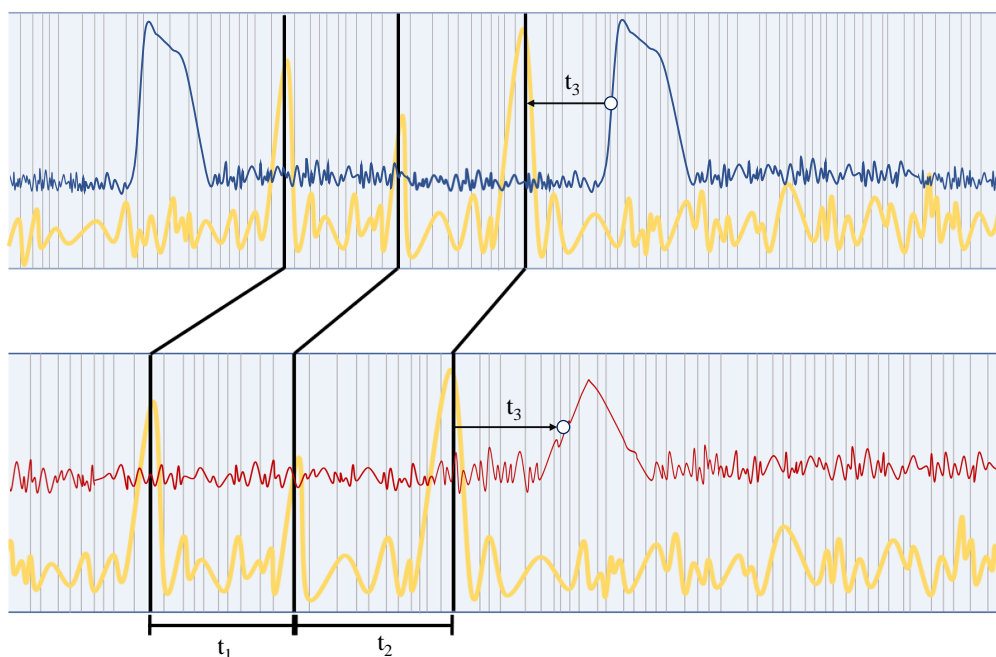


Figure 2.4 | Schematic illustration of (bipolar) volcanic synchronisation. Electrical conductivity signal (yellow) indicates an identical sequence of volcanic eruptions in both ice cores. Using these as (bipolar) reference horizons, the ice cores can be linked as they constitute the same timescale (t_1 , t_2). To ascertain the point in the Southern Hemisphere ice core which corresponds to the onset of a DO event, first the time from the onset in e.g. $\delta^{18}\text{O}$ or Ca^{2+} records (blue) to the closest matchpoint is defined (t_3). Subsequently, the same number of annual layers can be counted back from the bipolar volcanic matchpoint to the isotope profile in the Antarctic ice core (red).

It has to be noted, while local eruptions occurring proximate to the ice core drilling site often show a detectable ash content in the ice core, bipolar tephra layers usually are lacking due to the larger distance to the source, or the weak signal is masked by background dust signals. The volcanic signals can therefore not be matched geochemically, potentially leading to regional signals being misinterpreted as bipolar. The different geographical locations and atmospheric circulation, further prevent the magnitudes of the records to be concurrent, hampering the identification of bipolar eruptions. Hence, eruption sequences with about the same relative

spacing are used for synchronisation rather than relying on one single event. Coincidentally temporally similar occurring local events can still not be ruled out entirely. The uncertainty is, however, reduced by previous synchronisations based on methane and cosmogenic radioisotopes providing a constrained time frame.

2.2.3.4 Ice Core Chronologies

For the most recent half of the last ice age, all deep Greenland ice cores (NGRIP, GRIP, GISP2, NEEM, Camp Century, Renland, and DYE-3) are dated based on annual layer counting (Vinther et al. (2006); Rasmussen et al. (2006)). While for the Holocene annual layers have been mainly identified in the stable isotope signal, the ages of the period from 8-60 ka b2k are ascertained through seasonal impurities as the isotopic annual layers are obliterated by diffusion (Vinther et al. (2006)). Based on the DYE-3, GRIP, and NGRIP ice cores, a Greenland chronology has been constructed reaching back to 14.8 ka b2k ((Vinther et al. (2006); Rasmussen et al. (2006)). NGRIP reveals the most robust annual layer signal throughout the entire ice core due to basal melt of approximately 1 cm per year in combination with a moderate annual accumulation rate. This results in a different ice flow pattern than in the other deep ice cores and consequently in thicker annual layers (Rasmussen et al. (2006)). The common Greenland Ice Core Chronology 2005 (GICC05), therefore, has been extended until 42 ka b2k using independent multi-parameter layer counting in the NGRIP ice core data (Andersen et al. (2004)). Applying a glaciological flow model, the GRIP record has been extended until the interglacial-glacial transition (~ 120 ka b2k) (Johnsen et al. (2001); Wolff et al. (2010)). Internally synchronising the ice cores by shared volcanic signals, finally the common GICC05modelext chronology has been established (Svensson et al. (2005)).

All the Antarctic deep ice cores (WDC, EDML, EDC, Dome F, Talos Dome, Byrd, Vostok, Talyor Dome, and Low Dome) are assigned to individual timescales (Stenni et al. (2011) and references herein). Due to generally lower accumulation rates in Antarctica compared to Greenland, the chronologies are predominantly based on ice flow models supported by orbital tuning and stratigraphic marker horizons (e.g. Parrenin et al. (2016); Salamatin et al. (2004)). The WAIS Divide ice core, on the contrary, shows a reliable annual layer record until around 31.2 ka b2k and is afterwards dated through CH_4 -matching with Greenland ice cores, favoured by a high-resolution gas record and a small Δage as result of low accumulation (WAIS Divide Project Members (2015)). However, for one decade now, some of the deep ice cores share a common timescale, the Antarctic Ice Core Chronology 2012 (AICC2012) which has been linked to Greenland through greenhouse gas concentrations, bipolar volcanoes, and cosmogenic isotope records for the past 60 k years (Veres et al. (2013)).

3. Data and Methods

The phasing of Greenland and Antarctic climate evolution around the abrupt temperature transitions associated with Dansgaard-Oeschger events has previously been analysed with a focus on the period up to 60 ka b2k (WAIS Divide Project Members (2015); Svensson et al. (2020)). This project AIM to expand the study by determining the exact Greenland-Antarctic climatic phasing at all of the DO warming transitions of the entire Last Glacial Period (11.7 ka to about 115 ka b2k). For this, firstly, the DO events are defined in the NGRIP ice core and dated according to the GICC05modelext timescale (Section 3.3). Applying proposed ice-core-based volcanic synchronisation of the entire last glacial, the corresponding depth of the DO events in the other studied ice cores of Greenland and Antarctica has been provided by Anders Svensson. This enables the investigation of individual and stacked climate records to describe the pattern of the climate signal for mean or weaker transitions compared to DO events succeeding a Heinrich Event, as well as the first half compared to the second half of the last ice age. Furthermore, the bipolar coupling between Greenland and Antarctica has been qualified by determining the time delay of Antarctic cooling in response to Greenland abrupt warming (Section 3.4). Lastly, the climatic profiles across the transitions are compared to computed surface temperatures from a global climate model simulating DO events under varying greenhouse gas forcing (Section 3.2 and 4.4.2). The ice core data as well as the model output have been processed in MATLAB.

3.1 Ice Core Records

The study is based on existing stable water isotope records from the Greenland NGRIP, GRIP, GISP2, and NEEM, and the Antarctica WAIS Divide (WDC), Talos Dome (TAL), Dome F, EDC, and EDML ice cores. The respective drilling site locations can be seen in Figure 3.1. Due to their wide distribution across the ice sheets, the features such as elevation, accumulation, and surface snow temperature vary widely between sites. An overview of the ice core characteristics can be found in Table 3.1.

The NGRIP ice core has been drilled in the centre of the ice sheet and provides the only dataset used in this study which covers the entire last glacial. A moderately high accumulation rate (19 cm ice equivalent per year at modern time) and basal melt ensure thick annual layers throughout the entire core. Even though data from the last interglacial have been lost to melting annual layers of 1 cm even close to the bedrock enabling precise dating of the whole last ice age (Rasmussen et al. (2006)). Close to the summit of the Greenland Ice Sheet, the GRIP and GISP2 drilling sites are located in proximate (< 30 km) distance from each other. With a depth of > 3 km to the bedrock, both ice core records reach around 200 ka back in time. However, ice flow over an uneven bedrock topography causes the stratigraphies of the bottom to be disturbed and results in folded layers older than 105.5 k years. Located near the ice divide, which separates

3. Data and Methods

the east- and west-flowing parts, the NEEM ice core contains the oldest ice found in Greenland. Moderately high precipitation at this location ensures clear, thick annual layers without increasing the ice flow resulting in the thinning of older layers. However, the temperature proxy data in this work only cover the last ice age. All four Greenland ice core records are dated using the annual-layer counted and model-extended Greenland Ice Core Chronology 2005 (hereafter GICC05modelext) based on the NGRIP record (Rasmussen et al. (2014)).

Table 3.1: Ice core characteristics. Geographical location, drilling site elevation (m above sea level (a.s.l)), length of the core (m), temporal coverage of the data in thousands of years (ka), and sampling resolution for the four Greenlandic ice cores (NGRIP, GRIP, NEEM, GISP2 and the five Antarctic ice cores (Wais Divide (WDC), Talos Dome (TAL), Dome F, EPICA Dome C (EDC), and Epica Dronning Maud Land (EDML)), respectively.

Ice Core	Location	Elevation (m a.s.l)	Length (m)	Coverage (ka)	Resolution (cm)	
NGRIP	75°01'N, 42°32'W	2917	3090	122	5	NGRIP Members (2004); Gkinis et al. (2014)
GRIP	72°35'N, 37°38'W	3230	3022	106	6	Dansgaard et al. 1993; Johnsen et al. (2001)
NEEM	77°27'N, 51°3.6'W	2484	2539	109	5	Gkinis et al. (2021)
GISP2	72°35'N, 38°27'W	3203	3040	106	6	Grootes et al. (1993); Grootes and Stuiver (1999)
WDC	79°28'S, 112°5'W	1766	3403	67	5	WAIS Divide Project Members (2013); WAIS Divide Project Members (2015)
TAL	72°49'S, 159°11'E	2315	1282	60	10	Stenni et al. (2011) ; Landais et al. (2015)
Dome F	77°19'S, 39°42'E	1151	2416	72	50	Watanabe et al. (2003); Kawamura et al. (2007)
EDC	75°05'S, 123°19'E	3233	1488	110	11	EPICA Community Members (2004)
EDML	75°00'S, 0°04'E	2892	2416	110	50	EPICA Community Members (2006)

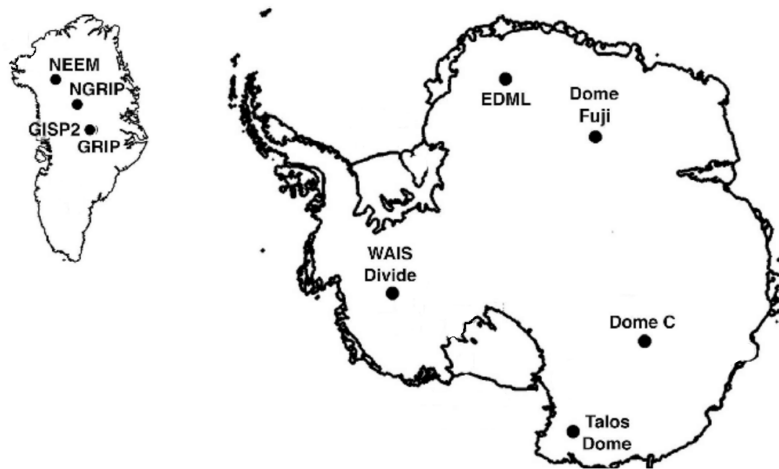


Figure 3.1 | Map of Greenland and Antarctica. Geographic locations of the polar drill sites in Greenland and Antarctica, whose ice core records are used in this work. Exact coordinates and characteristics can be found in Table 3.1. Figure modified from Neff (2014).

Drilled at the ice flow divide of the West Antarctic Ice Sheet around 1040 km from the geographical South Pole, low surface temperatures prevent surface melt and result in thick annual layers. At the Talos Dome (TAL) drilling site, the modern annual accumulation amounts to 8.5 cm ice equivalent due to its near-coastal location (~ 300 km to both the Southern Indian Ocean and the Ross Sea) (Buiron et al. (2011)). Dome F is located on a stable ice dome on the ice divide on the Antarctic Plateau at the second-highest Antarctic summit and is with 10 m-snow temperature of -58°C one of the coldest places on Earth (Watanabe et al. (2003)). The EDC ice core provides one of the longest climate records. However, the small annual layer thickness and flow disturbance of the basal layers complicate the dating of the older ice (Parrenin et al. (2016)). The continuous $\delta^{18}\text{O}$ record originates from two separate ice cores (EDC96, started in 1996, with 786 m length and EDC99, started in 1999, reaching a depth of approximately 3200 m) (Augustin et al. (2007)). Here, all EDC depths are given on the EDC99 depth scale. The Antarctic ice core records are dated using their respective chronology different to the one that the Greenland ice cores are dated based on. In order to determine the bipolar phasing, the depths of the ice cores are linearly interpolated on the NGRIP depth enabling the GICC05modelext to be used as a common chronology.

All of the data series are equidistant in depth and thus, have an inconsistent individual temporal resolution, which changes with depth as the annual layers get compressed. The depth resolutions vary between ice core records from a fine resolution of 2.5 cm up to a coarse 0.5 m-resolution, as shown in Figure A.1 in the Appendix.

3.2 Abrupt Climate Change Simulations

Modelling the climate based on different prehistorical climate conditions enables to verify the ability of a climate model to predict future climatic scenarios. A comprehensive climate model has determined the past global temperature changes during DO events under different atmospheric CO_2 concentrations (Vettoretti et al. (2022)). The Community Climate System Model (CCSM4) is composed of five separate geophysical models, coupling the atmosphere, ocean, sea ice, land, and land ice (Gent et al. (2011)). Despite being a highly complex model it agrees with the basic mechanisms described by Stocker and Johnsen (2003) mimicking bipolar seesaw behaviour. A combined thermohaline buoyancy flux is the main forcing driving changes in the global ocean circulation. During stadials, the heat content in the Southern Hemisphere and below North Atlantic sea ice is increased, leading to a buoyancy gain on millennial timescales. The energy influx to the ocean lowers atmospheric temperatures and increases the thermohaline stratification of the global ocean. Eventually, the heat is released from the ocean during warm interstadial periods. The buoyancy gradient determines the fluctuating strength of the AMOC resulting in DO event characteristics. In the conceptual ocean box model, the temperature changes happen instantaneously in the Northern Hemisphere, while the large thermal reservoir in the ocean causes heat in the Southern Hemisphere to decay exponentially, resulting in the characteristic bipolar seesaw pattern as seen in Figure 1.2 (Stocker and Johnsen (2003)). In the CCSM4, the thermal memory is defined by timescales related to the heat capacity of the ocean and eddy diffusion. Not resolved by the coarse grid resolution of the model, eddies are

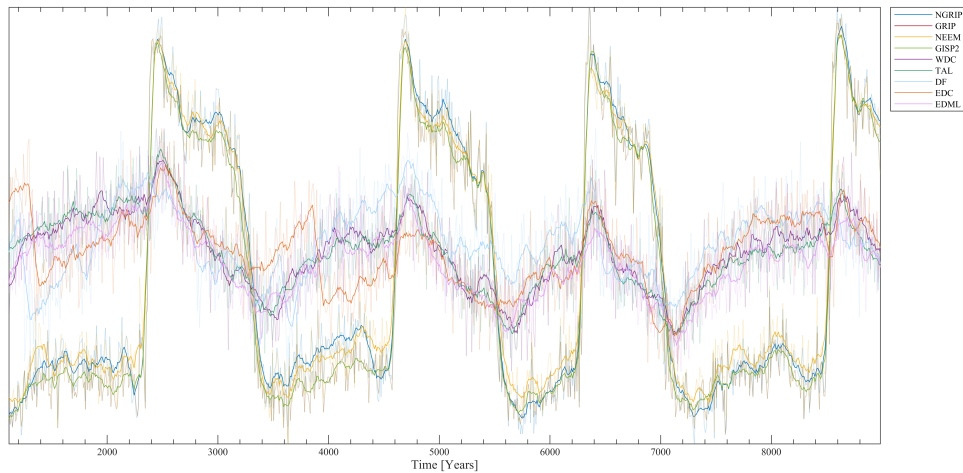


Figure 3.2 | Simulated temperature under a CO₂ forcing of 210 ppm. CCSM4 model output representing temperature profiles over Greenland and Antarctica under a constant CO₂ forcing of 210 ppm (Vettoretti et al. (2022)). The simulation reveals abrupt temperature increases over the North Atlantic and corresponding rising temperatures over Antarctica, similar to DO events and AIM of the last ice age.

parameterised in a subgrid scale as originally proposed by Gent and McWilliams (1990). The basic features of the heat transport through the atmosphere capture solar insolation and wind patterns modified by the Intertropical Convergence Zone (ITCZ). A set of 10 000-year-long equilibrated glacial simulations furnishes a global surface temperature profile with a grid resolution of $3^{\circ} \times 3^{\circ}$ and temporal resolution of ten years for distinct atmospheric CO₂ concentrations in the range of 170-240 ppm (Vettoretti et al. (2022)). Additionally, Heinrich events are simulated by adding a freshwater forcing of 0.05 Sv ($1 \text{ Sverdrup} = 1 \times 10^6 \text{ m}^3 \text{ s}^{-1}$) imitating extensive ice-berg melt. On the basis of these mechanisms, the model succeeds to produce a set of abrupt temperature rises over Greenland and respective small-scale temperature increases over Antarctica, resembling Northern Hemisphere DO events and corresponding Southern Hemisphere AIM (Figure 3.2). Despite a constant pattern of the events, the duration varies in accordance with the background CO₂ forcing.

Since the model is driven by mathematical descriptions of the physical processes in the climate system, the mechanisms behind the climate coupling between the Northern and Southern Hemisphere in the last glacial period can be understood, if the model output fits the actual palaeoclimatic data of the Greenland and Antarctic ice cores. For this study, the temperatures at the respective Greenlandic and Antarctic drilling sites are extracted from the global record, and the interhemispherical climate signal across the DO events is analysed in comparison to the isotope ice core data.

3.3 Defining the Onsets of Dansgaard-Oeschger Events

In order to study the interhemispherical interplay and for this purpose determine the phasing between Antarctica and Greenland across the Northern Hemisphere abrupt warming events, first the absolute timing of the DO events has to be determined. More precisely, the onset of the individual warming events has to be ascribed to a certain age on the common timescale, which all the individual ice cores can be assigned to. The identified 25 DO events are in some cases internally interrupted by several warming and cooling transitions. In this work, the onset of in total 32 interstadials as well as the abrupt warming through the Younger Dryas-Preboreal transition (YD-PB) has been dated.

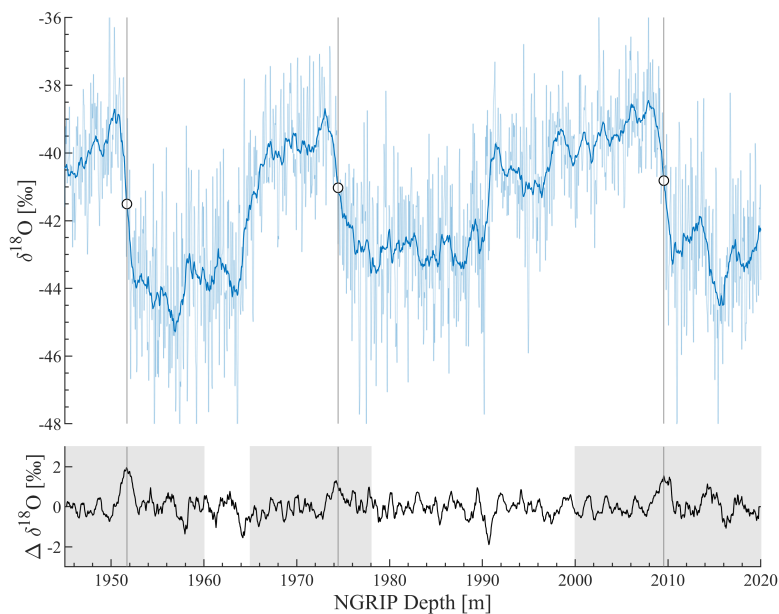


Figure 3.3 | Defining onsets of Dansgaard-Oeschger events. NGRIP $\delta^{18}\text{O}$ as a function of NGRIP depth including the Greenland interstadials GI-5.2, GI-6, and GI-7. Dots denote the midpoint defined as the steepest point in the transition from stadial to interstadial conditions. The slope is represented by $\Delta\delta^{18}\text{O}$ as a function of depth. Grey vertical lines mark the depth associated with the largest $\Delta\delta^{18}\text{O}$ gradient over ten data points in a 15-point smoothed isotope profile in the predefined search interval indicated by the grey shading.

The onset of the DO event, here, is defined as the midpoint of the transition from a cold stadial to a warm interstadial period in the NGRIP $\delta^{18}\text{O}$ record. The NGRIP ice core provides the longest continuous high-spatial-resolution isotope record assigned to the prehistorical ages with a 20-year temporal resolution. Corresponding to the number of events, 33 search intervals have been prescribed, each covering the respective DO event including interstadial initiation and subsequent termination. In order to reduce the noise, the data are smoothed by calculating the moving mean over a subset of a number of datapoints varying for the different depth intervals. Aiming to provide a method as objective as possible, it has to be noted that the number of averaged data points has been decided based on a visual inspection of the dataset and varies between 10 and 20 datapoints. The midpoint is then determined as the depth of the

smoothed isotope record with the steepest $\delta^{18}\text{O}$ gradient during the transition between stadial and interstadial. By determining the depth of the ice core where the change in $\delta^{18}\text{O}$ is largest over at least ten datapoints (i.e. 0.5 m), the influence of short-term fluctuations has further been reduced. Figure 3.3 illustrates the determined onsets of three DO events. Seeking to ascertain the Antarctic climate response time to Greenland abrupt warming, the midpoints of the stadial-interstadial transitions on a depth scale are assigned to the corresponding age of the NGRIP ice core by linearly interpolating the depth-dependent high-resolution record onto the GICC05modelext timescale with a temporal resolution of 20 years.

3.4 Determining the Bipolar Phasing

Based on the determined onsets of the DO events in this work, the corresponding depth of the stadial-interstadial transitions in the three other Greenland ice cores (GRIP, GISP2, and NEEM) as well as the depth in the four Antarctic ice cores (WDC, TAL, Dome F, EDC, and EMDL) corresponding to the respective DO events have been provided by Anders Svensson, applying annual layer counting in combination with (bipolar) volcanic reference horizons, as described in Section 2.2.3.3. Again, linear interpolation concatenating the depth-dependent $\delta^{18}\text{O}$ data with interpolants to create a continuous timeline corresponding to the depth data yields the age of the respective DO onsets in all the other ice cores.

The synchronisation allows to study the bipolar phasing of the abrupt warming events for different periods of the last glacial as well as for different assemblies of individual DO events. To precisely analyse the timing, the $\delta^{18}\text{O}$ record of each individual event for all the different ice cores is aligned at the determined ages for the transitions on the GICC05modelext time scale. For this, a time vector, τ , is defined to span from $t = -1\,200$ years to $t = +1\,200$ years in 1-year increments. The midpoint age is set to $t = 0$ and the isotope record is linearly interpolated onto the time vector. This results in an oversampled record spanning from 1 200 years before the transition to 1 200 years after the relative transition with equal annual spacing for each individual DO event and the corresponding synchronous Antarctic $\delta^{18}\text{O}$ -profile. For a more pronounced signal the individual, synchronised events are averaged to obtain a stacked record.

Within this 2 400-year window, occasionally multiple events occur. The series of closely-spaced events including GI-14 to GI-17.2 comprises seven events within around 5 500 years, with a minimum temporal difference between the midpoints of GI-16.1 and GI-16.2 of 220 years. To avoid the signal of the individual transitions being disturbed by closely following or preceding events, those signals could be replaced by a constant value matching an average boundary value. However, due to the generally largely varying timing and duration of the events, the signal is expected to be averaged out away from the transition in a stack of multiple events and thus, not to be influenced by transitions occurring shortly before or after a certain event.

Stacking the events is especially advantageous when defining the precise bipolar phasing from the highly variable climate signal. The small signal-to-noise ratio in the Antarctic profile due to wind-driven redeposition generally observed at low-accumulation sites complicates the identification of the breakpoint where warming switches to cooling in the individual AIM. Therefore, the change point is found by determining the $\delta^{18}\text{O}$ maximum in the common climate signal of all events and ice cores. Stacked records further reveal a more general phasing relationship which

can more easily be compared to climate models as these often are not able to mirror the details of each individual event. For Greenland, in total 128 events were stacked for four different ice cores over the course of the last ice age, as the records from GRIP and GISP2 only are reaching up to and including GI-24.1 while the ice cores from NGRIP and NEEM cover the entire range of 33 interstadials. The data from Talos Dome and Wais Divide only embrace the last 60 ka, and the signal from Dome F ends after GI-19.2. Thus, for the five Antarctic ice cores, overall 136 events are averaged.

Antarctica has been observed to warm in response to abrupt warming of the Northern Hemisphere and subsequently cool until reaching temperatures lower than prior to the corresponding DO events, indicated by increasing and decreasing $\delta^{18}\text{O}$ values, respectively. Based on previous studies, global heat circulation mechanisms, and general climate timescales, Antarctica is expected to respond within a maximum of 300 years after the DO onset (Blunier et al. (1998); Blunier and Brook (2001); WAIS Divide Project Members (2015); Svensson et al. (2020)). Hence, the breakpoint between Antarctic warming and cooling is defined as the maximum in the $\delta^{18}\text{O}$ -record occurring within this time interval of 300 years after the transition from stadial to interstadial conditions.

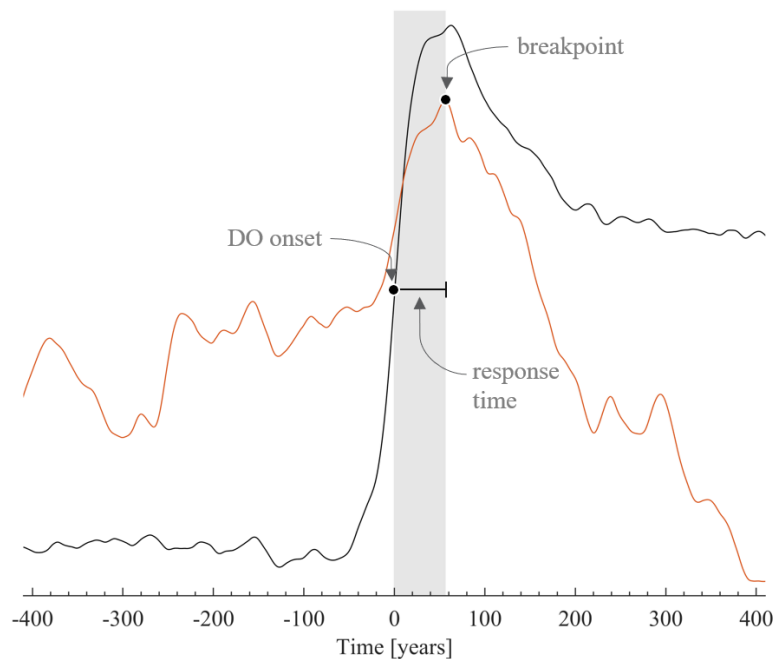


Figure 3.4 | Illustration of the procedure of determining the bipolar phasing between Greenland and Antarctica. The climate records from the different ice cores across the individual DO events are oversampled by interpolating the record onto a time vector, $\tau = -1200 : 1 : 1200$ years, where the onset of the DO event corresponds to $t = 0$ years. Subsequently, the events are averaged to create a stacked record for Greenland (black) and Antarctica (orange), respectively. The breakpoint marks the onset of Antarctic cooling found as the maximum in the Antarctic stack. The bipolar phasing is then defined as the time Antarctica needs to respond with cooling to Greenland abrupt warming as the average time between the DO onset and the breakpoint.

Different from the Greenland isotope signals, the Antarctic $\delta^{18}\text{O}$ -values vary widely between the individual ice cores. Therefore, the records have been normalised according to the min-max scaling before the stacking procedure. For subsequent comparison to Greenland isotope signals, Antarctic records are transformed into the interval $[-0.3; 0.3]$ while the Greenland data are min-max normalised in the range $[-1;1]$. Normalising with respect to the extreme values is not expected to change the maximum of the stacked record. Since the maximum can be hidden in noise the profiles are smoothed creating a 15-point moving mean before determining the breakpoint. The influence of smoothing the Antarctic stack as well as normalisation has been tested for different smoothing windows showing similar results (Figure D.2) supporting the robustness of this method. Furnishing an almost constant value of the response time regardless of the number of averaged points between zero and 30, the bipolar phasing has been calculated based on a stack smoothed over a window of 15 years. The procedure of determining the bipolar phasing between Greenland and Antarctica is illustrated in Figure 3.4.

Different ensembles are studied by grouping the DO events into distinct classifications defined by the time of occurrence and size. Namely, the last glacial period is divided into the first (older) half spanning from 115 ka until 60 ka b2k and the second (more recent) half covering the period from 60 ka until the onset of the Holocene (~ 11.7 ka b2k). Another separation considers major and minor events, where the large events are specified by those with a preceding Heinrich event (Figure 1.1). Small events comprise the remaining events. Table 3.2 presents an overview of the DO events associated with the respective four classifications.

Table 3.2: DO event classification. Analysed groups of DO events classified by time of occurrence in the first and second half of the last glacial and by size. Major events refer to DO events arising from a Heinrich stadial, whereas minor events comprise the remaining DO events. Additionally, the total number of events averaged for the different classes is given for the four Greenlandic (GL) and five Antarctic (AA) ice cores, respectively, as the different datasets do not uniformly cover the same period and thus number of events.

	DO Events	DOs GL	DOs AA
Entire Last Glacial			
(10-115 ka b2k)	YD-PB to GI-24.2	128	136
First Half			
(65-115 ka b2k)	GI-19.1 to GI-24.2	36	22
Second Half			
(10-65 ka b2k)	YD-PB to GI-18	92	114
Major Events	GI-1, 2.2, 4, 8, 12, 14 17.2, 19.2, 20, 21.1 22, 23.1	48	46
Minor Events	YD-PB, GI-3, 5.1, 5.2, 6, 7 9, 10, 11, 13, 15.1, 15.2 16.1, 16.2, 17.1, 18, 19.1, 21.2	80	90

3.5 Uncertainty Evaluation

The bipolar phasing across DO events is based on the determination of the transitions in the Greenlandic record, the subsequent bipolar synchronisation, and finally, the examination of the breakpoint in the Antarctic stacked isotope profile. Each of these determinations is fraught with uncertainties and contributes to an absolute error on the Antarctic response time relative to Northern Hemisphere warming. In the following, the different error sources are discussed and corresponding estimates are given.

The transitions from stadial to interstadial have been defined in the NGRIP $\delta^{18}\text{O}$ record with an equidistant resolution of 5 cm. Smoothing the data points over a window between five and maximum 20 datapoints reduces the noise in the signal facilitating the examination of the transition without decreasing the number of data points. A high noise level is thought to hamper the definition of the steepest point and the smoothing process is therefore considered necessary to evaluate the midpoint of the transition. Other approaches approximate the abrupt change by a ramp fit. By only averaging over a few data points the potentially non-linear characteristics and the abruptness of the change are conserved while reducing the noise level. Therefore, smoothing the data is considered to favour the midpoint determination and is not included in the uncertainty estimate. Instead, the sample resolution is said to contribute to the overall error, as some years might be masked if the annual layer thickness is smaller than the spatial resolution. After interpolating the depth onto the chronology to assign a corresponding age, the temporal resolution has been found around the transition age and is taken as the respective uncertainty for each DO event, with the mean of all events comprising the uncertainty contribution of the transition determination, denoted as δ_T , to the Antarctic response time.

The ages are ascertained with reference to the GICC05modelext timescale with a 20-year resolution. Down to 60.2 ka b2k the chronology is based on annual layer counting where the dating uncertainty is quantified in terms of MCE (Section 2.2.2.1). This cumulative error amounts to 99 years at the onset of the Holocene and accumulates to 2.6 ka at 60 ka b2k. Beyond this age the chronology has been extended, applying a glaciological model based on the simple Dansgaard-Johnsen model combined with $\delta^{18}\text{O}$ data without an instinct error estimate (Rasmussen et al. (2014)). This error of about 5% is approximately constant throughout the last glacial period. When synchronising records across hemispheres, only the relative timing is of importance rather than the absolute age. The bipolar matching is, however, sensitive to annual layer counting. Accounting for the error of 5% associated with the chronology, a relative uncertainty on the bipolar synchronisation is given as 10% of the distance to the closest bipolar matchpoint (Svensson et al. (2020)), with the uncertainty consequently increasing proportionally to the number of annual layers between the onset and the matchpoint. The bipolar matching uncertainty ranges between 0 and 50 years (Table E.1). With respect to the distribution of the error (Figure D.3), the median of the bipolar matching uncertainties, rather than the mean, is taken as an error estimate on the stack of all transitions, termed δ_M .

The Antarctic response time to Greenland warming is defined as the time passed between the DO event and the isotopic maximum in the $\delta^{18}\text{O}$ record. Meaning it is determined by the maximum

in the stacked Antarctic isotope profiles past the stadial-interstadial transition (Section 3.4). Here, a noisy signal again complicates the precise determination of the breakpoint and the data have been smoothed prior to the examination. The influence of smoothing as well as normalisation of the Antarctic stack has been tested for different smoothing windows and gives a maximum deviation of 16 years for the response time defined from raw data and smoothed over maximum 80 years. Accounting for the different shapes and data resolutions of the individual ice core records, one uncertainty on the breakpoint determination has been estimated for each Antarctic ice core (Table D.1). For this, the data fluctuation has been quantified by calculating the residuals relative to the data smoothed over a window of 80 years in order to remove the noise and to solely represent the trend of the isotope profile. The value corresponding to the maximum of the smoothed curve has been found within the upper level represented by one standard deviation of the residuals (Figure D.4). This gives a time range of where the maximum of the raw data can be located accounting for the noisiness of the data. Even though the maximum is not necessarily the midpoint of the maximum range, the uncertainty is taken as half the range to account for the maximum time deviation. The mean of the uncertainties of the individual ice cores corresponds to the phasing contribution of the error on the stacked Antarctic record, referred to as δ_{BP} . Since EDML does not show a maximum prior to the cooling trend in response to Northern Hemisphere warming, it is excluded from the error evaluation. To achieve a conservative error estimate, each uncertainty contributes equally to the overall uncertainty on the average Antarctic response time. Presuming the errors to be independent, the law of error propagation can be used to calculate the final uncertainty on the Antarctic response time for the whole glacial as well for different ensembles, δ_{RT} , as can be seen in Equation 3.1.

$$\delta_{RT} = \sqrt{\delta_T^2 + \delta_M^2 + \delta_{BP}^2} \quad (3.1)$$

An overview of the estimates can be found in Table 3.3 for the different subsets of events. It has to be noted that this is only a rough error estimate and might be influenced by additional factors. For instance, the sample resolution has been assumed to be captured by the uncertainty on the individual break points which in reality might not be certainly true.

Table 3.3: Uncertainty estimates. Error estimates on the definition of the midpoint in the NGRIP ice core (δ_T), on the bipolar volcanic synchronisation (δ_M), and the determination of the breakpoint (δ_{BP}) in the Antarctic records in years (yr). Each estimate contributes equally to the uncertainty on the bipolar phasing, i.e. Antarctic response time to Greenland warming, (δ_{RT}), for all the different classifications; entire Last Glacial Period (10-115 ka b2k), the first half (65-115 ka b2k), the second half (10-65 ka b2k), as well as minor and major events (DOs with preceding Heinrich Event). See Table 3.2 for the events comprising the different classifications. The error estimate on the breakpoint is the mean of the estimates on the maximum for the individual Antarctic ice cores are listed in Table D.1.

	δ_T [yr]	δ_M [yr]	δ_{BP} [yr]	δ_{RT} [yr]
Entire last glacial	3	7	39	40
First half	4	7	56	57
Second half	3	7	38	38
Minor DOs	3	7	52	53
Major DOs	3	4	51	51

4. Results and Discussion

4.1 Stadal-Interstadial Transitions

The timing of the onsets of the Dansgaard-Oeschger events, defined as the midpoint of the transition from stadial to interstadial conditions, have been determined in the NGRIP $\delta^{18}\text{O}$ -record as part of this work. The depth and the corresponding age on the GICC05modelext timescale of the respective DO events are presented in Table 4.1. It has to be kept in mind, that the onset of abrupt warming from a cold stadial precedes the onset as it is defined here, namely as the midpoint of the transition. Based on the last isotopic minimum in the $\delta^{18}\text{O}$ record before the stadial-interstadial transition in the NGRIP stacks, the midpoint occurs 25 years later on average than the initiation of the interstadials (Figure 4.1). This is in strong agreement with a recent study, suggesting the midpoint to be delayed by 25 ± 7 years compared to the stadial termination/interstadial initiation in NGRIP $\delta^{18}\text{O}$ -data (Erhardt et al. (2019)). Note, however, that the timing is influenced by the smoothing of the data, differs between proxies (Erhardt et al. (2019); Svensson et al. (2020)), and strongly depends on how the initiation of the DO event is defined.

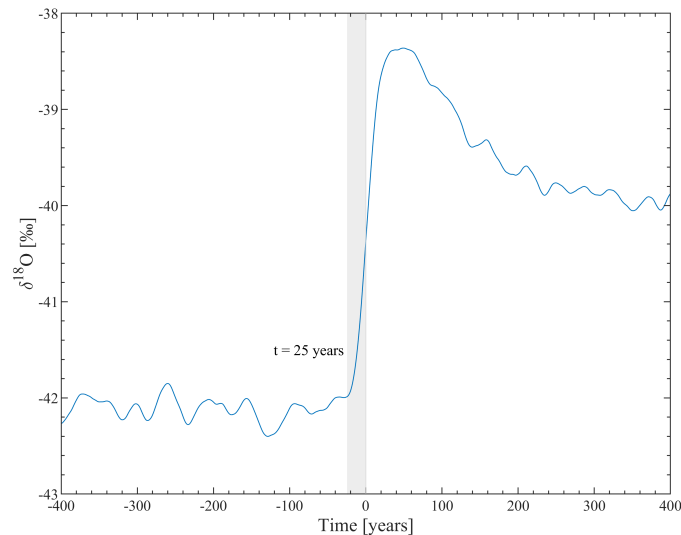


Figure 4.1 | Temporal delay of midpoint compared to the onset of DO events. Stacked isotope record of 33 events in the period between 10 ka and 120 ka b2k of the NGRIP ice core showing the delay of the defined midpoint used for aligning the stacks at $t = 0$ compared to the interstadial initiation at $t = -25$ years on average.

Table 4.1: Onsets of the DO events. Depth and corresponding age on the GICC05modelext timescale with reference to the year 2000 CE (b2k) of the Greenland Interstadial onsets. The onsets are defined as the midpoint of the transition during the last glacial period based on the NGRIP $\delta^{18}\text{O}$ -record. YD-PB refers to the Younger Dryas-Preboreal transition.

Interstadial	NGRIP Depth [m]	Age [yr b2k]
YD-PB	1 492.40	11 702
GI-1e	1 604.50	14 688
GI-2.2	1 793.45	23 349
GI-3	1 869.00	27 778
GI-4	1 891.35	28 890
GI-5.1	1 919.55	30 783
GI-5.2	1 951.70	32 501
GI-6	1 974.45	33 734
GI-7c	2 009.55	35 483
GI-8c	2 069.90	38 214
GI-9	2 099.70	40 164
GI-10	2 124.05	41 460
GI-11	2 157.50	43 339
GI-12c	2 221.95	46 842
GI-13c	2 256.60	49 263
GI-14e	2 345.35	54 210
GI-15.1	2 355.20	54 990
GI-15.2	2 366.15	55 785
GI-16.1c	2 398.70	58 035
GI-16.2	2 402.20	58 255
GI-17.1c	2 414.85	59 067
GI-17.2	2 420.35	59 434
GI-18	2 465.80	64 094
GI-19.1	2 507.55	69 614
GI-19.2	2 535.95	72 337
GI-20c	2 579.10	76 436
GI-21.1e	2 687.35	84 762
GI-21.2	2 691.00	85 049
GI-22g	2 746.60	90 044
GI-23.1	2 891.50	104 035
GI-23.2	2 896.40	104 499
GI-24.1c	29 20.60	106 758
GI-24.2	2 938.30	108 289
GI-25c	3 003.30	115 391

The determination of onsets of the abrupt climate events has been addressed in several studies applying different methods. After the initial definition of the events by Johnsen et al. (1992), the

event stratigraphy has been extended with new short-lived oscillations by visually identifying the event onsets in the synchronised $\delta^{18}\text{O}$ -records in combination with Ca^{2+} concentrations from three Greenlandic ice cores (Rasmussen et al. (2014)). Instead of defining the midpoint of the stadial-interstadial transition directly, Buizert et al. (2015) manually determined pre-event and post-event averages to set the start- and the endpoint of the transitions and subsequently defined the time when 50% of the transition was completed by linear interpolation. Another approach is based on an algorithm designed by Erhardt et al. (2019) using a probabilistic model which describes the transition between stadial and interstadial as linear. Fitting a ramp model to the transition in a carefully predefined window, the temporal midpoint and the duration of the transition are used as parameters in the fitting function to define the onset of the DO event (Capron et al. (2021); Myrvoll-Nilsen et al. (2022)). The age of the onsets detected in the NGRIP $\delta^{18}\text{O}$ data in these studies are plotted together with the onsets determined in this work in Figure 4.3, where only this work and Rasmussen et al. (2014) extend beyond GI-18. It has been noticed, that in some cases the age is given in years before present (BP), with 'present' corresponding to the year 1950. The ages have been adjusted to fit the transition ages in years prior to 2000 CE (b2k) and are therefore offset by 50 years from the originally published transition ages.

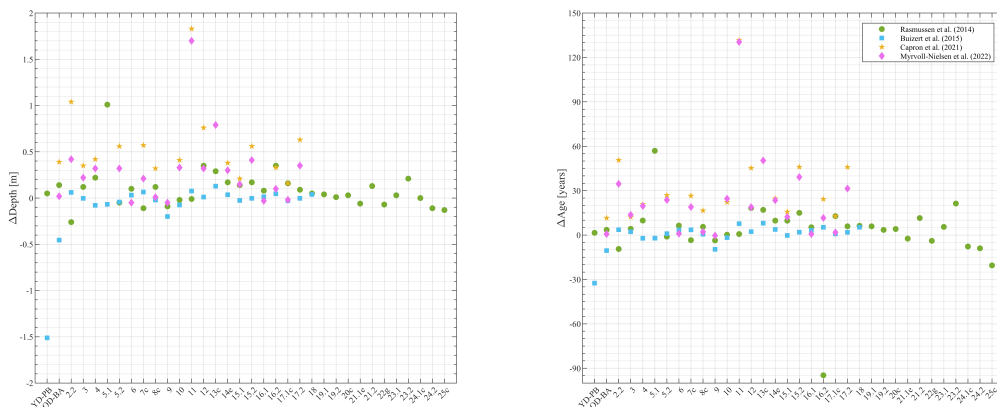


Figure 4.2 | Deviation of determined transitions. Differences in the NGRIP depth [m] (Δ Depth, left panel) and GICC05modelext age [ka b2k] (Δ Age, right panel) of the abrupt climate transitions determined as the midpoint from stadial to interstadial in this work based on the NGRIP $\delta^{18}\text{O}$ [‰] proxy record compared Rasmussen et al. (2014) (green), Buizert et al. (2015) (blue), and the onset as defined in Capron et al. (2021) (yellow), and Myrvoll-Nilsen et al. (2022) (pink).

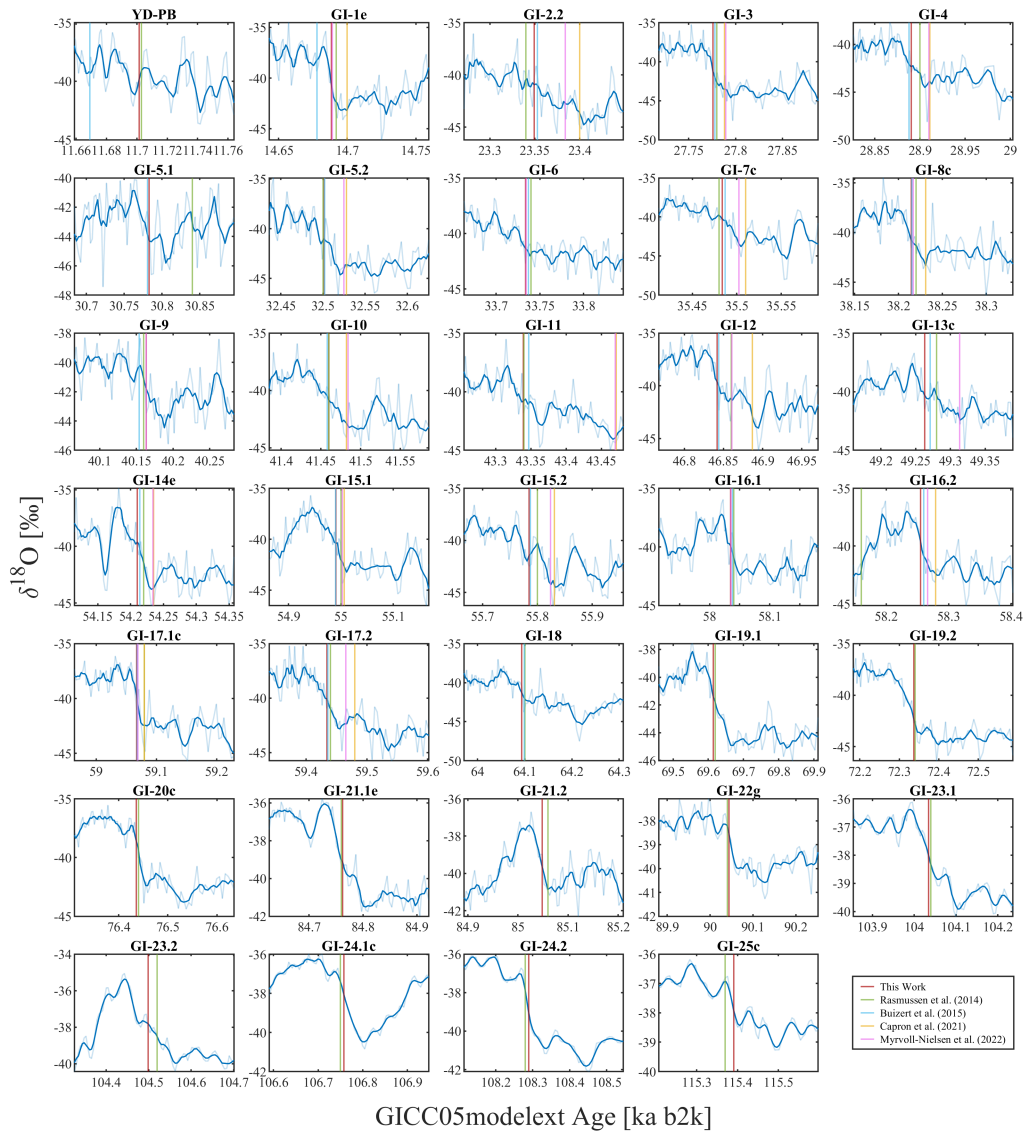


Figure 4.3 | Ages of the abrupt climate transitions. Onset and midpoint ages in ka b2k of the stadial-interstadial transitions for the NGRIP $\delta^{18}\text{O}$ [‰] proxy record determined in this work (red). The results are compared to the midpoint ages presented in Rasmussen et al. (2014) (green) and Buizert et al. (2015) (blue), and the initiation ages from Capron et al. (2021) (yellow), and Myrvoll-Nilsen et al. (2022) (pink).

To compare the approach used in this work to previous studies, the respective depths and ages relative to this work have been calculated and plotted in Figure 4.2 as depth and age differences, respectively. A positive value implies that the onset has been found deeper in the ice core (i.e. at greater age), meaning that the transition is occurring earlier in time in the other studies compared to this work, and vice versa. The onsets determined in this work are in considerable agreement with the onset depths and ages defined by Rasmussen et al. (2014) and Buizert

et al. (2015) showing generally low deviations of maximum 95 years and 32 years, respectively (Rasmussen et al. (2014); Buizert et al. (2015)). With the differences almost equally distributed around zero, the method is not thought to systematically under- or overestimate the midpoints of the transitions. The ramp-fitting approach, on the contrary, systematically ascertains the onsets to occur earlier in time with a maximum of around 130 years for GI-11 in both studies. Despite being in agreement with the midpoint to occur after the initiation of the event, the transitions from stadial to interstadial usually are of shorter duration than 260 years. The different results regarding the timing of the events show the high sensitivity to the method. Visually analysing the isotope signal (Figure 4.3) the onsets determined in this work seem to be a good estimate for the midpoint of an abrupt warming event. Furthermore, averaging all 33 abrupt warming events for the NGRIP isotope record and aligning the profiles at the determined midpoint of the transition ($t = 0$), the isotopic minimum before the stadial termination and the isotopic maximum marking the end of the warming phase, are in approximately equal distance to the determined DO onset (i.e. midpoint of warming transition) in the stacked signal (Figure B.1 in Appendix). This validates the method of defining depth with the steepest $\delta^{18}\text{O}$ gradient as the midpoint of the interstadial-stadial transition. Figure B.1 in the Appendix further shows that the previous statement is valid for the other ice cores as well, as the onset on average corresponds to about the midpoint between a pre-transition $\delta^{18}\text{O}$ minimum and a post-transition $\delta^{18}\text{O}$ maximum in all the four Greenland ice cores.

4.2 Climate Across Dansgaard-Oeschger Events

The Greenland ice cores are internally synchronised and subsequently interhemispherically linked with the Antarctic ice cores using volcanic reference markers to achieve a bipolar climate signal across the Northern Hemisphere abrupt climate events. An overview of the onset depth based on the midpoints defined in the NGRIP isotopic record can be found in Table E.1 in the Appendix as provided by Anders Svensson. Considering the individual warming events the overall associated climate signal is very similar over the course of the last glacial period for all four Greenlandic ice cores showing an abrupt warming and subsequent gradual cooling. The duration of the interstadial and the rate of temperature change, however, varies between events but not significantly between the deep Greenland ice cores. This is due to the drilling sites being located at proximate distance to each other and thus, are characterised by a highly similar climate. Despite the higher elevation, GRIP and GISP2 situated at the summit show higher temperatures as indicated by higher $\delta^{18}\text{O}$ -values compared to NGRIP and NEEM (Figure 4.5), suggesting that the latitudinal effect dominates the lapse rate effect. The latitudinal effect masks the effect of the proximity to the moisture source, which suggests higher $\delta^{18}\text{O}$ values for NGRIP and NEEM being located closer to the coast than the summit drilling sites, GRIP and GISP2 (see Figure 3.1 and Table 3.1). For these more northern ice cores, NGRIP and NEEM, the different influences on the isotopic composition of the ice, elevation, latitude, and distance to moisture source seem to be balanced as indicated by similar temperature proxy values. It has, however, to be kept in mind that the isotopic composition is further influenced by factors such as distance to the moisture source.

In Antarctica, on the contrary, the drilling sites are spread widely across the continent experi-

encing climate impacts from different ocean basins and larger variations in elevation (see Figure 3.1 and Table 3.1). Thus, different isotope compositions of the moisture source, distance from the ocean, and air temperatures impact the individual $\delta^{18}\text{O}$ values. Therefore, the climate signal fluctuates not only slightly between events but also varies between ice cores to a higher degree than in Greenland, making the Antarctic isotope profiles difficult to compare directly. As examples of DO events of different classes, the climate signal across the DO event GI-18, GI-21.1, and GI-21.2 is shown in Figure 4.4. The former represents the second half of the last ice age, and the other the first half. GI-21.1 is further an example of a major DO event initiating from a Heinrich stadial. The climate signal associated with all the remaining events is presented in Figure E.1 in the Appendix.

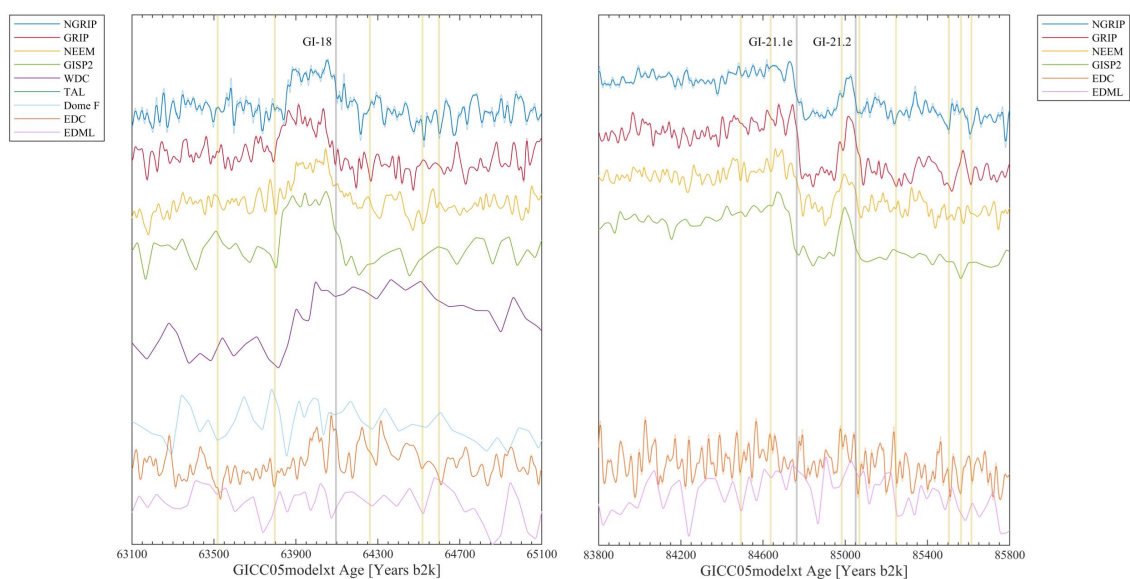


Figure 4.4 | Interhemispherical climate signal across Dansgaard-Oeschger events. Normalised $\delta^{18}\text{O}$ records across the onset of GI-18, and GI-21.1 and GI-21.2 (grey vertical line) for four Greenlandic and four Antarctic ice cores aligned using bipolar volcanic synchronisation. The applied bipolar volcanic matchpoints are marked as yellow vertical lines. The synchronisation across GI-18 is hampered by a lack of volcanic matchpoints during this period, potentially explaining the less precise alignment of the Greenland ice core records.

These climate signals show a generally similar pattern for the four Greenland ice cores with low $\delta^{18}\text{O}$ values indicating the cold stadial and a rapid increase in $\delta^{18}\text{O}$ across the determined DO onset until warm stadial conditions characterised by higher $\delta^{18}\text{O}$ values, as previously well established from Greenland ice cores (e.g. Rasmussen et al. (2014); Landais et al. (2018); Capron et al. (2021)). Contrary to a strong inter-core consistency related to the transition duration and amplitude, the individual ice cores suggest variability in the transition duration and even larger differences in the duration of the entire DO event from one event to the other despite agreeing on the overall pattern. Towards earlier DO events found in the lower part of the ice core, this consistency in the duration pattern is disturbed by flow-induced thinning and potential basal

melt lowering the temporal resolution of the datasets, as each sample contains a longer time period for each average $\delta^{18}\text{O}$ value the thinner the annual layers. This also erases the variability of the climate signal itself and can explain the smoother curves in the GISP2, which has a low temporal resolution, and the NEEM ice core, which has a stronger thinning rate compared to NGRIP (Capron et al. (2021)).

The Antarctic isotope records, on the other hand, do not reveal any uniform pattern across the individual Northern Hemisphere stadial-interstadial transitions. Instead, the signal varies in amplitude, i.e. change in $\delta^{18}\text{O}$ from Greenland stadial to interstadial, timing and a general trend of the isotopic composition, both between ice cores and from event to event. The inter-core heterogeneity observed in both Greenland and Antarctica may be owed to local artefacts, such as different seasonalities, changes in the moisture source origin or transport mechanisms, and atmospheric or/and oceanic mesoscale dynamics (Charles et al. (1994); Guillevic et al. (2012)). The event-to-event differences, however, point towards different processes underlying the individual abrupt climate changes. Alternatively, and supporting the common hypothesis of DO events originating from a unique trigger, the underlying mechanisms potentially are expressed differently due to internal climate variability controlling the propagation of the climate signal or perturbation both on a regional and hemispherical scale (Erhardt et al. (2019)).

Under the assumption, that the events and the triggering mechanisms are considerably similar, the $\delta^{18}\text{O}$ profiles across the individual DO events are stacked for the different ice cores in order to investigate a more general climate behaviour of Antarctica in response to Northern Hemisphere abrupt warming. As seen from the stacked isotope records in Figure 4.5, the Antarctic profiles from WDC, Dome F, Talos Dome, and EDC show initial warming synchronous with Greenland DO events followed by a gradual cooling while the Northern Hemisphere temperatures stay elevated as suggested by the bipolar seesaw theory. The variations in the Antarctic isotope composition during the AIM are hereby in the order of one magnitude lower than experienced in Greenland when transitioning from stadial to interstadial. While the synchronous, sharp warming is distinctly presented in all four of the mentioned Antarctic ice cores, the gradual cooling is most clearly pronounced in the WDC stack, whereas the signal is more difficult to distinguish from noise in the isotope records from Talos Dome, Dome F and EDC. Nevertheless, a general decrease in $\delta^{18}\text{O}$ is detectable after a certain lag time. Different from the East Antarctic ice cores (Dome F, Talos Dome, and EDC), as well as WDC, EDML is cooling across the transition associated with DO events, continuing the same general trend afterwards.

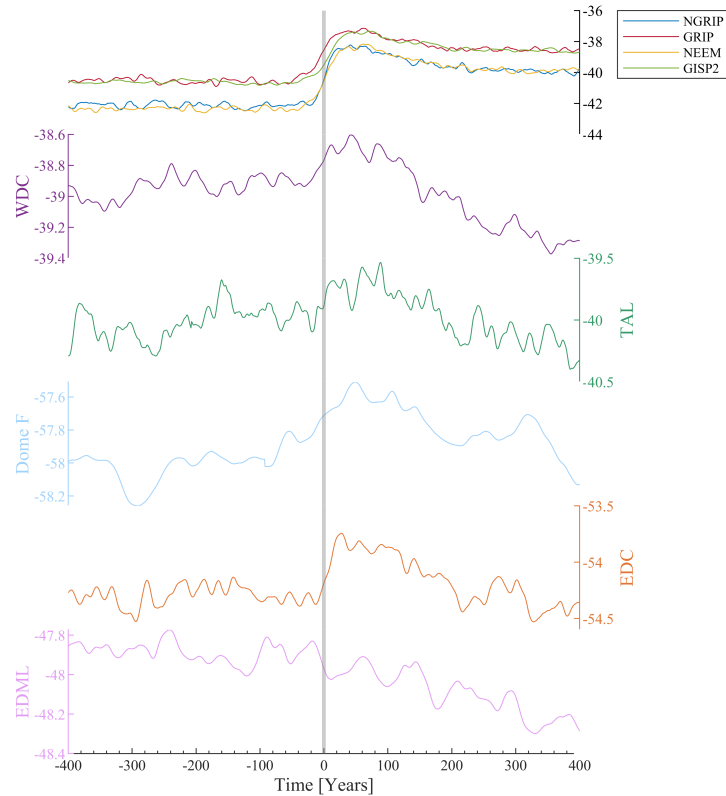


Figure 4.5 | Average interhemispherical climate signal across Greenland abrupt warming transitions. Stacked $\delta^{18}\text{O}$ [‰] signals from the Greenlandic NGRIP, GRIP, GISP2, and NEEM ice cores (upper panel) and the Antarctic Wais Divide (WDC), Talos Dome (TAL), Dome F, Epica Dome C (EDC) and Epica Dronning Maude Land (EDML) ice cores around the transition from stadial to interstadial conditions as marked by $t = 0$ years. Years < 0 represent the time before the DO event and years > 0 the period after the warming transition. The timescale is thereby reversed with respect to Figure 4.4.

4.3 Bipolar Phasing

With the precise volcanic synchronisation, the coupling between DOs and AIM can be analysed and the Antarctic response time with respect to Northern Hemisphere abrupt warming quantified. The initial bipolar seesaw hypothesis predicts an anti-phase behaviour between the Northern and the Southern Hemisphere (Stocker and Johnsen (2003)). The ice core synchronisation, however, suggests an in-phase relationship characterised by a time lag between Antarctica and Greenland (Section 4.2 and Blunier et al. (1998); WAIS Divide Project WAIS Divide Project Members (2015); Svensson et al. (2020)). Holding onto the bipolar seesaw theory, the time lag can be explained by adding a heat reservoir to the system, typically the interior of the Southern Ocean, delaying the Antarctic cooling after the Northern Hemisphere temperature increase. Averaging the shared climate signals from the five Antarctic ice cores, the Antarctic temperature decrease after reaching an isotopic maximum has been found to lag the Greenland abrupt

warming by 57 ± 40 years on average (Figure 4.6). This is about 150 years faster than determined based on methane synchronisation (WAIS Divide Project WAIS Divide Project Members (2015)). Svensson et al. (2020) argue for an underestimation of Δ age between the enclosed gas and the surrounding ice leading to imprecise interhemispherical matching, which potentially results in overestimating the Southern Hemisphere response time. Applying volcanic synchronisation, a delay of 122 ± 24 years of the onset of Antarctic cooling relative to Greenland warming has been proposed (Svensson et al. (2020)). While foreshortening the time lag compared to gas matching it is still about twice as long as estimated in this work. Both estimates are based on the same fitting routine (WAIS Divide Project WAIS Divide Project Members (2015); Svensson et al. (2020)) whereas the breakpoint in the Antarctic stacked isotope records marking the initiation of the cooling after Northern Hemisphere warming in this work has been defined by a simple maximum determination. Further, while the previous studies only address the more recent half of the last glacial consisting of the events up to and including GI-17.2, this work covers the entire glacial with the exception of GI-25. The bipolar phasing of the first half only (prior 65 ka b2k) is more difficult to define precisely compared to the second half post 65 ka b2k, perhaps due to a weaker mean comprised of fewer events. First of all, only one third of the analysed DO events occur during the earlier period, where the isotope data from WDC and Talos Dome do not expand past GI-18 (~ 65 ka b2k), and Dome F only contributes with two events to the Antarctic mean of the first half. The climate signal at Dome F as well as EDC further are highly variable with generally small-scale temperature fluctuations (Figure 4.4 and 4.6) but without any distinct cooling trend after the breakpoint. Thus, the three-core mean of in total only 22 events is dominated by the EDML isotope record during the cooling period past the breakpoint. Furthermore, decreasing temporal resolution due to annual layer thinning disguises the isotope profile and hampers the exact phasing determination. Given by the post-transition isotopic maximum (i.e. breakpoint) in the stack, the switch from warming to cooling in the course of the AIM has been determined in this work to occur on average 62 ± 57 years after the onset of the DO events in the first half of the last ice age (Figure 4.6). Despite the response time attributed to the first half being in overall agreement with the response time of the whole last glacial, the estimate has to be taken with caution. The breakpoint determination is sensitive to smoothing of the signals and outliers in the individual $\delta^{18}\text{O}$ -record. For instance, since the result is based on the normalised stack the large fluctuations in the EDML and Dome F records damp the profile of the mean. Excluding these two signals from the mean, the response time can be prolonged to 88 ± 62 years (Figure F.4) for the entire last glacial period. However, it can be ventured that the Antarctic response time is consistently shorter during the last ice age than suggested by methane synchronisation and the increased abruptness of the shifting climate indicates an improvement in the bipolar synchronisation when using volcanic reference sequences rather than well-mixed atmospheric gases.

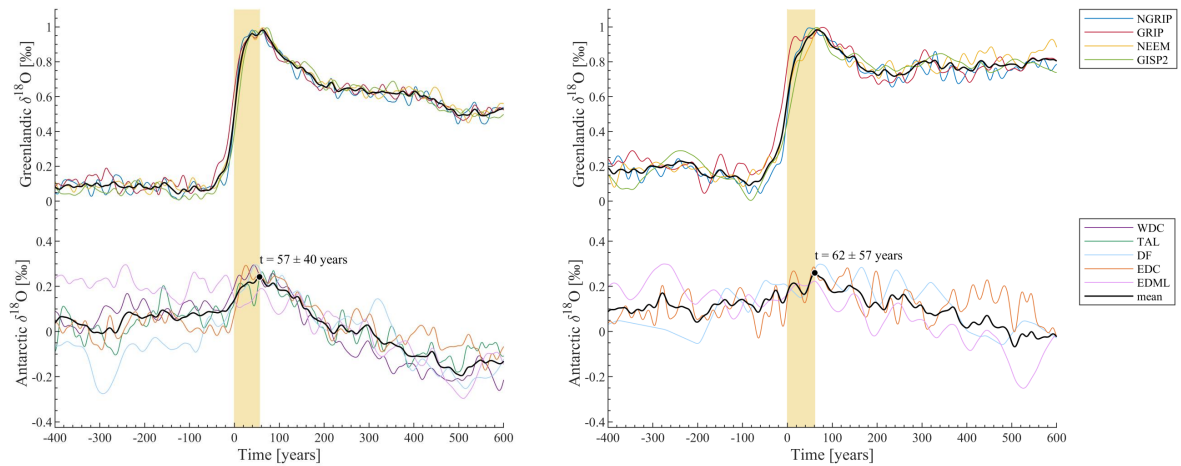


Figure 4.6 | Bipolar phasing during the entire last glacial and its early half. Normalised stacks of the isotopic records across the Greenland interstadials YD-PB until GI-24.2 (left panel), and GI-19 to GI-24.2 (right panel), with $t = 0$ marking the onset determined in the NGRIP $\delta^{18}\text{O}$ profile as listed in Table 4.1. The breakpoint, defined as the maximum in the Antarctic multi-core mean at $t = 57 \pm 40$ years and $t = 63 \pm 57$ years marks the temporal delay of the Antarctic cooling relative to Northern Hemisphere abrupt warming for the whole glacial period and its first half, respectively. See Section 3.4 for normalisation and stacking procedure, as well as the determination of the bipolar phasing. The number of events stacked for the period of the entire glacial and the first half, respectively, can be seen in Table 3.2. Note that the Antarctic stacks of EDML and Dome F are offset for better visualisation. Further, note that the poor alignment of the GRIP ice core compared to the remaining is probably not caused by a climate artefact but rather due to a lack of volcanic matchpoints complicating the precise synchronisation.

4.4 Towards an Understanding of the Mechanisms Behind Dansgaard-Oeschger Events

In order to investigate the physical mechanisms behind the abrupt climatic changes the events are classified by size and time of occurrence (see Table 3.2) and the groups studied individually for each ice core as well as averaged for Greenland and Antarctica respectively to determine the bipolar phasing. Figure 4.7 compares the averaged climate signal of Greenland and Antarctica between the first and the second half, and between major and minor events, respectively. In addition, the bipolar phasing has been computed for a model output simulating DO events under different levels of CO_2 concentrations to examine the potential of the model to explain possible processes of abrupt climate change and the ability to project comparable changes in the future.

4.4.1 Comparing Classes of DO Events

The first half of the last ice age is characterised by higher $\delta^{18}\text{O}$ -values across DO events in both the Greenlandic and Antarctic ice core records compared to the more recent 50k years. This is very likely an imprint of the preceding interglacial and thus attributable to generally higher global temperatures during this period and lower elevations of the ice sheets as a result of ice-sheet hysteresis. Regional variations in $\delta^{18}\text{O}$ therefore might be related to a changing shape of the ice sheets. The Greenland ice sheet, for instance, reached its maximum extent at the Last Glacial Maximum around 21 ka b2k with a global ice sheet volume equivalent to 110 to 130 m sea level compared to 60 to 90 m sea-level equivalent during the early time of the last glacial (Onac et al. (2012)). The Dome F ice core has the only record with lower $\delta^{18}\text{O}$ -values during the early half compared to the period of 10-65 ka b2k, potentially suggesting lower temperatures during the early half of the last glacial. However, it has to be kept in mind that the stacked record representing the early 55 ka years comprises of solely two single events, namely GI-19.1 and GI-19.2, occurring right at the temporal boundary to what has been defined as the second half (~ 65 ka b2k), where global temperatures have distinctly decreased. Therefore, the two events might not be truly representative of the first half and differences in the isotope profiles between the first and the second half cannot be confidently connected to local geography or climate variations at the Dome F drilling site.

Early Greenland interstadials are on average longer than those occurring during the more recent half. Higher temperatures over the North Atlantic potentially prolong the termination of the AMOC extending the time the system spends in the warmer state (Vettoretti et al. (2022)). Further, higher early-glacial air temperatures are closely coupled to an increased atmospheric CO_2 concentration, which in return modulates the DO oscillations. Observed in a modelling study (Section 3.2), the CO_2 levels have shown to control the duration of stadial and interstadial by impacting the ocean heat content and mean sea ice volume in the North Atlantic and Arctic Ocean (Vettoretti et al. (2022)). Higher CO_2 levels in the first half of the last glacial in comparison with the second half resulted in warmer waters of the North Atlantic and Arctic Ocean to a higher degree than in other parts of the global ocean due to important climate feedbacks and consequently a reduced mean sea-ice volume. Cooling after the transitions from stadial to interstadial conditions is, on the contrary, of shorter duration than during the more recent period. This is supported by the climate model simulating longer interstadials under elevated CO_2 levels relative to the ensemble mean. A weak AMOC state, in return, reduces the northward transport of warm, saline waters and leads to a saltwater build-up in the low-latitude Atlantic. Under high CO_2 concentrations, this saltwater pool has the potential to re-invigorate the AMOC and consequently, foreshorten the stadial period (Vettoretti et al. (2022)). The reduced time spent in the stadial in addition to higher background temperatures in the first half compared to the second half might explain the smaller absolute change in $\delta^{18}\text{O}$ across the abrupt warming event as seen in all the nine ice core records from Greenland and Antarctica (Figure 4.8).

A similar behaviour as seen contrasting the two periods of the last glacial can be observed when comparing minor events to those arising from a Heinrich stadial (referred to as major events). Here, the average $\delta^{18}\text{O}$ anomaly of the stadial is less pronounced than it might have been expected from exceptional cold Heinrich stadials. It has to be noticed, however, that

4. Results and Discussion

Heinrich events occurring during the warmer younger ice age are taken into account, potentially lowering the average. The average $\delta^{18}\text{O}$ variation across the abrupt warming transition is more distinct during major events leading to warmer Greenland interstadials than associated with minor events. A complete shutoff of the AMOC prevents any ocean surface heat transport in the Atlantic from low to high latitudes. Extensive energy accumulation in the ocean interior and massive iceberg discharge being a source of freshwater could have triggered dramatic changes in the overturning circulation leading to enhanced warming during Heinrich stadials.

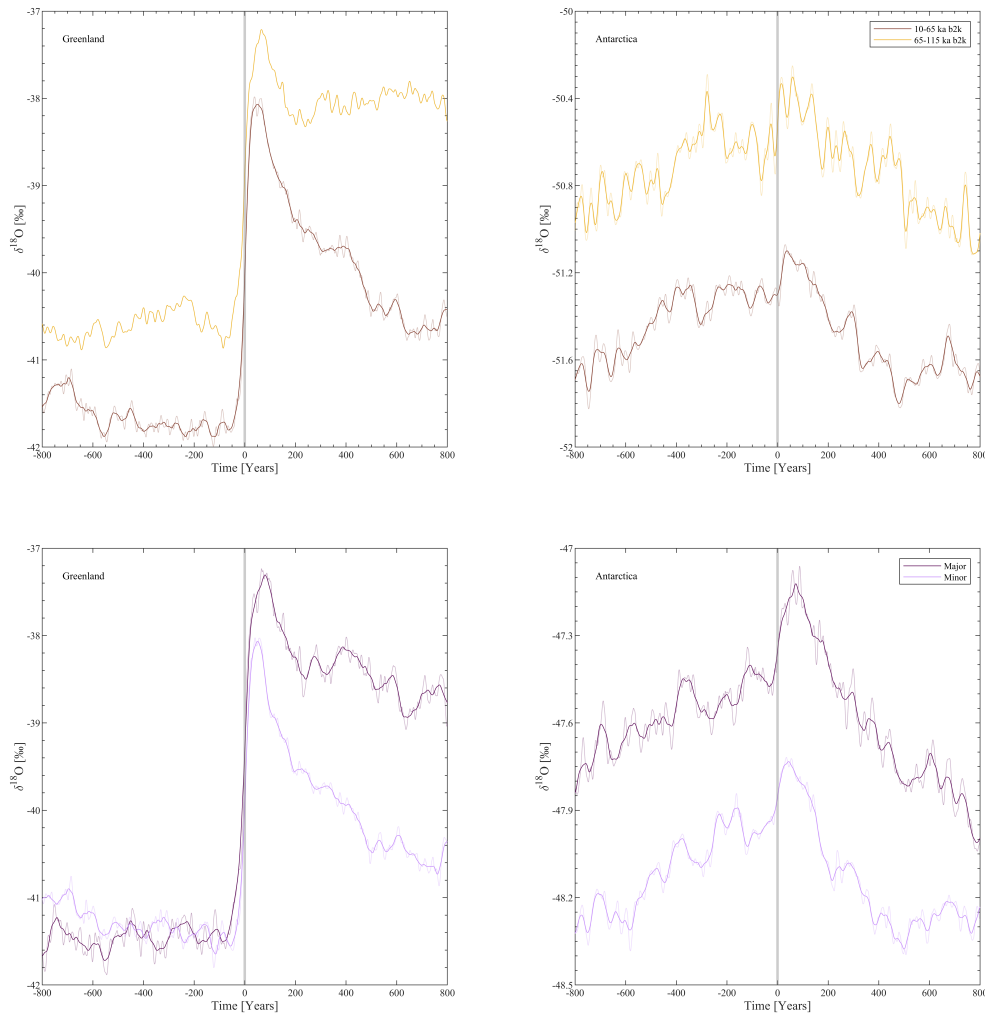


Figure 4.7 | Stadal-Interstadial transitions for different classes of DO events. Stacked $\delta^{18}\text{O}$ records of different groups of events for the Greenlandic and Antarctic ice cores, respectively. The upper panel compares transitions occurring during the first half of the last glacial (65-115 ka b2k) and the second half (10-65 ka b2k). Due to a lack of data for WDC, Talos Dome, and Dome F only the data from EDC and EDML are included in the stacked signal of the early ice age. The right panel shows the events grouped by size, where major events correspond to DOs with preceding Heinrich stadial and minor events classify the remaining events. See Table 3.2 for the respective events comprising the different classifications.

A generally elevated $\delta^{18}\text{O}$ level during major DO events can likewise be observed in the Antarctic

isotope signal. This might be attributed to the complete shut-off of the AMOC during Heinrich events trapping thermal energy in the Southern Hemisphere and consequently increasing atmospheric temperatures around Antarctica. Similar to a warmer North Atlantic prolonging Greenland interstadials, the enhanced heat reservoir in the Southern Ocean potentially explains the increased delay of Southern Hemisphere cooling relative to Northern Hemisphere abrupt warming, which has been found to 88 ± 51 years for major DO events. By contrast, the bipolar phasing associated with the remaining smaller events as well as the first and the second half is about equal to the average bipolar phasing determined for all events during the entire Last Glacial Period. Namely, the Antarctic response time related to minor events has been determined to be 55 ± 53 years. As this classification comprises the majority of the total averaged events, their signal dominates the mean of the entire last glacial and a similar time delay satisfies expectations.

The same applies to the more recent half (10-65 ka b2k), which includes two-thirds of the total number of analysed events, showing an Antarctic climatic lag of 56 ± 38 years (Figure F.1 in the Appendix). Despite comprising distinct ensembles of events, the ice core records averaged for the four different classifications (first and second half; minor and major DO events) show the same pattern for Greenland and Antarctica, respectively. The Antarctic isotope signal sharply increases synchronously with Greenland abrupt warming until reaching a maximum from where the $\delta^{18}\text{O}$ -value follows a decreasing trend (Figure 4.7). Here, the profiles only differ in the amplitude of the transition (Figure 4.8), and average duration of the respective stadials and interstadials (Figure G.4 in the Appendix). The only exception is found in the EDML record. While the $\delta^{18}\text{O}$ -value decreases across the onset of the DO events during the later half of the glacial it is increasing in the early half equal to the general Antarctic isotope behaviour (Figure 4.8). An increase in EDML $\delta^{18}\text{O}$ across the transition is also experienced during minor events. Directly at the transition, the trend is negative but the signal highly fluctuates (Figure G.4). This results in a smaller positive change within 50 years after the onset (Figure 4.8). It has to be kept in mind that the temporal resolution of the EDML isotope data is almost 50 years on average during the first half of the last ice age (Figure A.1). The accurate behaviour across the transition of about the same duration might therefore be lost in the sample resolution and/or noise of the record. Striking is, however, that the EDML record generally shows a maximum occurring before the transition (Figure 4.5) resulting in an overall negative trend on longer timescales compared to the remaining Antarctic signals (Figure 4.8). An explanation for the contrary behaviour of EDML compared to the other Antarctic ice cores has not been provided yet, but is potentially related to local artefacts. The atmospheric setting around Antarctica is dominated by strong westerlies driving the Antarctic Circumpolar Current (ACC). Surface waves, such as Kelvin waves, travelling along topographic boundaries and other waveguides as the equator and the ACC, and are therefore not able to propagate into the Southern Ocean (Kusahara and Ohshima (2014)). Thus, the climate signal is transported across the ACC predominantly by slow Rossby waves in the interior of the ocean (Taylor et al. (2018); Pedro et al. (2018)). The fast ACC meanwhile guides the warm climate signal clockwise (as seen from the South Pole) around Antarctica and thereby away from the EDML drilling site and the nearby sea ice cover. While the warm signal interacts with the sea ice close to the WDC drilling site, potentially resulting in higher temperatures during Northern Hemisphere stadial-interstadial transitions, the sea ice

cover close to EDML, in the near term, might be unaffected by warmer climates transported to the Southern Hemisphere, keeping down local atmospheric temperatures. With a higher sea level in the early glacial a different sea ice extent and consequently a different climate response cannot be ruled out (Buizert et al. (2018); Lefebvre et al. (2004)).

This hypothesis does not capture all the details of the transitions nor explain the similar climate behaviour mirrored in remaining East Antarctica ice cores compared to WDC. Nevertheless, it emphasises the complexity of the climate system being shaped by external components. Further, it supports the theory that the short-term warming response occurring approximately synchronous to Northern Hemisphere temperature increases is attributed to the atmospheric circulation such as shifts in the Southern Westerlies in reaction to the movement of the ITCZ during climate changes, while long-term responses in the order of multiple decades are related to ocean circulation (WAIS Divide Project WAIS Divide Project Members (2015)).

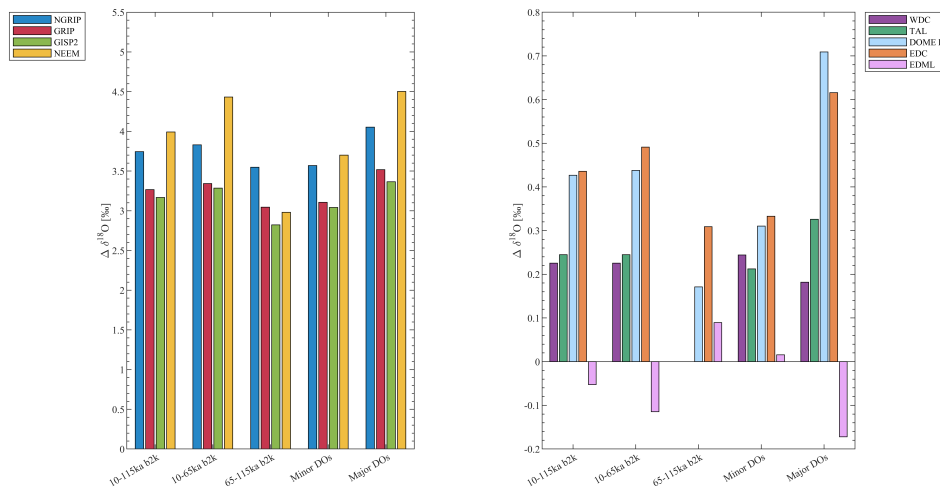


Figure 4.8 | Variation in $\delta^{18}\text{O}$ across DO transitions. Average change in $\delta^{18}\text{O}$ for the individual Greenlandic (left panel) and Antarctic ice cores (right panel) across the stadial-interstadial transition associated with Northern Hemisphere abrupt warming. The associated events are grouped in different classes according to their time of occurrence and size as can be seen in Table 3.2. Note the different order of magnitude of Antarctica compared to Greenland.

4.4.2 Modelling Abrupt Climate Change

In order to gain a better understanding of the mechanisms behind the abrupt climate changes the determined Antarctic response time based on the ice core records can be compared to the output of the comprehensive climate model simulating the climate of the last glacial period for distinct atmospheric CO_2 concentrations introduced in Section 3.2.

According to the WDC CO_2 record (Bauska et al. (2021)), the mean atmospheric CO_2 concentration during the more recent half of the last ice age (10-65 ka b2k) was approximately 210 ppm, disregarding the abrupt CO_2 increase at around 17 ka b2k (Figure H.1 in Appendix). For this intermediate CO_2 concentration of 210 ppm, the Antarctic response time relative to Greenland abrupt warming has been determined to be about $t = 110$ years applying the same approach as

for the isotope data as described in Section 3.4 (Figure 4.9).

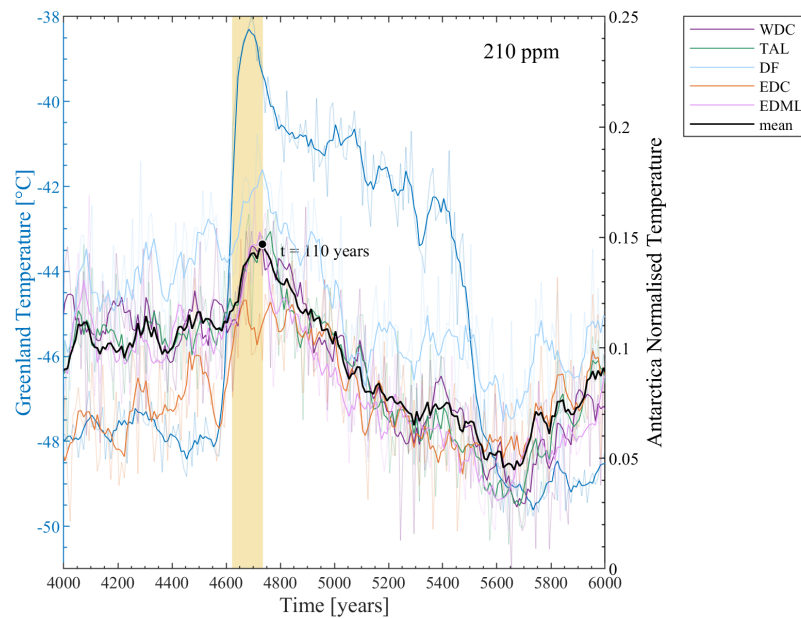


Figure 4.9 | Bipolar phasing during a background CO_2 concentration of 210 ppm. Mean Greenland and Antarctic temperature profiles from a CCSM4 model simulation (Vettoretti et al. (2022)) showing the Antarctic response time relative to Greenland abrupt warming to be $t = 110$ years for a single DO event. The signal from Antarctica is normalised with respect to its extreme values and scaled for better visualisation and are not representative for the actual simulated temperature.

This estimate corresponds to only one single event. The individual simulated events are however coherent under equal CO_2 forcing as can be seen in Figure 3.2. Decreasing the CO_2 concentration to 200 ppm, the Antarctic response time is reduced to $t = 70$ years. This estimated timescale is thereby in strong agreement with the determined average bipolar phasing during the Last Glacial Period and with regards to different classifications of DO events. This might lead to the anticipation that the response time tends to decrease with decreasing CO_2 level. This prediction is supported by the Antarctic response time determined in the isotope signal to be higher during the period of 65 ka to 115 ka b2k, where the average background CO_2 levels were elevated compared to the more recent half. However, the high uncertainties regarding this estimate have to be kept in mind. Nevertheless, this expectation is refuted by the model simulations, showing no clear trend between the different runs. Except for the response time related to 210 ppm, the general response time is almost consistent between simulations with different background CO_2 concentrations, varying between $t = 110$ and $t = 130$ years (Figure H.4). Thereby, this time lag overall lies within the uncertainty ranges of the response time determined from ice core data. Further, the model captures the characteristic pattern with a fast warming response synchronous with Greenland warming and the delayed long-term cooling trend after reaching a maximum. Even though the similarity to the data does not prove that the model is a correct representation of the past, this leads to the assumption that the model potentially captures the

overall underlying physical processes triggering DO events.

Describing the main features of an ocean circulation driven by a meridional density gradient, the model simulates the fluctuations in the strength of the AMOC during DO oscillations. The stadials are associated with a sea ice expansion and a weak AMOC resulting in subsurface temperature and salinity increases favouring vertical stratification and transporting freshwater northward out of the North Atlantic into the Arctic Ocean. While the sea ice extent may reach a maximum as it approaches the sea ice maximum latitude, the ocean interior continues to accumulate thermal heat as a consequence of constant solar radiation warming the water at low latitudes. In the Southern Hemisphere, the Antarctic Bottom Water (AABW) formation weakens and water temperatures rise, leading to a thinning of the Southern Ocean sea ice cover. This allows more heat to escape from the surface ocean consequently increasing atmospheric temperatures around Antarctica while Northern Hemisphere temperatures are low, which is partly modulated by a strong sea-ice-albedo feedback. While the Arctic Ocean freshens, salt convergence increases in the North Atlantic. With a strongly positive salt-advection feedback, the AMOC and consequent North Atlantic Deep Water (NADW) formation fluctuations are amplified. Satisfying conservation laws, the NADW volume needs to increase when AABW production is reduced. The destabilisation tendency of a positive salt-advection feedback causes thermohaline instability of the vertical stratification breaking the protective cold and fresh boundary layer between the sea ice and the warm interior. With rapid sea ice loss in the North Atlantic, Greenland warms abruptly as the accumulated heat rapidly escapes to the atmosphere. As shown by accurate bipolar volcanic synchronisation, Antarctica reacts simultaneously to Northern Hemisphere warming with a rapid temperature increase. This raises the question whether the same process as in the North Atlantic could happen in the Southern Ocean at the same time as the stadial termination. With the ocean around Antarctica warming and the sea ice thinning, an abrupt release of thermal energy seems conceivable. The excessive heat loss and old sea ice transported from the Arctic Ocean favour sea ice growth gradually cooling Greenland and Antarctica as the meridional density gradient weakens and AABW reactivates (Vettoretti et al. (2022)). The hypothesis considering atmospheric changes to abruptly alter the Antarctic climate can still be valid. Shifting southern westerlies following the ITCZ northward as a consequence of a decreasing temperature gradient between northern high latitudes and the equator when Greenland warms, potentially accompanies or even amplifies the effect of rapid sea ice loss. In fact, the temperature profiles provided by the model express two different slopes, both indicating a temperature increase. During cold Northern Hemisphere stadials, the Antarctic temperature increases steadily but comparatively slowly, as suggested by the bipolar seesaw theory. This presumably oceanic response is hereby related to the ocean's large heat capacity and/or eddy diffusion velocity. Synchronously with Greenland abrupt warming, the Antarctic temperature gradient steepens indicating a fast meridional transport through the atmosphere. These features are, however, not clearly resolved in the ice core data but potentially are masked by internal climate artefacts such as atmospheric turbulence and storms in the Southern Ocean perturbing the signal.

Climate models can help to understand the physical processes behind climate observations. In

return, comparisons to (palaeo)climate data help to evaluate the model. This is a crucial process in order to make accurate climate change predictions. The global climate model, comprehensively describing air-sea-ice interactions, is able to simulate the DO oscillations including short- and long-term Antarctic responses to Northern Hemisphere abrupt warming. It however fails to completely capture the abruptness seen in the Antarctic ice core data, and the climate characteristics of the individual DO events and drilling sites. For instance, the contrary behaviour of EDML is not expressed by the model, indicating that the behaviour is due to very local anomalies which get lost in the coarse grid resolution or that the underlying mechanisms are not fully described by the physical processes driving the climate system in the model. Precisely simulating DO events is especially important when these models are used to address future abrupt changes and potential tipping points in the climate system.

4.4.3 Major Volcanic Eruptions as Potential Trigger of DO Events

The CCSM4 model suggests the ocean oscillatory mechanisms to arise from stochastic elements associated with internal climate variability (Vettoretti et al. (2022)) supported by a statistical analysis of tipping point behaviour (Ditlevsen et al. (2007)). This might be long-term variations in solar or volcanic forcing (Solanki (2002); Abbott et al. (2021); Lohmann and Svensson (2022)). The irregularity of DO events does not coincide with any solar cycle. However, a cooperative process between periodic solar forcing and noise has been shown to produce climate oscillations in agreement with DO events (Braun et al. (2008)). Similar studies could not provide convincing evidence for this causality (Muscheler and Beer (2006)), and the coherence remains uncertain. A potential volcanic influence has been analysed by examining the number of bipolar volcanoes occurring within a few decades prior to the interstadial initiation by Lohmann and Svensson (2022).

In this work, the DO events have been dated by the midpoint of the stadial-interstadial transition. Based on the NGRIP $\delta^{18}\text{O}$ record the initiation occurs on average 25 years prior to the midpoint (Figure 4.1). To allow for shorter transitions (Kindler et al. (2014)) and uncertainties on the midpoint determination, potential impacting volcanic eruptions have been said to occur between 15 and 65 years prior to the transition midpoint. This way, the record of seven volcanoes potentially triggering DO events during the first half of the last ice age (Lohmann and Svensson (2022)) could be extended to ten bipolar volcanoes. The eruptions are related to GI-1e, GI-3, GI-4, GI-8, GI-9, GI-13, GI-19.1, GI-19.2, and GI-21.2 (Figure 4.10). The inconsistency of this previous study compared to this work arises from different definitions of the DO onset.

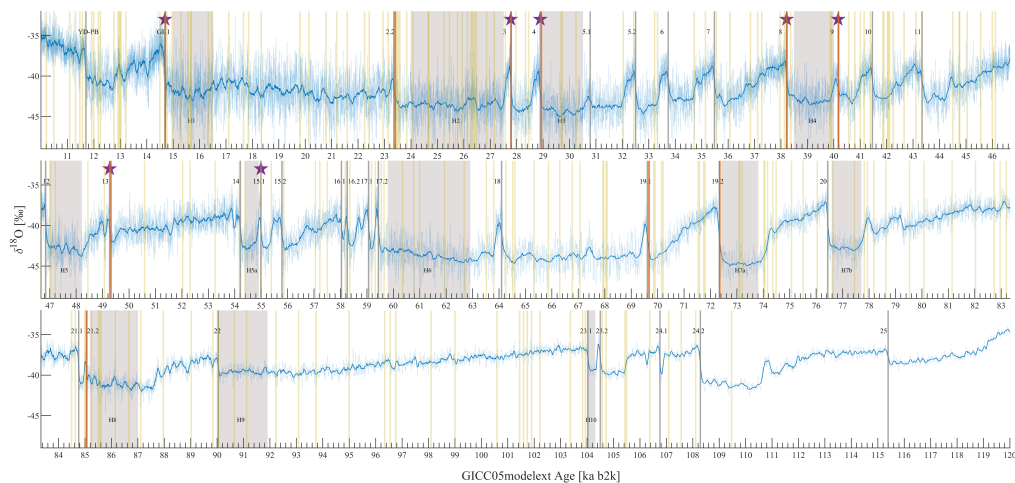


Figure 4.10 | Bipolar volcanic eruptions during the Last Glacial Period. NGRIP isotope record with large volcanic eruptions detected in at least one ice core from both the Northern and the Southern Hemisphere (yellow vertical lines). Red vertical lines mark volcanic eruptions occurring between 15 and 65 years prior to the transition midpoint. Stars indicate the seven interstadials for which the onset occurs within 50 years after a bipolar volcanic eruption according to Lohmann and Svensson (2022).

Bipolar volcanoes are chosen as they are assumed to be large enough to act as short-term triggers for climate variability. Counterintuitively, large volcanic eruptions, usually responsible for local or even global temperature decrease, here, are associated with Greenland abrupt warming. This is based on the hypothesis, that volcanic aerosol-induced cooling of the ocean leads to an intensification of the AMOC as the water density increases. It is speculated that this direct cooling influence on the AMOC tips the system from stadial to interstadial conditions if the AMOC is close to the threshold as large eruptions only occur occasionally imminent to some transitions, but are statistically unrelated to interstadial terminations (Lohmann and Svensson (2022)). However, a causal relationship between large-scale volcanic eruptions and abrupt Northern Hemisphere warming cannot be supported without any statistical analysis.

The distribution of these ten volcanoes does not indicate a certain pattern or trend, nor any correlation to amplitude and duration of the respective DO events. However, the lack of major volcanic eruptions occurring shortly before the majority of the DO events does not eliminate the possibility for them to initiate abrupt climate changes. It rather supports the thesis that the physical mechanisms behind DO events differ between events, or alternatively, that the same underlying mechanism is triggered by different processes in the climate system. Different from larger events with long interstadials and stadials in between, precursor events, as for instance GI-21.2 and GI-23.2, occurring shortly before another DO event, may not be solely explained by the bipolar seesaw theory since the observed timescales disagree with those related to long-term ocean mechanisms. Here, extensive volcanic cooling could potentially anticipate the process. Other phenomena as large-scale ocean turbulence initiated by earthquakes and ensuing tsunamis are not necessarily visible in ice core data but cannot be completely neglected in the discussion

about possible triggers of Northern Hemisphere abrupt warming.

4.5 Potential for Future Abrupt Climate Change

Dansgaard-Oeschger events are evidence of the capability of elements in the climate system to change rapidly and trigger dramatic local abrupt changes with global consequences. A change is defined as abrupt when the climate system is transitioning into a different state on a timescale shorter than the responsible forcing (National Research Council (2002)). Anthropogenic greenhouse gas forcing has drastically altered the climate system over the past decades increasing the global mean temperature. Due to crucial climate feedbacks the Arctic is exceptionally vulnerable to warmer temperatures. This phenomenon of Arctic amplification has led to a temperature increase of 4°C in the past 40 years (Jansen et al. (2020)). According to past temperature reconstructions based on ice core isotope data, the temperature at NGRIP likewise changed by >1°C per decade on average over the course of stadial-interstadial transitions (Kindler et al. (2014)). This arises the concern that abrupt changes similar to DO events could happen in the future if temperature increases are not sufficiently mitigated. It is, however, important to note that the $\delta^{18}\text{O}$ profile, extracted from ice cores, mirrors the temperature over the interior of the Greenland Ice Sheet, whereas the temperature rise under modern climate change addressed in simulations is most pronounced in the Central Arctic and over the Arctic Ocean (Jansen et al. (2020)). The temperature anomaly in this area is therefore expected to be considerably higher during the last ice age. This is also caused by generally higher sea ice extent and consequently stronger feedback effects. However, warming projections under the high-end, unmitigated emissions scenario (RCP 8.5) meet the amplitude as seen in palaeoclimatic reconstructions (Hoff et al. (2016)).

Further, the analysis and reconstruction of DO events have shown that the key element of the oscillations is very likely the fast sea ice retreat during sudden changes in the overturning circulation. Linking tephra layers in ice to sediment cores, the sea ice diminution has been shown to precede the initiation of DO event supporting this thesis (Sadatzki et al. (2019)). Over the last ~ 40 years, the monthly September sea ice extent has decreased by about 12% per decade relative to the average of this period in the same area experiencing a warming rate of 1°C per decade (Fetterer et al. (2017)), emphasising the interplay between high-amplitude warming and large-scale sea ice retreat. With ocean warming, a stable vertical stratification is essential in order to maintain a sea ice cover. Higher temperatures increase evaporation and the atmospheric water-holding capacity, in return enhancing the hydrological cycle. As a consequence, more precipitation in combination with amplified seasonal sea ice melt increases the freshwater influx, preventing salinification of the surface ocean and separating the sea ice from the warm ocean interior. As the stratification of the Arctic Ocean is predominantly controlled by salinity (Timmermans and Marshall (2020)), the stratification of the upper and intermediate ocean is predicted to be retained under current climate change scenarios for at least the next century. This is supported by global climate model simulations to not initiate deep ocean convection in the Arctic Ocean under future warming scenarios with only a few exceptions (e.g. Behrens et al. (2016)). However, Arctic Ocean stratification is often poorly represented in global models and a possible instability might not be captured properly (Ilıcak et al. (2016)), in addition

to model simulations of sea ice decline often being too conservative (Vihma (2014)). Further, it is alarming that modern Atlantification of the Arctic Ocean similar to what is believed to initiate DO events has been observed to a larger extent over the past decades. Here, the meridional heat transport in the Northern Barents Sea and Fram Strait has dramatically increased, resulting in a large-scale sea ice retreat (Lind et al. (2018); Årthun et al. (2019)). The sea ice loss is further amplified by strengthened greenhouse gas-induced radiative forcing. Accompanied by the heat increase, the salinity in this region has increased due to the intrusion of Atlantic waters edging the meltwater from sea ice further into the Arctic Ocean (Jansen et al. (2020)). This describes the same mechanism triggering the abrupt warming in the model simulating DO events by freshening the Arctic Ocean and destabilising the strong vertical stratification (Vettoretti et al. (2022)). Even though the surface waters might have been warmer during DO cycles (Sessford et al. (2018); Sessford et al. (2019)) and consequently the stratification more sensitive to instability than the modern Arctic Ocean it cannot be ruled out that future warming could trigger warm-water convection, which finally can result in dramatic sea ice loss compared to the initiation of DO events. Most models tend, however, to underestimate the abruptness of climate changes both under glacial and pre-industrial boundary conditions, even though the tipping point seems not to be reached yet (Jensen et al. (2016); Sessford et al. (2019)). Nevertheless, crossing the threshold becomes more likely in high-concentration pathways (Jansen et al. (2020)) emphasising the acuteness of reducing fossil fuel emissions and mitigating climate change.

5. Conclusion and Outlook

Using provided bipolar volcanic synchronisation the phasing between Antarctica and Greenland across DO variability during the Last Glacial Period has been studied. Based on $\delta^{18}\text{O}$ ice core data, the average Antarctic response time to Northern Hemisphere abrupt warming has been significantly reduced as against previous studies. Different groups of DO events classified by the time of occurrence and magnitude, hereby, all reveal similar bipolar phasing. This suggests bipolar volcanic synchronisation to improve the exact interhemispherical linking compared to methane synchronisation and the bipolar volcanic framework to have been refined over the past years. The response time estimates, however, are determined by a simple method and partly hampered by low-resolution data and therefore fraught with uncertainties. Thus, the estimated delay needs to be taken with caution. Nevertheless, the method is considerably robust in order to constrain the overall timeframe of the Antarctic response time. To achieve more accurate estimates, high-resolution data are necessary; especially regarding the early half of the Last Glacial Period. Further, a fitting routine accounting for both slopes visible in the Antarctic record during the warming transition can potentially improve the determination of the Antarctic breakpoint hampered by a noisy isotope signal.

Accounting for uncertainties, the timescale may still be consistent with the original hypothesis embracing the bipolar seesaw. Antarctic temperatures increase during cold Northern Hemisphere stadials and decrease over the course of warm interstadials. At the time of the DO onset, Antarctica warms synchronously with the abrupt Greenland temperature rise, supporting the theory of the climate signal being transported across hemispheres through atmospheric teleconnection. The subsequent cooling continues to be very likely related to ocean mechanisms. However, the increased synchronicity between Greenland and Antarctica, both at the DO onset and after the stadial-interstadial transition, ignites a debate about whether there is a clear antiphase behaviour of the two hemispheres and warrants further investigation. This requires accurate dating and synchronisation, which further could be improved by utilising additional proxies to define the bipolar phasing, such as d-excess and calcium ions. Furthermore, determining the response time regarding interstadial terminations can contribute to a better understanding of possible mechanisms behind DO events.

Distinct differences between the individual DO events, especially on a local scale, argue against the uniformity of the mechanisms causing the abrupt climate changes. Instead, the underlying process could be triggered by different phenomena in the climate system; for instance, extensive volcanic eruptions occasionally occurring before DO events. However, considered out of the scope of the project, the correlation has not been statistically tested. To investigate the causality a statistical analysis extending the previous study by Lohmann and Svensson (2022) is recommended. Moreover, by linking the observations to different palaeoclimatic archives, possible mechanisms unrelated to ice cores can be investigated.

Whereas the individuality of the DO events is not captured by the comprehensive climate

model, the simulated general climate signal and interhemispherical phasing are concurrent with the isotope profiles. This argues for the ability of the model to explain the physical mechanisms related to DO events and to simulate abrupt climate change. Under progressive anthropogenic climate change, this is crucial to predict potential tipping points as mechanisms similar to those suspected to cause DO events have been observed over the past decades. Even though the threshold has not been crossed yet, future climate change scenarios have the potential to trigger tipping points. Here, the Arctic Ocean is currently closest to experiencing abrupt changes, which can lead to cascading effects having unpredictable consequences. This emphasises the need for ongoing refinement of climate models as well as the urge for immediate climate change mitigation.

6. Bibliography

- Abbott, P.M., Niemeier, U., Timmreck, C., Riede, F., McConnell, J.R., Severi, M., Fischer, H., Svensson, A., Toohey, M., Reinig, F., and Sigl, M. Volcanic climate forcing preceding the inception of the Younger Dryas: Implications for tracing the Laacher See eruption. *Quaternary Science Reviews*, 274:107260, 2021. ISSN 0277-3791. doi: <https://doi.org/10.1016/j.quascirev.2021.107260>. URL <https://www.sciencedirect.com/science/article/pii/S0277379121004674>.
- Alley, R. B., Meese, D. A., Shuman, C. A., Gow, A. J., Taylor, K. C., Grootes, P. M., White, J. W. C., Ram, M., Waddington, E. D., Mayewski, P. A., and Zielinski, G. A. Abrupt increase in Greenland snow accumulation at the end of the Younger Dryas event. *Nature*, 362(6420): 527–529, 1993. ISSN 1476-4687. doi: 10.1038/362527a0. URL <https://doi.org/10.1038/362527a0>.
- Andersen, K., Azuma, N., Barnola, J. M., Bigler, M., Biscaye, P., Caillon, N., Chappellaz, J., Clausen, H., Dahl-Jensen, D., Fischer, H., Flückiger, J., Fritzsche, D., Fujii, Y., Goto-Azuma, K., Grønvold, K., Gundestrup, N., Hansson, M., Huber, C., Hvidberg, C., and White, J. High-resolution record of Northern Hemisphere climate extending into the last interglacial period. *Nature*, 431:147–51, 2004. doi: 10.1038/nature02805.
- Arias, P.A., Bellouin, N., Coppola, E., Jones, R.G., Krinner, G., Marotzke, J., Naik, V., Palmer, M.D., Plattner, G.-K., Rogelj, J., Rojas, M., Sillmann, J., Storelvmo, T., Thorne, P.W., Trewin, B., Achuta Rao, K., Adhikary, B., Allan, R.P., Armour, K., Bala, G., Barimalala, R., Berger, S., Canadell, J.G., Cassou, C., Cherchi, A., Collins, W., Collins, W.D., Connors, S.L., Corti, S., Cruz, F., Dentener, F.J., Dereczynski, C., Di Luca, A., Diongue Niang, A., Doblus-Reyes, F.J., Dosio, A., Douville, H., Engelbrecht, F., Eyring, V., Fischer, E., Forster, P., Fox-Kemper, B., Fuglestedt, J.S., Fyfe, J.C., Gillett, N.P., Goldfarb, L., Gorodetskaya, I., Gutierrez, J.M., Hamdi, R., Hawkins, E., Hewitt, H.T., Hope, P., Islam, A.S., Jones, C., Kaufman, D.S., Kopp, R.E., Kosaka, Y., Kossin, J., Krakovska, S., Lee, J.-Y., Li, J., Mauritsen, T., Maycock, T.K., Meinshausen, M., Min, S.-K., Monteiro, P.M.S., Ngo-Duc, T., Otto, F., Pinto, I., Pirani, A., Raghavan, K., Ranasinghe, R., Ruane, A.C., Ruiz, L., Sallée, J.-B., Samset, B.H., Sathyendranath, S., Seneviratne, S.I., Sörensson, A.A., Szopa, S., Takayabu, I., Tréguier, A.-M., Hurk, B.van den , Vautard, R., Schuckmann, K.von , Zaehle, S., Zhang, X., and Zickfeld, K. *Technical Summary*, page 33144. Cambridge University Press, Cambridge, United Kingdom and New York, NY, USA, 2021. doi: 10.1017/9781009157896.002.
- Årthun, M., Eldevik, T., and Smedsrud, L. H. The Role of Atlantic Heat Transport in Future Arctic Winter Sea Ice Loss. *Journal of Climate*, 2019.

- Augustin, L., Panichi, S., and Frascati, F. EPICA Dome C 2 drilling operations: performances, difficulties, results. *Annals of Glaciology*, 47(1):68–72, 2007. ISSN 0260-3055. doi: 10.3189/172756407786857767. URL <https://dx.doi.org/10.3189/172756407786857767>.
- Ballinger, T. J., Overland, J. E., Wang, M., Bhatt, U. S., Brettschneider, B., Hanna, E., Hanssen-Bauer, I., Kim, S. J., Thoman, R. L., and Walsh, J. E. Surface Air Temperature. 2021. doi: <https://doi.org/10.25923/53xd-9k68>. URL <https://repository.library.noaa.gov/view/noaa/34475>. (GOMO).
- Bauska, T. K., Marcott, A., S., and Brook, E. J. Abrupt changes in the global carbon cycle during the last glacial period. *Nature Geoscience*, 14(2):91–96, 2021. ISSN 1752-0908. doi: 10.1038/s41561-020-00680-2. URL <https://doi.org/10.1038/s41561-020-00680-2>.
- Bazin, L., Landais, A., Lemieux-Dudon, B., Toyé Mahamadou Kele, H., Veres, D., Parrenin, F., Martinerie, P., Ritz, C., Capron, E., Lipenkov, V., Loutre, M. F., Raynaud, D., Vinther, B., Svensson, A., Rasmussen, S. O., Severi, M., Blunier, T., Leuenberger, M., Fischer, H., Masson-Delmotte, V., Chappellaz, J., and Wolff, E. An optimized multi-proxy, multi-site Antarctic ice and gas orbital chronology (AICC2012): 120–800 ka. *Climate of the Past*, 9(4):1715–1731, 2013. ISSN 1814-9332. doi: 10.5194/cp-9-1715-2013. URL <https://dx.doi.org/10.5194/cp-9-1715-2013>.
- Bazin, L., Landais, A., Capron, E., Masson-Delmotte, V., Ritz, C., Picard, G., Jouzel, J., Dumont, M., Leuenberger, M. C., and Prié, F. Phase relationships between orbital forcing and the composition of air trapped in Antarctic ice cores. *Climate of The Past*, 12:729–748, 2015.
- Behrens, E., Rickard, G., Morgenstern, O., Martin, T., Osprey, A., and Joshi, M. Southern Ocean deep convection in global climate models: A driver for variability of subpolar gyres and Drake Passage transport on decadal timescales. *Journal of Geophysical Research: Oceans*, 121(6):3905–3925, 2016. doi: <https://doi.org/10.1002/2015JC011286>. URL <https://agupubs.onlinelibrary.wiley.com/doi/abs/10.1002/2015JC011286>.
- Bender, M., Sowers, T., and Labeyrie, L. The Dole Effect and its variations during the last 130,000 years as measured in the Vostok Ice Core. *Global Biogeochemical Cycles*, 8(3):363–376, 1994. ISSN 0886-6236. doi: <https://doi.org/10.1029/94GB00724>. URL <https://agupubs.onlinelibrary.wiley.com/doi/abs/10.1029/94GB00724>.
- Bender, M. L. Orbital tuning chronology for the Vostok climate record supported by trapped gas composition. *Earth and Planetary Science Letters*, 204:275–289, 2002.
- Blunier, T. and Brook, E. J. Timing of millennial-scale climate change in Antarctica and Greenland during the last glacial period. *Science*, 291(5501):109–12, 2001. doi: 10.1126/science.291.5501.109.
- Blunier, T. and Schwander, J. Gas enclosure in ice: age difference and fractionation. 2000.

- Blunier, T., Chappellaz, J., Schwander, J., Dällenbach, A., Stauffer, B., Stocker, T. F., Raynaud, D., Jouzel, J., Clausen, H. B., Hammer, C. U., and Johnsen, S. J. Asynchrony of Antarctic and Greenland climate change during the last glacial period. *Nature*, 394(6695):739–743, 1998. ISSN 0028-0836. doi: 10.1038/29447. URL <https://dx.doi.org/10.1038/29447>.
- Bond, G., Heinrich, H., Broecker, W., Labeyrie, L., McManus, J., Andrews, J., Huon, S., Jantschik, R., Clasen, S., Simet, C., Tedesco, K., Klas, M., Bonani, G., and Ivy-Ochs, S. Evidence for massive discharges of icebergs into the North-Atlantic ocean during the Last Glacial Period. *Nature*, 360:245–249, 11 1992. doi: 10.1038/360245a0.
- Bradley, R. *Paleoclimatology (3rd edition)*. 2014. ISBN 978-0-12-386913-5.
- Braun, H., Ditlevsen, P., and Chialvo, D. R. Solar forced Dansgaard-Oeschger events and their phase relation with solar proxies. *Geophysical Research Letters*, 35(6), 2008. ISSN 0094-8276. doi: <https://doi.org/10.1029/2008GL033414>. URL <https://agupubs.onlinelibrary.wiley.com/doi/abs/10.1029/2008GL033414>.
- Buiron, D., Chappellaz, J., Stenni, B., Frezzotti, M., Baumgartner, M., Capron, E., Landais, A., Lemieux-Dudon, B., Masson-Delmotte, V., Montagnat, M., Parrenin, F., and Schilt, A. TALDICE-1 age scale of the Talos Dome deep ice core, East Antarctica. *Climate of the Past*, 7(1):1–16, 2011. ISSN 1814-9332. doi: 10.5194/cp-7-1-2011. URL <https://dx.doi.org/10.5194/cp-7-1-2011>.
- Buizert, C. The Ice Core Gas Age-Ice Age Difference as a Proxy for Surface Temperature. *Geophysical Research Letters*, 48, 2021.
- Buizert, C., Cuffey, K. M., Severinghaus, J. P., Baggenstos, D., Fudge, T. J., Steig, E. J., Markle, B. R., Winstrup, M., Rhodes, R. H., Brook, E. J., Sowers, T. A., Clow, G. D., Cheng, H., Edwards, R. L., Sigl, M., McConnell, J. R., and Taylor, K. C. The WAIS Divide deep ice core WD2014 chronology – Part 1: Methane synchronization (68–31 ka BP) and the gas age–ice age difference. *Climate of the Past*, 11(2):153–173, 2015. ISSN 1814-9332. doi: 10.5194/cp-11-153-2015. URL <https://dx.doi.org/10.5194/cp-11-153-2015>.
- Buizert, C., Sigl, M., Severi, M., Markle, B. R., Wettstein, J. J., McConnell, J. R., Pedro, J. B., Sodemann, H., Goto-Azuma, K., Kawamura, K., Fujita, S., Motoyama, H., Hirabayashi, M., Uemura, R., Stenni, B., Parrenin, F., He, F., Fudge, T. J., and Steig, E. J. Abrupt ice-age shifts in southern westerly winds and Antarctic climate forced from the north. *Nature*, 563(7733):681–685, 2018. ISSN 0028-0836. doi: 10.1038/s41586-018-0727-5.
- Capron, E., Rasmussen, S. O., Popp, T. J., Erhardt, T., Fischer, H., Landais, A., Pedro, J. B., Vettoretti, G., Grinsted, A., Gkinis, V., Vaughn, B., Svensson, A., Vinther, B. M., and White, J. W. C. The anatomy of past abrupt warmings recorded in Greenland ice. *Nature Communications*, 12(1), 2021. ISSN 2041-1723. doi: 10.1038/s41467-021-22241-w.
- Charles, C. D., Rind, D., Jouzel, J., Koster, R. D., and Fairbanks, R. G. Glacial-Interglacial Changes in Moisture Sources for Greenland - Influences on the Ice Core Record of Climate. *Science*, 263(5146):508–511, 1994. ISSN 0036-8075. doi: DOI10.1126/science.263.5146.508.

- Clark, P. U. and Mix, A. C. Ice sheets and sea level of the Last Glacial Maximum. *Quaternary Science Reviews*, 21(1):1–7, 2002. ISSN 0277-3791. doi: [https://doi.org/10.1016/S0277-3791\(01\)00118-4](https://doi.org/10.1016/S0277-3791(01)00118-4).
- Council, National Research. *Abrupt Climate Change: Inevitable Surprises*. The National Academies Press, Washington, DC, 2002. ISBN 978-0-309-07434-6. doi: 10.17226/10136. URL <https://nap.nationalacademies.org/catalog/10136/abrupt-climate-change-inevitable-surprises>.
- Cuffey, K. M. and Clow, G. D. Temperature, accumulation, and ice sheet elevation in central Greenland through the last deglacial transition. *Journal of Geophysical Research: Oceans*, 102(C12):26383–26396, 1997. doi: 10.1029/96JC03981. Export Date: 19 July 2022; Cited By: 383.
- Cuffey, K.M. and Paterson, W.S.B. 15 - Ice Core Studies. In PATERSON, W.S.B., editor, *The Physics of Glaciers (Third Edition)*, pages 378–409. Pergamon, Amsterdam, third edition edition, 1994a. ISBN 978-0-08-037944-9. doi: <https://doi.org/10.1016/B978-0-08-037944-9.50021-2>. URL <https://www.sciencedirect.com/science/article/pii/B9780080379449500212>.
- Cuffey, K.M. and Paterson, W.S.B. 3 - Mass Balance. In PATERSON, W.S.B., editor, *The Physics of Glaciers (Third Edition)*, pages 26–52. Pergamon, Amsterdam, fourth edition edition, 1994b. ISBN 978-0-08-037944-9. doi: <https://doi.org/10.1016/B978-0-08-037944-9.50009-1>.
- Dahl-Jensen, D., Johnsen, S. J., Hammer, C. U., Clausen, H. B., and Jouzel, J. Past accumulation rates derived from observed annual layers in the GRIP ice core from summit. 1993.
- Dahl-Jensen, D., Albert, M. R., Aldahan, A., Azuma, N., Balslev-Clausen, D., Baumgartner, M., Berggren, A. M., Bigler, M., Binder, T., Blunier, T., Bourgeois, J. C., Brook, E. J., Buchardt, S. L., Buizert, C., Capron, E., Chappellaz, J., Chung, J., Clausen, H. B., Cvijanovic, I., Davies, S. M., Ditlevsen, P., Eicher, O., Fischer, H., Fisher, D. A., Fleet, L. G., Gfeller, G., Gkinis, V., Gogineni, S., Goto-Azuma, K., Grinsted, A., Gudlaugsdottir, H., Guillevic, M., Hansen, S. B., Hansson, M., Hirabayashi, M., Hong, S., Hur, S. D., Huybrechts, P., Hvidberg, C. S., Iizuka, Y., Jenk, T., Johnsen, S. J., Jones, T. R., Jouzel, J., Karlsson, N. B., Kawamura, K., Keegan, K., Kettner, E., Kipfstuhl, S., Kjær, H. A., Koutnik, M., Kuramoto, T., Köhler, P., Laepple, T., Landais, A., Langen, P. L., Larsen, L. B., Leuenberger, D., Leuenberger, M., Leuschen, C., Li, J., Lipenkov, V., Martinerie, P., Maselli, O. J., Masson-Delmotte, V., McConnell, J. R., Miller, H., Mini, O., Miyamoto, A., Montagnat-Rentier, M., Mulvaney, R., Muscheler, R., Orsi, A. J., Paden, J., Panton, C., Pattyn, F., Petit, J. R., Pol, K., Popp, T., Possnert, G., Prié, F., Prokopiou, M., Quiquet, A., Rasmussen, S. O., Raynaud, D., Ren, J., Reutenauer, C., Ritz, C., Röckmann, T., Rosen, J. L., Rubino, M., Rybak, O., Samyn, D., Sapart, C. J., Schilt, A., Schmidt, A. M. Z., Schwander, J., Schüpbach, S., Seierstad, I., Severinghaus, J. P., and others., Eemian interglacial reconstructed from a Greenland folded ice core. *Nature*, 493(7433):489–494, 2013. ISSN 1476-4687. doi: 10.1038/nature11789. URL <https://doi.org/10.1038/nature11789>.

- Dansgaard, W. Stable isotopes in precipitation. *Tellus*, 16(4):436–468, 1964. doi: <https://doi.org/10.1111/j.2153-3490.1964.tb00181.x>. URL <https://onlinelibrary.wiley.com/doi/abs/10.1111/j.2153-3490.1964.tb00181.x>.
- Dansgaard, W. and Johnsen, S. J. A Flow Model and a Time Scale for the Ice Core from Camp Century, Greenland. *Journal of Glaciology*, 8:215 – 223, 1969.
- Dansgaard, W., Johnsen, S. J., Møller, J., and Langway, C. C. One Thousand Centuries of Climatic Record from Camp Century on the Greenland Ice Sheet. *Science*, 166:377 – 380, 1969.
- Dansgaard, W., Johnsen, S.J., and Clausen, H.B. *Stable Isotope Glaciology*. in: Meddelelser om Grønland, bd. 197, no. 2. C.A. Reitzels Forlag, 1973.
- Ditlevsen, P. *Tipping Points in the Climate System*, pages 33–53. Cambridge University Press, Cambridge, 2017. ISBN 9781107118140. doi: DOI:10.1017/9781316339251.003.
- Ditlevsen, P., Andersen, K., and Svensson, A. The DO-climate events are probably noise induced: Statistical investigation of the claimed 1470 years cycle. *Climate of the Past*, 3:129–134, 2007. doi: 10.5194/cp-3-129-2007.
- EPICA Community Members,. Eight glacial cycles from an Antarctic ice core. *Nature*, 429: 623–628, 07 2004. doi: 10.1038/nature02599.
- EPICA Community Members,. One-to-one coupling of glacial climate variability in Greenland and Antarctica. *Nature*, 444:195–198, 11 2006. doi: 10.1038/nature05301.
- Erhardt, T., Capron, E., Rasmussen, S. O., Schüpbach, S., Bigler, M., Adolphi, F., and Fischer, H. Decadal-scale progression of the onset of Dansgaard–Oeschger warming events. *Climate of the Past*, 15(2):811–825, 2019. ISSN 1814-9332. doi: 10.5194/cp-15-811-2019. URL <https://dx.doi.org/10.5194/cp-15-811-2019>.
- Fetterer, F., Knowles, K., Meier, W. N., Savoie, M., and Windnagel, A. K. Sea Ice Index, Version 3, 2017. URL <https://nsidc.org/data/G02135/versions/3>.
- Fischer, H., Siggaard-Andersen, M., Ruth, U, Röthlisberger, R., and Wolff, E. W. Glacial/interglacial changes in mineral dust and sea-salt records in polar ice cores: Sources, transport, and deposition. *Reviews of Geophysics*, 45, 2007.
- Gent, P., Danabasoglu, G., Donner, L., Holland, M., Hunke, E., Jayne, S., Lawrence, D., Neale, R., Rasch, P., Vertenstein, M., Worley, P., Yang, Z., and Zhang, M. The community climate system model version 4. pages 4973–4991, 10 2011.
- Gent, P. R. and McWilliams, J. C. Isopycnal Mixing in Ocean Circulation Models. *Journal of Physical Oceanography*, 20(1):150 – 155, 1990. doi: 10.1175/1520-0485(1990)020<0150:IMIOCM>2.0.CO;2.
- Gkinis, V., Simonsen, S. B., Buchardt, S. L., White, J. W., and Vinther, B. M. Water isotope diffusion rates from the NorthGRIP ice core for the last 16,000 years - Glaciological and paleoclimatic implications. *Earth and Planetary Science Letters*, 405:132–141, 2014.

- Gkinis, V., Vinther, B. M., Popp, T. J., Quistgaard, T., Faber, A., Holme, C. T., Jensen, C., Lanzky, M., Lütt, A., Mandrakis, V., Ørum, N., Pedersen, A., Vaxevani, N., Weng, Y., Capron, E., Dahl-Jensen, D., Hörhold, M., Jones, T. R., Jouzel, J., Landais, A., Masson-Delmotte, V., Oerter, H., Rasmussen, S. O., Steen-Larsen, H. C., Steffensen, J.P., Sveinbjörnsdóttir, Á., Svensson, A., Vaughn, B., and White, J. W. C. A 120,000-year long climate record from a NW-Greenland deep ice core at ultra-high resolution. *Scientific Data*, 8(1):141, 2021. ISSN 2052-4463. doi: 10.1038/s41597-021-00916-9. URL <https://doi.org/10.1038/s41597-021-00916-9>.
- Grotes, P. M. and Stuiver, M. GISP2 Oxygen Isotope Data, 1999. URL <https://doi.org/10.1594/PANGAEA.56094>.
- Grotes, P. M., Stuiver, M., White, J. W. C., Johnsen, S. J., and Jouzel, J. Comparison of oxygen isotope records from the GISP2 and GRIP Greenland ice cores. *Nature*, 366:552–554, 1993.
- Guillevic, M., Bazin, L., Landais, A., Kindler, P., Orsi, A. J., Masson-Delmotte, V., Blunier, T., Buchardt, S. L., Capron, E., Leuenberger, M. C., Martinerie, P., Prié, F., and Vinther, B. M. Spatial gradients of temperature, accumulation and $\delta^{18}\text{O}$ -ice in Greenland over a series of Dansgaard-Oeschger events. *Climate of The Past*, 9:1029–1051, 2012.
- Heinrich, H. Origin and consequences of cyclic ice rafting in the Northeast Atlantic Ocean during the past 130,000 years. *Quaternary Research*, 29(2):142–152, 1988. ISSN 0033-5894. doi: [https://doi.org/10.1016/0033-5894\(88\)90057-9](https://doi.org/10.1016/0033-5894(88)90057-9). URL <https://www.sciencedirect.com/science/article/pii/0033589488900579>.
- Herron, M. M. and Langway, C. C. Firn Densification: An Empirical Model. *Journal of Glaciology*, 25:373 – 385, 1980.
- Hoek, W. Z., Yu, Z. C., and Lowe, J. J. INTegration of Ice-core, MArine, and TERrestrial records (INTIMATE): refining the record of the Last Glacial–Interglacial Transition. *Quaternary Science Reviews*, 27(1):1–5, 2008. ISSN 0277-3791. doi: <https://doi.org/10.1016/j.quascirev.2007.11.020>.
- Hoff, U., Rasmussen, Tine L., Stein, R., Ezat, M. M., and Fahl, K. Sea ice and millennial-scale climate variability in the Nordic seas 90kyr ago to present. *Nature Communications*, 7(1): 12247, 2016. ISSN 2041-1723. doi: 10.1038/ncomms12247.
- Ilıcak, M., Drange, H., Wang, Q., Gerdes, R., Aksenov, Y., Bailey, D. A., Bentsen, M., Bias-toch, A., Bozec, A., Böning, C. W., Cassou, C., Chassignet, E. P., Coward, A. C., Curry, B., Danabasoglu, G., Danilov, S., Fernandez, E., Fogli, P. G., Fujii, Y., Griffies, S. M., Iovino, D., Jahn, A., Jung, T., Large, W. G., Lee, C. M., Lique, C., Lu, J., Masina, S., Nurser, A. J. G., Roth, C., Mélia, D. S., Samuels, B. L., Spence, P., Tsujino, H., Valcke, S., Voldoire, A., Wang, X., and Yeager, S. G. An assessment of the Arctic Ocean in a suite of interannual CORE-II simulations. Part III: Hydrography and fluxes. *Ocean Modelling*, 100:141–161, 2016.

- Jansen, E., Christensen, J. H., Dokken, T., Nisancioglu, K. H., Vinther, B. M., Capron, E., Guo, C., Jensen, M. F., Langen, P. L., Pedersen, R. A., Yang, S., Bentsen, M., Kjær, H. A., Sadatzki, H., Sessford, E., and Stendel, M. Past perspectives on the present era of abrupt Arctic climate change. *Nature Climate Change*, 10(8):714–721, 2020. ISSN 1758-678X. doi: 10.1038/s41558-020-0860-7. URL <https://dx.doi.org/10.1038/s41558-020-0860-7>.
- Jensen, M., Nilsson, J., and Nisancioglu, K. The interaction between sea ice and salinity-dominated ocean circulation: implications for halocline stability and rapid changes of sea ice cover. *Climate Dynamics*, 47, 11 2016. doi: 10.1007/s00382-016-3027-5.
- Johnsen, S. J., Clausen, H. B., Dansgaard, W., Fuhrer, K., Gundestrup, N., Hammer, C. U., Iversen, P., Jouzel, J., Stauffer, B., and Steffensen, J. P. Irregular glacial interstadials recorded in a new Greenland ice core. *Nature*, 359(6393):311–313, 1992. ISSN 1476-4687. doi: 10.1038/359311a0.
- Johnsen, S. J., Dahl-Jensen, D., Gundestrup, N., Steffensen, J., Clausen, H., Miller, H., Masson-Delmotte, V., Sveinbjörnsdóttir, A., and White, J. Oxygen isotope and palaeotemperature records from six Greenland ice-core stations: Camp Century, Dye-3, GRIP, GISP2, Renland and NorthGRIP. *Journal of Quaternary Science*, 16:299–307, 2001. doi: 10.1002/jqs.622.
- Jouzel, J., Masson-Delmotte, V., Cattani, O., Dreyfus, G., Falourd, S., Hoffmann, G., Minster, B., Nouet, J., Barnola, J. M., Chappellaz, J., Fischer, H., Gallet, J. C., Johnsen, S., Leuenberger, M., Loulergue, L., Luethi, D., Oerter, H., Parrenin, F., Raisbeck, G., Raynaud, D., Schilt, A., Schwander, J., Selmo, E., Souchez, R., Spahni, R., Stauffer, B., Steffensen, J. P., Stenni, B., Stocker, T. F., Tison, J. L., Werner, M., and Wolff, E. W. Orbital and Millennial Antarctic Climate Variability over the Past 800,000 Years. *Science*, 317(5839): 793–796, 2007. doi: doi:10.1126/science.1141038.
- Kahle, E. C., Holme, C., Jones, T. R., Gkinis, V., and Steig, E. J. A Generalized Approach to Estimating Diffusion Length of Stable Water Isotopes From Ice-Core Data. *Journal of Geophysical Research: Earth Surface*, 123(10):2377–2391, 2018. ISSN 2169-9003. doi: <https://doi.org/10.1029/2018JF004764>.
- Kawamura, K., Parrenin, F., Lisiecki, L., Uemura, R., Vimeux, F., Severinghaus, J., Hutterli, M., Nakazawa, T., Aoki, S., Jouzel, J., Raymo, M., Matsumoto, K., Nakata, H., Motoyama, H., Fujita, S., Goto-Azuma, K., Fujii, Y., and Watanabe, O. Northern Hemisphere forcing of climatic cycles in Antarctica over the past 360,000 years. *Nature*, 448:912–6, 09 2007. doi: 10.1038/nature06015.
- Kellerhals, T., Brütsch, S., Sigl, M., Knüsel, S., Gäggeler, H. W., and Schwikowski, M. Ammonium concentration in ice cores: A new proxy for regional temperature reconstruction? *Journal of Geophysical Research: Atmospheres*, 115(D16), 2010. doi: <https://doi.org/10.1029/2009JD012603>. URL <https://agupubs.onlinelibrary.wiley.com/doi/abs/10.1029/2009JD012603>.
- Kindler, P., Guillevic, M., Baumgartner, M., Schwander, J., Landais, A., and Leuenberger, M.

- Temperature reconstruction from 10 to 120 kyr b2k from the NGRIP ice core. *Clim. Past*, 10(2):887–902, 2014. ISSN 1814-9332. doi: 10.5194/cp-10-887-2014. CP.
- Kreutz, K. J. ICE CORE METHODS — Glaciochemistry. 2007.
- Kusahara, K. and Ohshima, K. I. Kelvin Waves around Antarctica. *Journal of Physical Oceanography*, 44(11):2909–2920, 2014. doi: 10.1175/JPO-D-14-0051.1.
- Lal, D. and Peters, B. Cosmic ray produced radioactivity on the Earth. 1967.
- Landais, A., Masson-Delmotte, V., Stenni, B., Selmo, E., Roche, D. M., Jouzel, J., Lambert, F., Guillevic, M., Bazin, L., Arzel, O., Vinther, B., Gkinis, V., and Popp, T. A review of the bipolar see-saw from synchronized and high-resolution ice core water stable isotope records from Greenland and East Antarctica. *Quaternary Science Reviews*, 114:18–32, 2015. ISSN 0277-3791. doi: 10.1016/j.quascirev.2015.01.031. URL <GotoISI>://WOS:000353090000002.
- Landais, A., Capron, E., Masson-Delmotte, V., Toucanne, S., Rhodes, R., Popp, T., Vinther, B., Minster, B., and Prié, F. Ice core evidence for decoupling between midlatitude atmospheric water cycle and Greenland temperature during the last deglaciation. *Clim. Past*, 14(10):1405–1415, 2018. ISSN 1814-9332. doi: 10.5194/cp-14-1405-2018. CP.
- Langway, C. C., Clausen, H. B., and Hammer, C. U. An Inter-Hemispheric Volcanic Time-Marker in Ice Cores from Greenland and Antarctica. *Annals of Glaciology*, 10:102–108, 1988. ISSN 0260-3055. doi: 10.3189/S0260305500004250. URL <https://www.cambridge.org/core/article/an-interhemispheric-volcanic-timemarker-in-ice-cores-from-greenland-and-antarctica/B49D4AC170CA0B9612CA191D7770B1DB>.
- Lefebvre, W., Goosse, H., Timmermann, R., and Fichet, T. Influence of the Southern Annular Mode on the sea ice-ocean system. *Journal of Geophysical Research*, 109, 2004.
- Lenton, T. M., Rockström, J., Gaffney, O., Rahmstorf, S., Richardson, K., Steffen, W., and Schellnhuber, H. J. Climate tipping points — too risky to bet against. *Nature*, 575:592 – 595, 2019.
- Lin, J., Svensson, A., Hvidberg, C. S., Lohmann, J., Kristiansen, S., Dahl-Jensen, D., Steffensen, J. P., Rasmussen, S. O., Cook, E., Kjær, H. A., Vinther, B. M., Fischer, H., Stocker, T., Sigl, M., Bigler, M., Severi, M., Traversi, R., and Mulvaney, R. Magnitude, frequency and climate forcing of global volcanism during the last glacial period as seen in Greenland and Antarctic ice cores (60–9ka). *Climate of the Past*, 18(3):485–506, 2022. ISSN 1814-9332. doi: 10.5194/cp-18-485-2022. URL <https://dx.doi.org/10.5194/cp-18-485-2022>.
- Lind, S., Ingvaldsen, R. B., and Furevik, T. Arctic warming hotspot in the northern Barents Sea linked to declining sea-ice import. *Nature Climate Change*, 8:634–639, 2018.
- Lohmann, J. and Svensson, A. Ice core evidence for major volcanic eruptions at the onset of Dansgaard–Oeschger warming events. *Climate of the Past*, 18(9):2021–2043, 2022. ISSN 1814-9332. doi: 10.5194/cp-18-2021-2022. URL <https://dx.doi.org/10.5194/cp-18-2021-2022>.

- Masson-Delmotte, V., Kageyama, M., Braconnot, P., Charbit, S., Krinner, G., Ritz, C., Guillard, E., Jouzel, J., Abe-Ouchi, A., Crucifix, M., Gladstone, R. M., Hewitt, C. D., Kitoh, A., LeGrande, A. N., Marti, O., Merkel, U., Motoi, T., Ohgaito, R., Otto-Bliesner, B., Peltier, W. R., Ross, I., Valdes, P. J., Vettoretti, G., Weber, S. L., Wolk, F., and Yu, Y. Past and future polar amplification of climate change: climate model intercomparisons and ice-core constraints. *Climate Dynamics*, 26(5):513–529, 2006. ISSN 1432-0894. doi: 10.1007/s00382-005-0081-9. URL <https://doi.org/10.1007/s00382-005-0081-9>.
- McHargue, L. R. and Damon, P. E. The global Beryllium 10 cycle. *Reviews of Geophysics*, 29(2):141–158, 1991. doi: <https://doi.org/10.1029/91RG00072>. URL <https://agupubs.onlinelibrary.wiley.com/doi/abs/10.1029/91RG00072>.
- Milankovitch, M. Canon of insolation and the ice-age problem: (kanon der Erdbestrahlung und seine Anwendung auf das Eiszeitenproblem) Belgrade, 1941. 1941.
- Muscheler, R. and Beer, J. Solar forced Dansgaard/Oeschger events? *Geophysical Research Letters*, 33(20), 2006. ISSN 0094-8276. doi: <https://doi.org/10.1029/2006GL026779>. URL <https://agupubs.onlinelibrary.wiley.com/doi/abs/10.1029/2006GL026779>.
- Muscheler, R., Beer, J., Wagner, G., and Finkel, R. C. Changes in deep-water formation during the Younger Dryas event inferred from 10Be and 14C records. *Nature*, 408(6812):567–570, 2000. ISSN 1476-4687. doi: 10.1038/35046041. URL <https://doi.org/10.1038/35046041>.
- Myrvoll-Nilsen, E., Riechers, K., Rypdal, M. W., and Boers, N. Comprehensive uncertainty estimation of the timing of Greenland warmings in the Greenland ice core records. *Climate of the Past*, 18(6):1275–1294, 2022. ISSN 1814-9332. doi: 10.5194/cp-18-1275-2022. URL <https://dx.doi.org/10.5194/cp-18-1275-2022>.
- Neff, P.D. A review of the brittle ice zone in polar ice cores. *Annals of Glaciology*, 55(68):72–82, 2014. ISSN 0260-3055. doi: 10.3189/2014AoG68A023. URL <https://www.cambridge.org/core/article/review-of-the-brittle-ice-zone-in-polar-ice-cores/73F743BA75BAA38500B6CBB90528EC49>.
- NGRIP Members,. High-resolution record of Northern Hemisphere climate extending into the last interglacial period. *Nature*, 431(7005):147–151, 2004. ISSN 0028-0836. doi: 10.1038/nature02805. URL <https://dx.doi.org/10.1038/nature02805>.
- NOAA National Centers for Environmental Information,. Monthly Global Climate Report for Annual 2021, 2022. URL <https://www.ncei.noaa.gov/access/monitoring/monthly-report/global/202113>.
- Nye, J. F. Correction Factor for Accumulation Measured by the Thickness of the Annual Layers in an Ice Sheet. *Journal of Glaciology*, 4:785 – 788, 1963.
- Onac, B., Ginés, A., Gines, J., Fornós, J., and Dorale, J. A. Late quaternary sea-level history: A Speleothem perspective. *Monografies de la Societat d’Historia Natural de les Balears*, 18: 147–162, 2012.

- Parrenin, F., Fujita, S., Abe-Ouchi, A., Kawamura, K., Masson-Delmotte, V., Motoyama, H., Saito, F., Severi, M., Stenni, B., Uemura, R., and Wolff, E. W. Climate dependent contrast in surface mass balance in East Antarctica over the past 216 ka. *Journal of Glaciology*, 62 (236):1037–1048, 2016. ISSN 0022-1430. doi: 10.1017/jog.2016.85. URL <https://dx.doi.org/10.1017/jog.2016.85>.
- Pedro, J. B., Jochum, M., Buizert, C., He, F., Barker, S., and Rasmussen, S. O. Beyond the bipolar seesaw: Toward a process understanding of interhemispheric coupling. *Quaternary Science Reviews*, 192:27–46, 2018. ISSN 0277-3791. doi: <https://doi.org/10.1016/j.quascirev.2018.05.005>. URL <https://www.sciencedirect.com/science/article/pii/S0277379117310351>.
- Rahmstorf, S. Ocean circulation and climate during the past 120,000 years. *Nature*, 419(6903): 207–214, 2002. ISSN 1476-4687. doi: 10.1038/nature01090. URL <https://doi.org/10.1038/nature01090>.
- Raisbeck, G. M., Yiou, F., Cattani, O., and Jouzel, J. ^{10}Be evidence for the Matuyama–Brunhes geomagnetic reversal in the EPICA Dome C ice core. *Nature*, 444:82–84, 2006.
- Rashid, H., Hesse, R., and Piper, D. J. W. Evidence for an additional Heinrich event between H5 and H6 in the Labrador Sea. *Paleoceanography*, 18(4), 2003. ISSN 0883-8305. doi: <https://doi.org/10.1029/2003PA000913>. URL <https://agupubs.onlinelibrary.wiley.com/doi/abs/10.1029/2003PA000913>. For H events.
- Rasmussen, S., Bigler, M., Blockley, S. P., Blunier, T., Buchardt, S. L., Clausen, H. B., Cvi-janovic, I., Dahl-Jensen, D., Johnsen, S. J., Fischer, H., Gkinis, V., Guillevic, M., Hoek, W. Z., Lowe, J. J., Pedro, J. B., Popp, T., Seierstad, I. K., Steffensen, J. P., Svensson, A., Val-lelonga, P., Vinther, B. M., Walker, M. J. C., Wheatley, J. J., and Winstrup, M. A stratigraphic framework for abrupt climatic changes during the Last Glacial period based on three synchronized Greenland ice-core records: refining and extending the INTIMATE event stratigraphy. *Quaternary Science Reviews*, 106:14–28, 2014. ISSN 0277-3791. doi: 10.1016/j.quascirev.2014.09.007.
- Rasmussen, S. O., Andersen, K. K., Svensson, A. M., Steffensen, J. P., Vinther, B. M., Clausen, H. B., Siggaard-Andersen, M.-L., Johnsen, S. J., Larsen, L. B., Dahl-Jensen, D., Bigler, M., Röthlisberger, R., Fischer, H., Goto-Azuma, K., Hansson, M. E., and Ruth, U. A new Greenland ice core chronology for the last glacial termination. *Journal of Geophysical Research: Atmospheres*, 111(D6), 2006. ISSN 0148-0227. doi: <https://doi.org/10.1029/2005JD006079>. URL <https://agupubs.onlinelibrary.wiley.com/doi/abs/10.1029/2005JD006079>.
- Rasmussen, S. O., Abbott, P. M., Blunier, T., Bourne, A. J., Brook, E., Buchardt, S. L., Buizert, C., Chappellaz, J., Clausen, H. B., Cook, E., Dahl-Jensen, D., Davies, S. M., Guillevic, M., Kipfstuhl, S., Laepple, T., Seierstad, I. K., Severinghaus, J. P., Steffensen, J. P., Stowasser, C., Svensson, A., Vallelonga, P., Vinther, B. M., Wilhelms, F., and Winstrup, M. A first chronology for the North Greenland Eemian Ice Drilling (NEEM) ice core. *Climate of the Past*, 9(6):2713–2730, 2013. ISSN 1814-9332. doi: 10.5194/cp-9-2713-2013. URL <https://dx.doi.org/10.5194/cp-9-2713-2013>.

- Rasmussen, T. L., Oppo, D. W., Thomsen, E., and Lehman, S. J. Deep sea records from the southeast Labrador Sea: Ocean circulation changes and ice-rafting events during the last 160,000 years. *Paleoceanography*, 18(1), 2003. ISSN 0883-8305. doi: <https://doi.org/10.1029/2001PA000736>. URL <https://agupubs.onlinelibrary.wiley.com/doi/abs/10.1029/2001PA000736>. H Events from IRD and low benthic d18O.
- Ritz, C., Rommelaere, V., and Dumas, C. Modeling the evolution of Antarctic ice sheet over the last 420,000 years: Implications for altitude changes in the Vostok region. *Journal of Geophysical Research: Atmospheres*, 106(D23):31943–31964, 2001. ISSN 0148-0227. doi: 10.1029/2001jd900232. URL <https://dx.doi.org/10.1029/2001jd900232>.
- Robin, G. Ice Cores and Climatic Change. *Philosophical Transactions of the Royal Society B*, 280:143–168, 1977.
- Ruth, U., Wagenbach, D., Steffensen, J. P., and Bigler, M. Continuous record of microparticle concentration and size distribution in the central Greenland NGRIP ice core during the last glacial period. *Journal of Geophysical Research: Atmospheres*, 108(D3), 2003. ISSN 0148-0227. doi: <https://doi.org/10.1029/2002JD002376>. URL <https://doi.org/10.1029/2002JD002376>. <https://doi.org/10.1029/2002JD002376>.
- Sadatzi, H., Dokken, T., Berben, S., Muschitiello, F., Stein, R., Fahl, K., Menviel, L., Timmermann, A., and Jansen, E. Sea ice variability in the southern Norwegian Sea during glacial Dansgaard-Oeschger climate cycles. *Science Advances*, 5, 03 2019. doi: 10.1126/sciadv.aau6174.
- Salamatin, A. N., Tsyganova, E. A., Lipenkov, V. Ya, and Petit, J. R. Vostok (Antarctica) ice-core time-scale from datings of different origins. *Annals of Glaciology*, 39:283–292, 2004. ISSN 0260-3055. doi: 10.3189/172756404781814023. URL <https://www.cambridge.org/core/article/vostok-antarctica-icecore-timescale-from-datings-of-different-origins/E318B364FD6BF65DCC7442481C22F6CD>.
- Sarnthein, M., Winn, K., Jung, S. J. A., Duplessy, J., Labeyrie, L., Erlenkeuser, H., and Ganssen, G. Changes in East Atlantic Deepwater Circulation over the last 30,000 years: Eight time slice reconstructions. *Paleoceanography*, 9(2):209–267, 1994. ISSN 0883-8305. doi: <https://doi.org/10.1029/93PA03301>. URL <https://doi.org/10.1029/93PA03301>. <https://doi.org/10.1029/93PA03301>.
- Sessford, E., Jensen, M., Tisserand, A., Muschitiello, F., Dokken, T., Nisancioglu, K., and Jansen, E. Consistent fluctuations in intermediate water temperature off the coast of Greenland and Norway during Dansgaard-Oeschger events. *Quaternary Science Reviews*, 223: 105887, 2019. doi: 10.1016/j.quascirev.2019.105887.
- Sessford, E. G., Tisserand, A., Risebrobakken, B., Andersson, C., Dokken, T. M., and Jansen, E. High-Resolution Benthic Mg/Ca Temperature Record of the Intermediate Water in the Denmark Strait Across D-O Stadial-Interstadial Cycles. *Paleoceanography and Paleoclimatology*, 33:1169 – 1185, 2018.

- Severinghaus, J. P. and Brook, E. J. Abrupt Climate Change at the End of the Last Glacial Period Inferred from Trapped Air in Polar Ice. *Science*, 286(5441):930–934, 1999. doi: [10.1126/science.286.5441.930](https://doi.org/10.1126/science.286.5441.930).
- Sharp, Z. Principles of Stable Isotope Geochemistry, 2nd Edition. 2017.
- Shumskiy, P. A. Density of Glacier Ice. *Journal of Glaciology*, 3(27):568–573, 1960. doi: [10.3189/S0022143000023686](https://doi.org/10.3189/S0022143000023686).
- Sigl, M., Winstrup, M., McConnell, J., Welten, K., Plunkett, G., Ludlow, F., Büntgen, U., Caffee, M., Chellman, N., Dahl-Jensen, D., Fischer, H., Kipfstuhl, S., Kostick, C., Maselli, O., Mekhaldi, F., Mulvaney, R., Muscheler, R., Pasteris, D., Pilcher, J., and Woodruff, T. Timing and climate forcing of volcanic eruptions for the past 2,500 years. *Nature*, 523, 07 2015. doi: [10.1038/nature14565](https://doi.org/10.1038/nature14565).
- Solanki, S. K. Solar variability and climate change: is there a link? *Astronomy Geophysics*, 43(5):5.9–5.13, 2002. ISSN 1366-8781. doi: [10.1046/j.1468-4004.2002.43509.x](https://doi.org/10.1046/j.1468-4004.2002.43509.x). URL <https://doi.org/10.1046/j.1468-4004.2002.43509.x>.
- Stauffer, B., Blunier, T., Dällenbach, A., Indermühle, A., Schwander, J., Stocker, T. F., Tschumi, J., Chappellaz, J., Raynaud, D., Hammer, C. U., and Clausen, H. B. Atmospheric CO₂ concentration and millennial-scale climate change during the last glacial period. *Nature*, 392(6671):59–62, 1998. ISSN 1476-4687. doi: [10.1038/32133](https://doi.org/10.1038/32133). URL <https://doi.org/10.1038/32133>.
- Steffensen, J. P., Andersen, K. K., Bigler, M., Clausen, H. B., Dahl-Jensen, D., Fischer, H., Goto-Azuma, K., Hansson, M., Johnsen, S. J., Jouzel, J., Masson-Delmotte, V., Popp, T., Rasmussen, S., Röhlisberger, R., Ruth, U., Stauffer, B., Siggaard-Andersen, M., Sveinbjörnsdóttir, A., Svensson, A., and White, J. W. C. High-Resolution Greenland Ice Core Data Show Abrupt Climate Change Happens in Few Years. *Science*, 321(5889):680–684, 2008. ISSN 0036-8075. doi: [10.1126/science.1157707](https://doi.org/10.1126/science.1157707). URL <https://dx.doi.org/10.1126/science.1157707>.
- Steinhilber, F., Abreu, J. A., Beer, J., and McCracken, K. G. Interplanetary magnetic field during the past 9300 years inferred from cosmogenic radionuclides. *Journal of Geophysical Research: Space Physics*, 115(A1), 2010. doi: <https://doi.org/10.1029/2009JA014193>. URL <https://agupubs.onlinelibrary.wiley.com/doi/abs/10.1029/2009JA014193>.
- Stenni, B., Buiron, Daphné, Frezzotti, M., Albani, Samuel, Barbante, C., Bard, Edouard, Barnola, J., Baroni, Mélanie, Baumgartner, Michelle, Bonazza, Mattia, Capron, Emilie, Castellano, E., Chappellaz, Jérôme, Delmonte, Barbara, Falourd, S., Genoni, L., Iacumin, Paola, Jouzel, Jean, Kipfstuhl, S., and Udisti, Roberto. Expression of the bipolar see-saw in Antarctic climate records during the last deglaciation. *Nature Geoscience*, 4: 46–49, 2011. doi: [10.1038/ngeo1026](https://doi.org/10.1038/ngeo1026).
- Stocker, T. F. and Johnsen, S. J. A minimum thermodynamic model for the bipolar seesaw. *Paleoceanography*, 18(4), 2003. ISSN 0883-8305. doi: <https://doi.org/10.1029/2003PA000920>. URL <https://agupubs.onlinelibrary.wiley.com/doi/abs/10.1029/2003PA000920>.

- Stommel, H. Thermohaline Convection with Two Stable Regimes of Flow. *Tellus*, 13(2):224–230, 1961. ISSN 0040-2826. doi: <https://doi.org/10.1111/j.2153-3490.1961.tb00079.x>. URL <https://doi.org/10.1111/j.2153-3490.1961.tb00079.x>. <https://doi.org/10.1111/j.2153-3490.1961.tb00079.x>.
- Stuecker, M. F., Bitz, C. M., Armour, K. C., Posescu, C., Kang, S. M., Xie, S., Kim, D., McGregor, S., Zhang, W., Zhao, S., Cai, W., Dong, Y., and Jin, F. Polar amplification dominated by local forcing and feedbacks. *Nature Climate Change*, 8(12):1076–1081, 2018. ISSN 1758-6798. doi: 10.1038/s41558-018-0339-y. URL <https://doi.org/10.1038/s41558-018-0339-y>.
- Svensson, A., Andersen, K., Clausen, H., Johnsen, S., Rasmussen, S., Steffensen, J., and Vinther, B. The Greenland Ice Core Chronology 2005 (GICC05). *AGU Fall Meeting Abstracts*, 2005.
- Svensson, A., Bigler, M., Blunier, T., Clausen, H., Dahl-Jensen, D., Fischer, H., Fujita, S., Goto-Azuma, K., Johnsen, S., Kawamura, K., Kipfstuhl, S., Kohno, M., Parrenin, F., Popp, T., Rasmussen, S., Schwander, J., Seierstad, I., Severi, M., Steffensen, J., and Winstrup, M. Direct linking of Greenland and Antarctic ice cores at the Toba eruption (74 ka BP), volume = 9, journal = *Climate of the Past*, doi = 10.5194/cp-9-749-2013. pages 749–766, 03 2013.
- Svensson, A., Dahl-Jensen, D., Steffensen, J. P., Blunier, T., Rasmussen, S. O., Vinther, B. M., Vallenga, P., Capron, E., Gkinis, V., Cook, E., Kjær, H. A., Muscheler, R., Kipfstuhl, S., Wilhelms, F., Stocker, T. F., Fischer, H., Adolphi, F., Erhardt, T., Sigl, M., Landais, A., Parrenin, F., Buizert, C., McConnell, J. R., Severi, M., Mulvaney, R., and Bigler, M. Bipolar volcanic synchronization of abrupt climate change in Greenland and Antarctic ice cores during the last glacial period. *Climate of the Past*, 16(4):1565–1580, 2020. ISSN 1814-9332. doi: 10.5194/cp-16-1565-2020. URL <https://dx.doi.org/10.5194/cp-16-1565-2020>.
- Taylor, J. R., Bachman, S., Stamper, M., Hosegood, P., Adams, K., Sallee, J., and Torres, R. Submesoscale Rossby waves on the Antarctic circumpolar current. *Science Advances*, 4(3): eaao2824, 2018. doi: 10.1126/sciadv.aao2824. URL <https://doi.org/10.1126/sciadv.aao2824>. doi: 10.1126/sciadv.aao2824.
- Thiede, J., Jessen, C., Knutz, P., Kuijpers, A., Mikkelsen, N., Nørgaard-Pedersen, N., and Spielhagen, R. F. Million years of Greenland Ice Sheet history recorded in ocean sediments. 2011.
- Thomas, E. Descent into the Icehouse. *Geology*, 36, 02 2008. doi: 10.1130/focus022008.1.
- Tierney, J. E., Zhu, J., King, J., Malevich, S. B., Hakim, G. J., and Poulsen, C. J. Glacial cooling and climate sensitivity revisited. *Nature*, 584(7822):569–573, 2020. ISSN 1476-4687. doi: 10.1038/s41586-020-2617-x. URL <https://doi.org/10.1038/s41586-020-2617-x>.
- Timmermans, M. and Marshall, J. Understanding Arctic Ocean Circulation: A Review of Ocean Dynamics in a Changing Climate. *Journal of Geophysical Research: Oceans*, 125(4): e2018JC014378, 2020. ISSN 2169-9275. doi: <https://doi.org/10.1029/2018JC014378>. URL <https://agupubs.onlinelibrary.wiley.com/doi/abs/10.1029/2018JC014378>.

- Veres, D., Bazin, L., Landais, A., Toyé Mahamadou Kele, H., Lemieux-Dudon, B., Parrenin, F., Martinerie, P., Blayo, E., Blunier, T., Capron, E., Chappellaz, J., Rasmussen, S. O., Severi, M., Svensson, A., Vinther, B., and Wolff, E. W. The Antarctic ice core chronology (AICC2012): an optimized multi-parameter and multi-site dating approach for the last 120 thousand years. *Clim. Past*, 9(4):1733–1748, 2013. ISSN 1814-9332. doi: 10.5194/cp-9-1733-2013. URL <https://cp.copernicus.org/articles/9/1733/2013/>. CP.
- Vettoretti, G., Ditlevsen, P., Jochum, M., and Rasmussen, S. O. Atmospheric CO₂ control of spontaneous millennial-scale ice age climate oscillations. *Nature Geoscience*, 15(4):300–306, 2022. ISSN 1752-0894. doi: 10.1038/s41561-022-00920-7. URL <https://dx.doi.org/10.1038/s41561-022-00920-7>.
- Vihma, T. Effects of Arctic Sea Ice Decline on Weather and Climate: A Review. *Surveys in Geophysics*, 35, 09 2014. doi: 10.1007/s10712-014-9284-0.
- Vincze, M., Bozóki, T., Herein, M., Borcia, I. D., Harlander, U., Horicsányi, A., Nyerges, A., Rodda, C., Pál, A., and Pálffy, J. The Drake Passage opening from an experimental fluid dynamics point of view. *Scientific Reports*, 11(1), 2021. ISSN 2045-2322. doi: 10.1038/s41598-021-99123-0. URL <https://dx.doi.org/10.1038/s41598-021-99123-0>.
- Vinther, B. M., Clausen, H. B., Johnsen, S. J., Rasmussen, S. O., Andersen, K. K., Buchardt, S. L., Dahl-Jensen, D., Seierstad, I. K., Siggaard-Andersen, M.-L., Steffensen, J. P., Svensson, A., Olsen, J., and Heinemeier, J. A synchronized dating of three Greenland ice cores throughout the Holocene. *Journal of Geophysical Research: Atmospheres*, 111 (D13), 2006. ISSN 0148-0227. doi: <https://doi.org/10.1029/2005JD006921>. URL <https://agupubs.onlinelibrary.wiley.com/doi/abs/10.1029/2005JD006921>.
- WAIS Divide Project Members,. Onset of deglacial warming in West Antarctica driven by local orbital forcing. *Nature*, 400:440–440.
- WAIS Divide Project Members,. Precise inter-polar phasing of abrupt climate change during the last ice age. *Nature*, 520(7549):661–665, 2015. ISSN 0028-0836. doi: 10.1038/nature14401. URL <https://dx.doi.org/10.1038/nature14401>.
- Wallace, J.M. and Hobbs, P.V. Climate Equilibria, sensitivity, and Feedbacks. pages 443–449. 2006.
- Watanabe, O, Jouzel, J., Johnsen, S., Parrenin, F., Shoji, H., and Yoshida, N. Homogeneous climate variability across East Antarctica over the past three glacial cycles. *Nature*, 422: 509–12, 05 2003. doi: 10.1038/nature01525.
- Wolff, E. W., Chappellaz, J., Blunier, T., Rasmussen, S. O., and Svensson, A. Millennial-scale variability during the last glacial: The ice core record. *Quaternary Science Reviews*, 29(21): 2828–2838, 2010. ISSN 0277-3791. doi: <https://doi.org/10.1016/j.quascirev.2009.10.013>. URL <https://www.sciencedirect.com/science/article/pii/S0277379109003588>.
- Zachos, J. C. 65 Ma to Present Trends, Rhythms, and Aberrations in Global Climate. 2007.

A. Ice Core Data Resolution

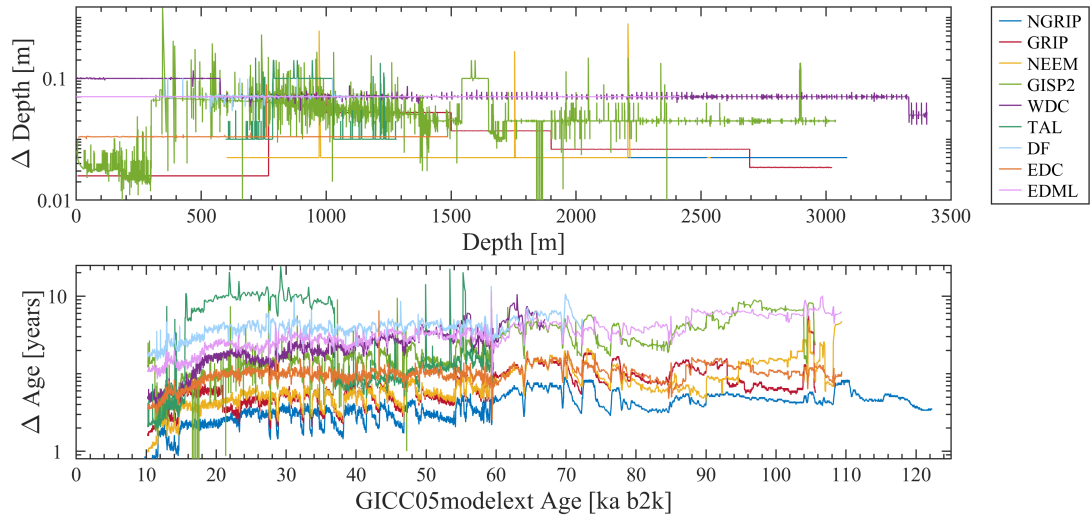


Figure A.1 | Ice core data resolution. Spatial resolution (Δ Depth in upper panel) and temporal resolution (Δ Age in lower panel) of the nine different ice core data sets for the last glacial period on a log-scale. The data are resampled in equidistance. The corresponding age is determined through linear interpolation on the NGRIP age scale. Thus, the age is based on the GICC05modelext ice chronology.

B. Stadial-Interstadial Transitions

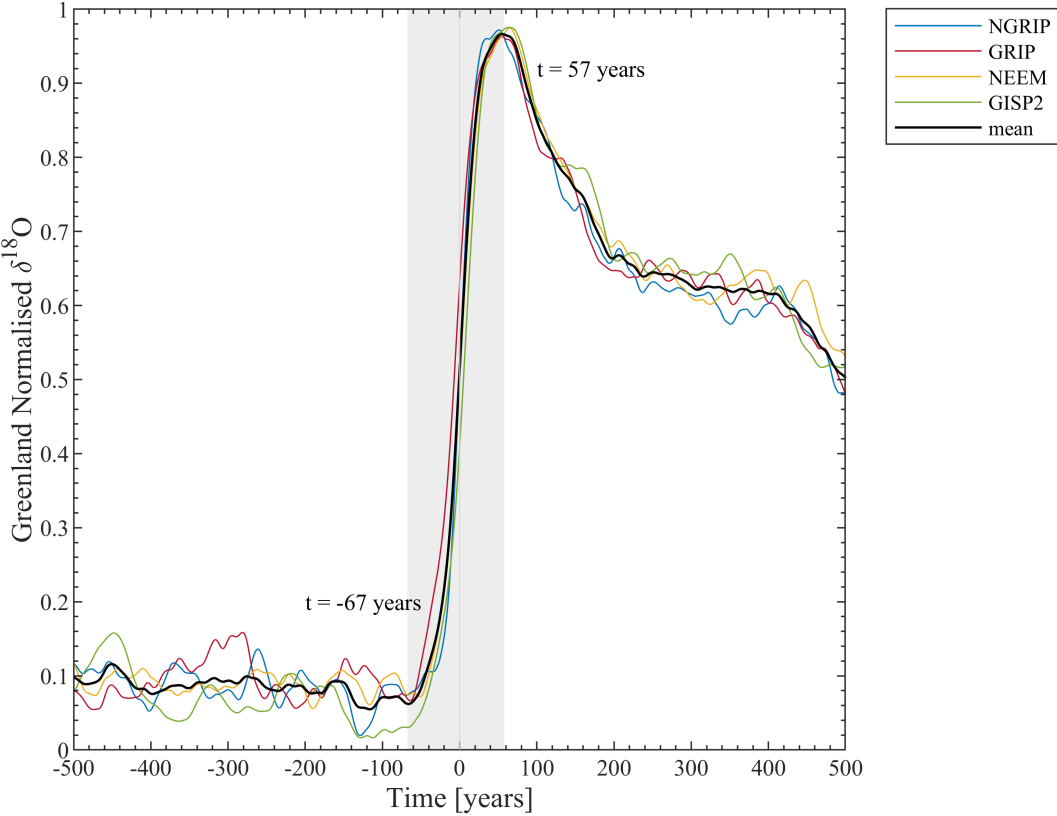


Figure B.1 | Average Greenland temporal difference between midpoint of stadial-interstadial transition, and initiation and termination of interstadials. Normalised stacked isotope records of 33 events in the period between 10 ka and 120 ka b2k of the four Greenlandic ice cores including their mean. Based on the minimum and maximum in the common climate signal (black) before and after the transition, respectively, the onset defined as the midpoint is validated. Note that the profiles are smoothed and normalised.

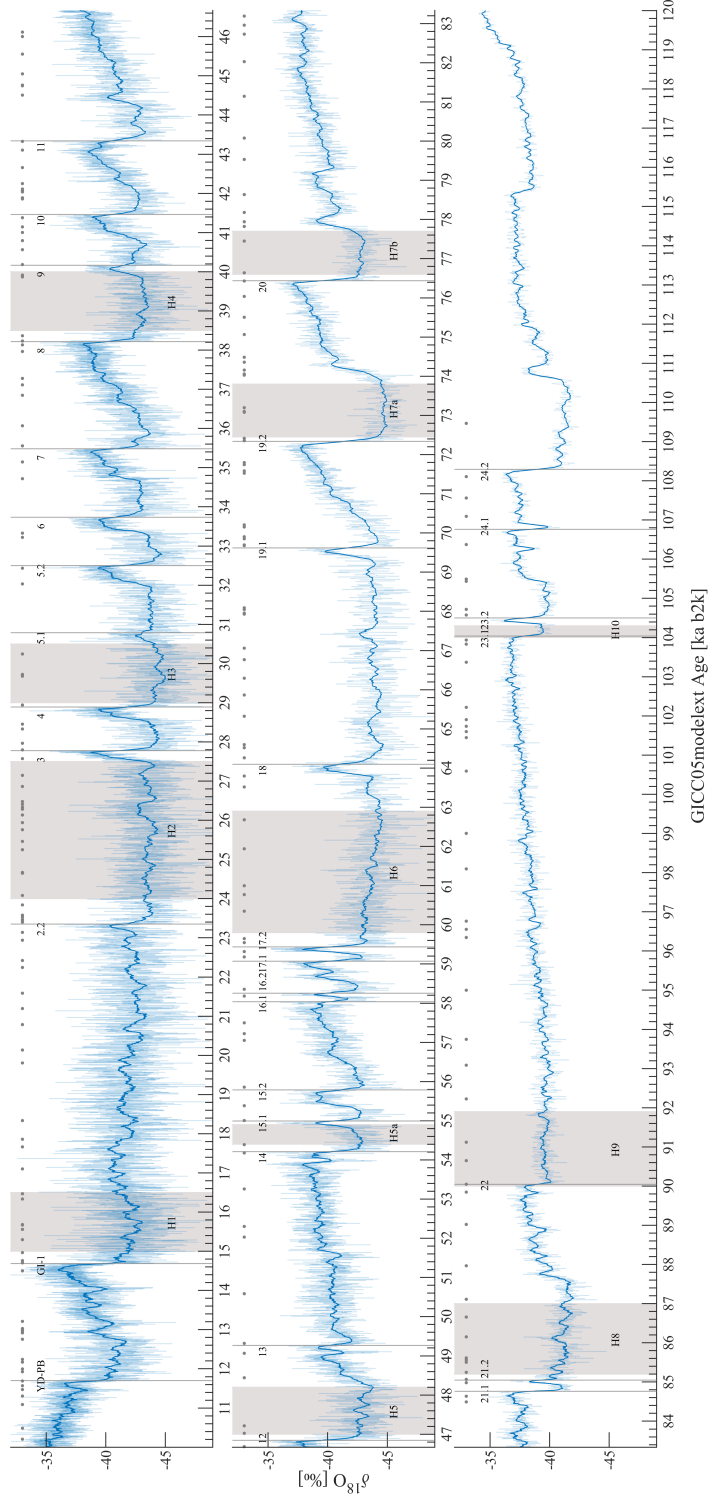


Figure B.2 | Climate signal during the Last Glacial Period. Stable water isotope signal from the Greenlandic NGRIP ice core for the last glacial period (10-120 ka b2k) on the GICC05modelext timescale including 33 Greenland interstadials and twelve Heinrich Events (H1-H10) which duration and timing are marked by the grey shading. The onset of the GIs as determined in this work is indicated by the vertical line. Grey dots represent bipolar volcanoes, which signal is found in at least one Greenlandic and one Antarctic ice core.

C. Amplitude of DO Events

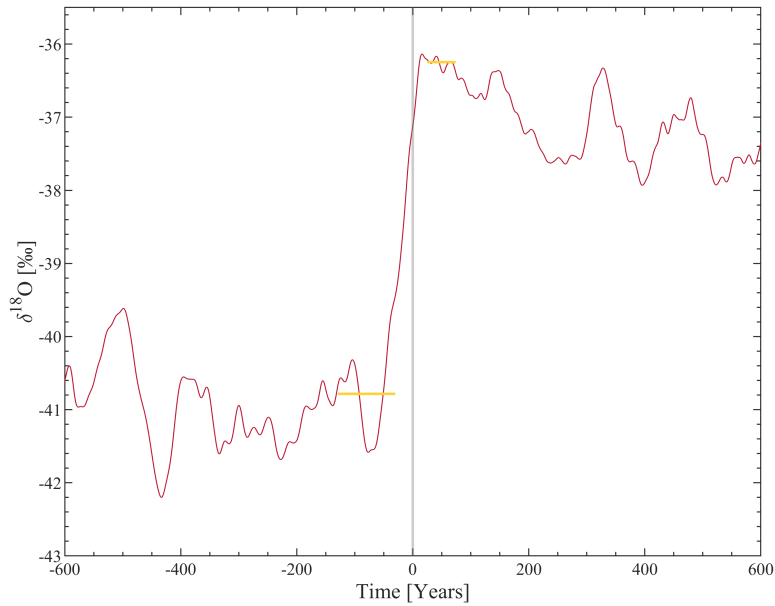


Figure C.1 | Determining the amplitude of a single Dansgaard-Oeschger event. Ascertaining the change in $\delta^{18}\text{O}$ over the course of a transition from stadial to interstadial for GI-12c in the GRIP isotope record. The midpoint of the transition is defined as $t = 0$. Pre-transitional (stadial) 100-year averages and post-transitional (interstadial) 50-year averages starting $t = \pm 30$ years respectively, are marked as horizontal bars (yellow) and determine the change, $\Delta \delta^{18}\text{O}$, across the Greenland abrupt warming event as presented in Figure 4.8.

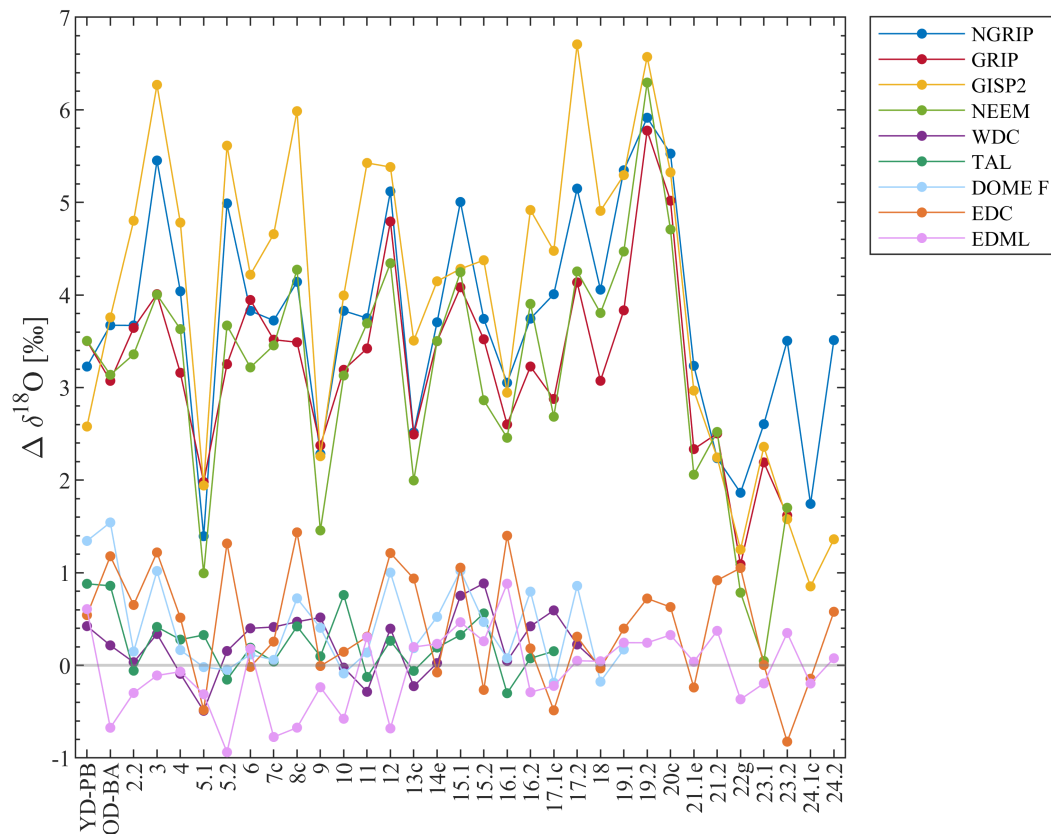


Figure C.2 | Amplitude of all stadial-interstadial transitions in the individual ice cores. Change in $\delta^{18}\text{O}$ [‰] over the course of each Greenland abrupt warming for the individual ice cores based on pre-transitional 100-year averages and 50-year post-transitional averages. Overall warming is designated by $\Delta \delta^{18}\text{O} > 0$, while $\Delta \delta^{18}\text{O} < 0$ indicate an overall cooling across the transition. See Figure C.1 in Appendix for an example of the determination of $\Delta \delta^{18}\text{O}$.

D. Uncertainty Estimations

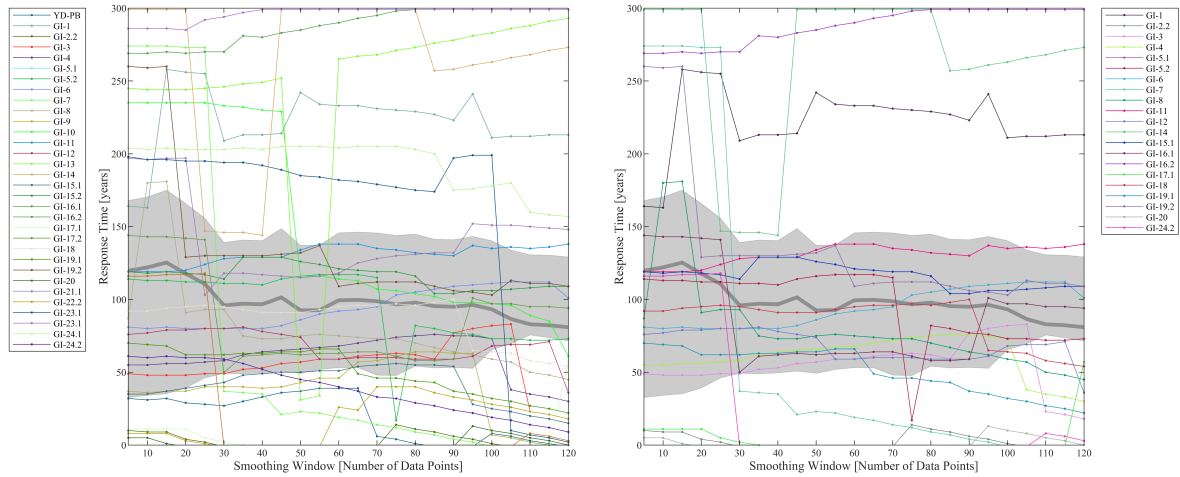


Figure D.1 | Antarctic response time depending on smoothing the data for individual DO events. Break points in the Antarctic $\delta^{18}\text{O}$ signal associated with Northern Hemisphere abrupt warming defined as the maximum occurring within 300 years after the transition ($t = 0\text{-}300$ years). The grey line marks the average response time of all events for each chosen smoothing window (left panel). The shading is based on $\pm \frac{1}{2} \sigma$. In the right panel, events without a distinct post-transitional cooling trend but with dominating noise level are excluded from the mean.

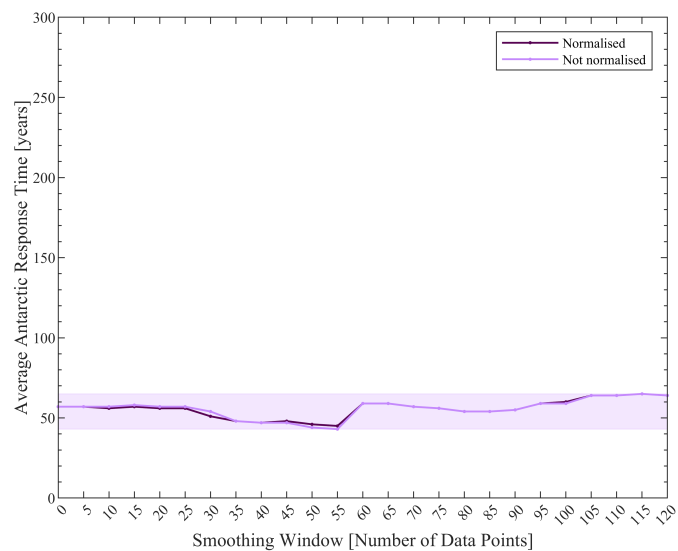


Figure D.2 | Antarctic response time to Greenland abrupt warming. Average response time based on break points in the normalised and non-normalised Antarctic stack record for different smoothing intervals. Break points are defined as the maximum $\delta^{18}\text{O}$ -signal within 300 years after the transition ($t = 0\text{-}300$ years). The shading describes the spread between the minimum and maximum determined response time from both methods of 16 years.

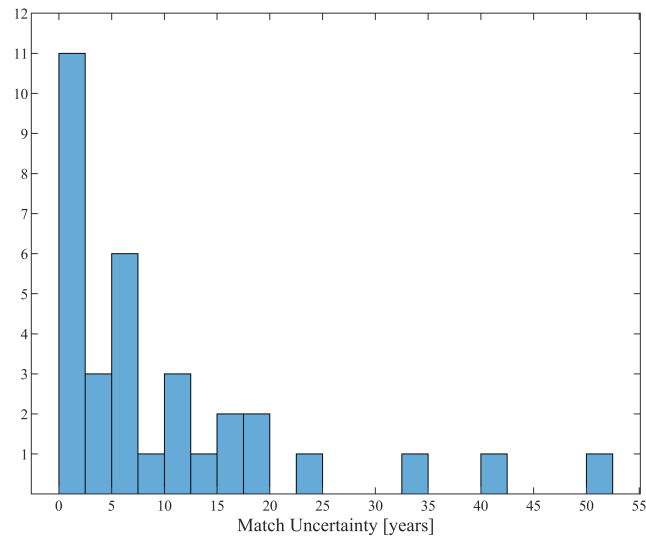


Figure D.3 | Uncertainty of bipolar volcanic synchronisation. The relative uncertainty of the bipolar matching to the Greenland Interstadials is defined as 10% of the temporal distance to the closest volcanic matchpoint (Svensson et al. (2020)).

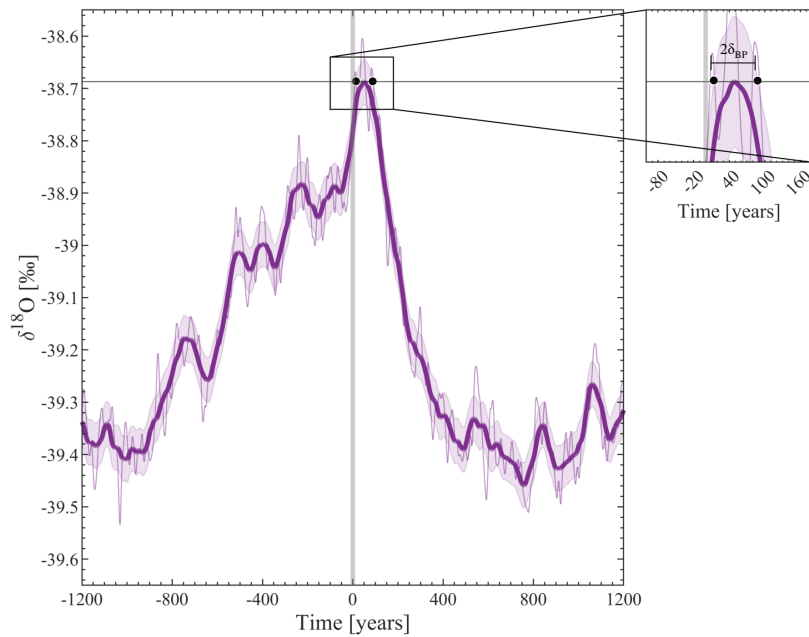


Figure D.4 | Determining the uncertainty on the Antarctic Breakpoint. Uncertainty arising from the determination of the breakpoint in the WDC stacked isotope profiles synchronous with DO events. Uncertainty is defined as half the temporal distance between the estimated maximum and the same value within half the standard deviation of the residuals ($\pm \frac{1}{2}\sigma$) as described in chapter 3.5.

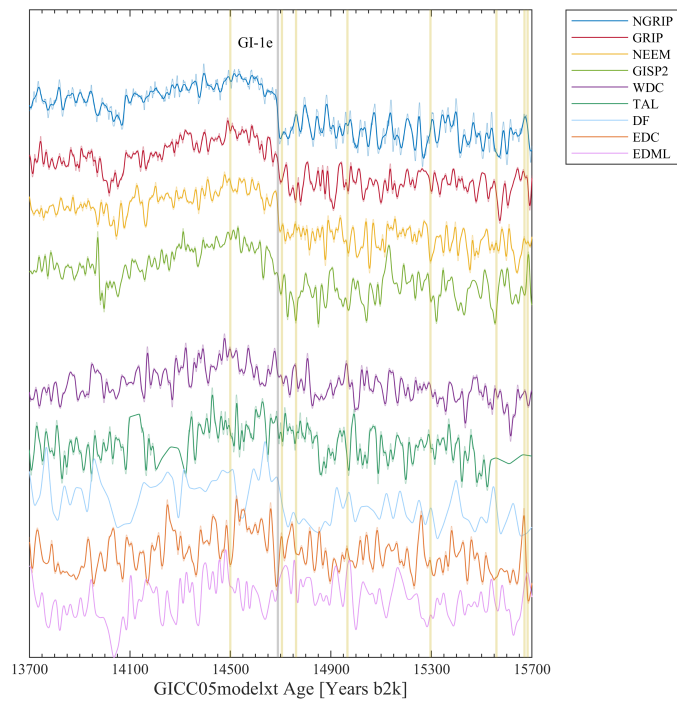
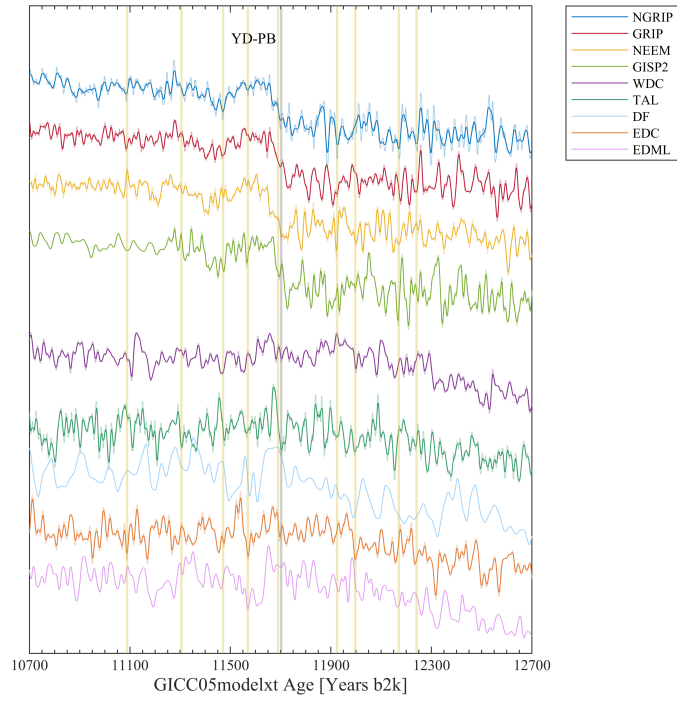
Table D.1: Uncertainty on the breakpoints. Uncertainties arising from the breakpoint determination as described in Section 3.4 for the individual ice cores given and respective classification in years. See Table 3.2 for the events representing the different classifications. As EDML does not show a clear maximum after the stadial-interstadial transition it is excluded from the determination. All uncertainties contribute equally to the mean, defining the uncertainty on the breakpoint for Antarctica, δ_{BP} (Table 3.3).

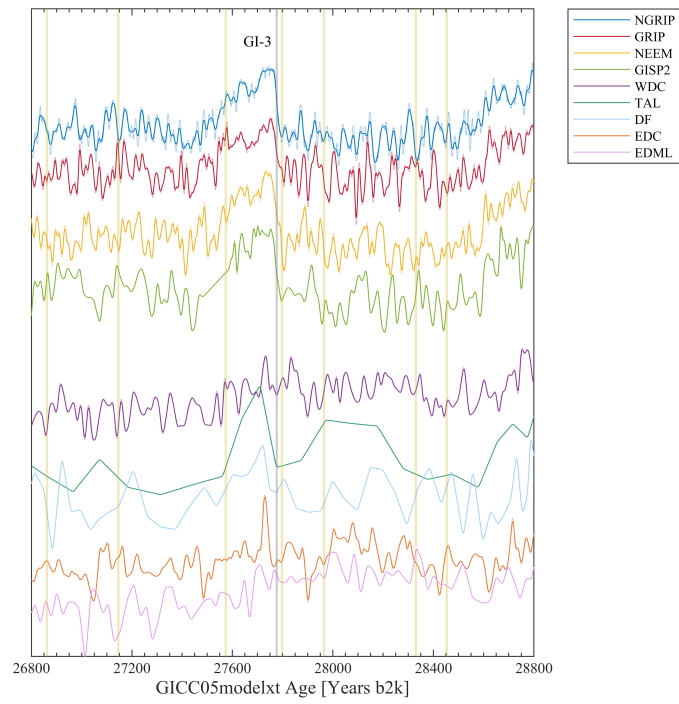
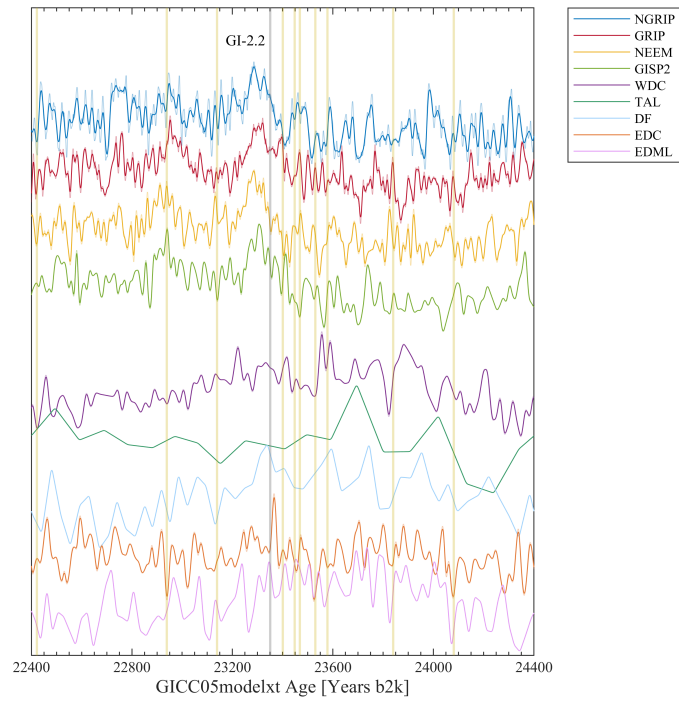
	WDC (yr)	TAL (yr)	Dome F (yr)	EDC (yr)	EDML (yr)
Entire last glacial	37	47	35	37	-
First half	-	-	51	62	-
Second half	37	47	37	31	-
Minor DOs	38	65	66	37	-
Major DOs	60	46	24	74	-

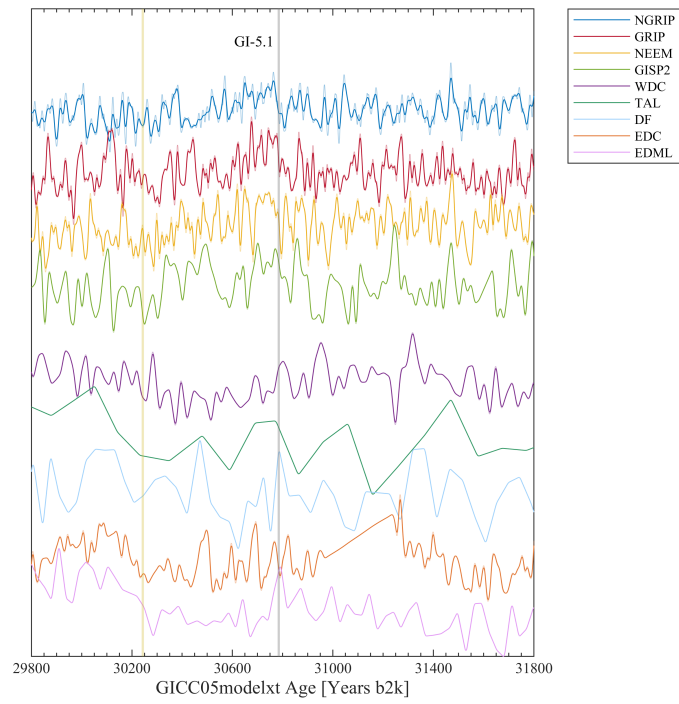
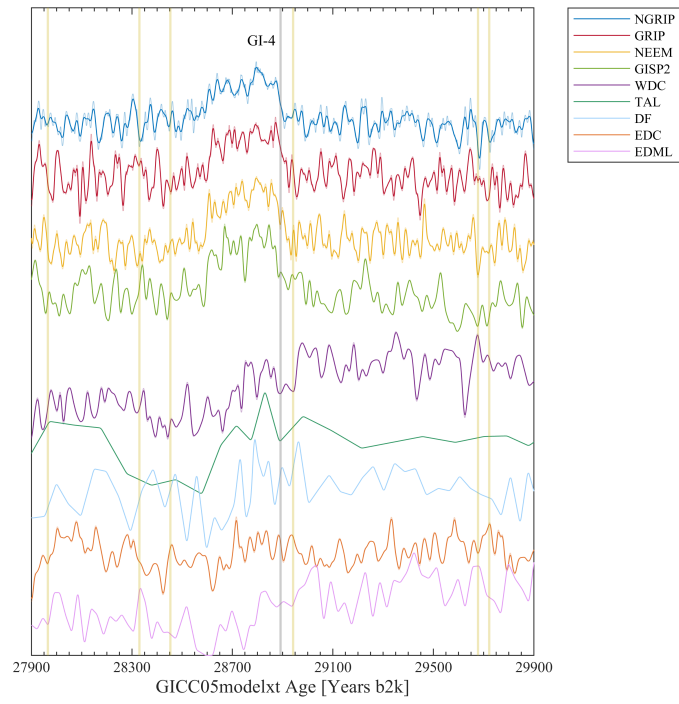
E. Climate Across DO Events

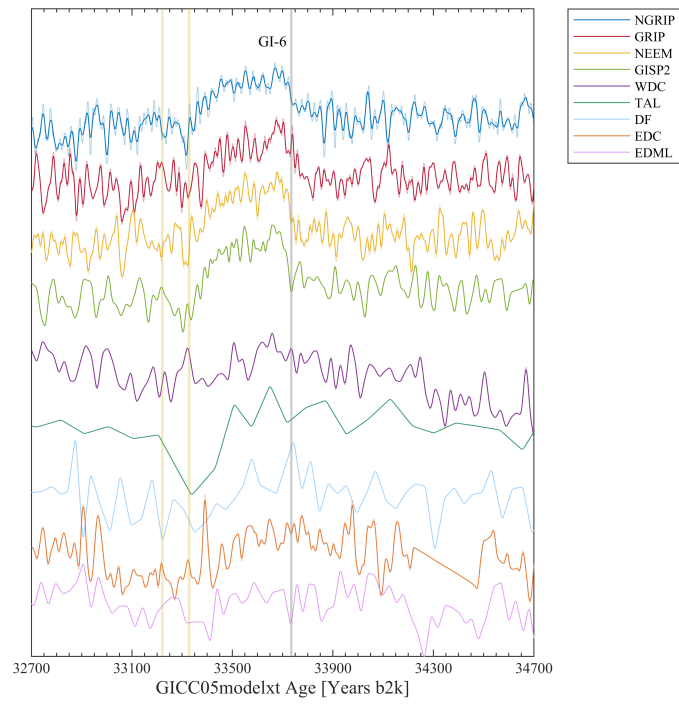
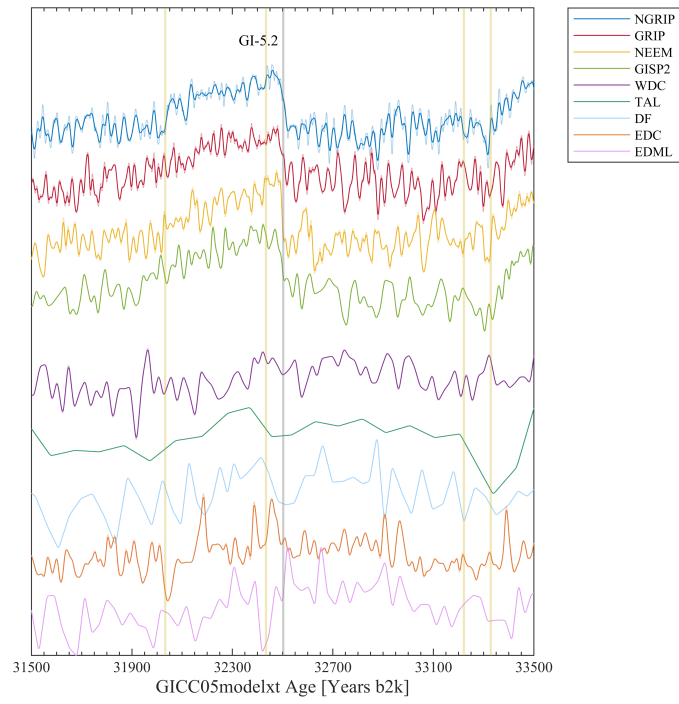
Table E.1: Timing of Dansgaard-Oeschger event onsets. Depths [m] of the Greenland interstadial onsets in the NGRIP, GRIP, GISP2, NEEM, WDC, TAL, DF, EDC, and EDML ice cores based on volcanic synchronisation. The onsets are defined as midpoints of the stadial-interstadial transition in the NGRIP $\delta^{18}\text{O}$ profile and linked to the other records applying bipolar volcanic matchpoints as described in Section 2.2.3.3 by Anders Svensson. Corresponding GICC05modelext ages of the onsets are given with reference to the year 2000 CE. "Distance" describes the temporal distance of the onset to the closest matchpoint, with negative values indicating the matchpoint occurring earlier in time than the corresponding transition onset. This distance is used to determine the relative uncertainty of the volcanic matching as 10% of the distance to the nearest volcanic matchpoint, accounting for an annual layer counting error of 5% for all the different ice cores Svensson et al. (2020). YD-PB refers to the Younger Dryas-Preboreal transition (glacial-interglacial transition or onset of the Holocene).

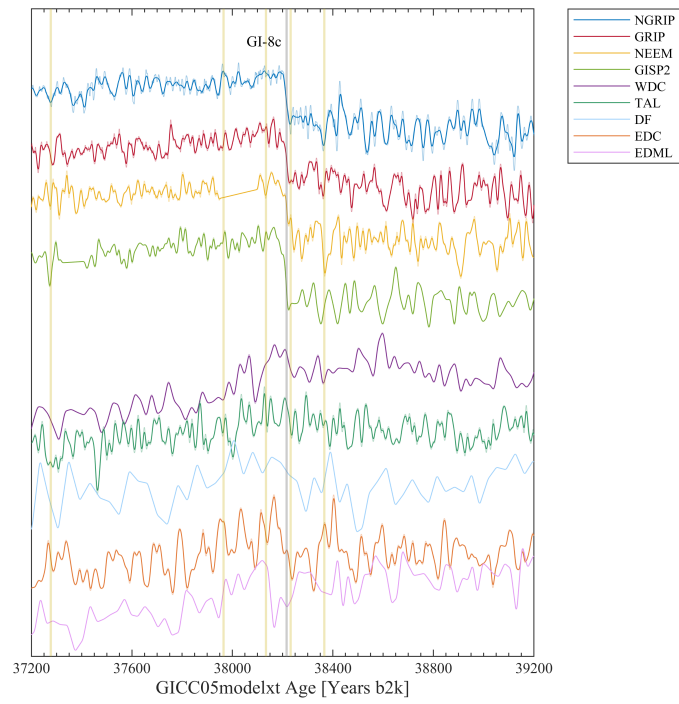
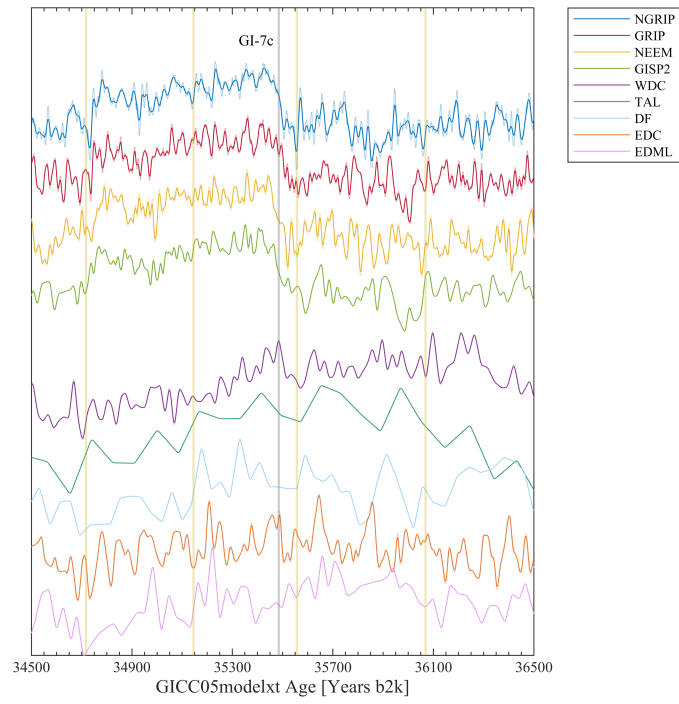
Interstadial	NGRIP	GRIP	GISP2	NEEM	WDC	TAL	DF	EDC	EDML	Age (b2k)	Distance (yr)	Uncertainty (yr)
YD-PB	1492.40	1623.81	1677.26	1419.78	1966.68	672.31	356.48	357.36	678.08	11702	12	1
GI-1e	1604.50	1753.18	1797.64	1489.19	2238.58	765.59	423.65	421.49	792.55	14689	-17	2
GI-2.2	1793.45	1950.77	1986.24	1598.17	2597.60	885.81	556.39	539.11	1021.86	23350	-46	5
GI-3	1869.00	2025.33	2056.57	1640.94	2742.08	928.54	611.49	586.05	1123.55	27777	-20	2
GI-4	1891.35	2045.88	2076.40	1654.16	2783.02	941.57	626.34	598.42	1146.04	28891	-48	5
GI-5.1	1919.55	2070.27	2100.02	1671.55	2835.58	959.63	650.55	619.10	1179.13	30784	501	50
GI-5.2	1951.70	2098.86	2127.56	1690.07	2874.06	977.02	671.92	637.18	1207.29	32502	70	7
GI-6	1974.45	2118.50	2147.00	1703.15	2902.93	990.70	687.98	650.62	1229.79	33735	407	41
GI-7c	2009.55	2148.74	2177.84	1723.22	2948.93	1011.37	710.59	670.21	1260.95	35484	-73	7
GI-8c	2069.90	2200.21	2232.05	1758.83	3012.43	1046.30	747.65	702.34	1312.70	38215	-18	2
GI-9	2099.70	2223.67	2256.04	1777.54	3057.67	1072.75	776.28	726.16	1354.33	40165	-15	1
GI-10	2124.05	2243.28	2276.36	1791.25	3085.83	1089.82	793.21	741.19	1378.58	41461	87	9
GI-11	2157.50	2270.76	2303.94	1810.12	3123.68	1113.76	817.19	762.41	1412.22	43341	14	1
GI-12c	2221.95	2323.97	2358.78	1846.27	3188.00	1156.57	858.57	800.56	1465.78	46843	-177	18
GI-13c	2256.60	2350.28	2385.29	1865.14	3231.10	1182.98	889.57	827.98	1506.50	49264	-55	5
GI-14e	2345.35	2420.66	2454.70	1911.84	3307.11	1223.14	948.36	882.66	1583.92	54212	34	3
GI-15.1	2355.20	2427.88	2461.39	1917.42	3317.77	1228.75	957.92	891.19	1596.47	54992	-14	1
GI-15.2	2366.15	2435.93	2469.03	1923.24	3326.14	1234.05	967.68	900.10	1608.86	55787	-71	7
GI-16.1c	2398.70	2460.17	2491.90	1940.25	3347.52	1248.65	995.27	925.24	1643.41	58036	-153	15
GI-16.2	2402.20	2462.71	2494.29	1942.03	3349.48	1250.09	998.23	927.97	1647.16	58256	-106	11
GI-17.1c	2414.85	2472.07	2503.04	1948.38	3356.72	1255.65	1008.73	937.93	1660.58	59069	-123	12
GI-17.2	2420.35	2476.15	2506.86	1951.11	3359.41	1257.39	1012.47	941.44	1665.45	59435	-241	24
GI-18	2465.80	2507.66	2535.60	1976.43	3387.42		1076.39	996.98	1743.63	64096	-169	17
GI-19.1	2507.55	2536.20	2563.19	1996.52			1125.16	1039.88	1806.31	69616	-72	7
GI-19.2	2535.95	2557.76	2584.27	2009.69			1149.56	1063.75	1842.97	72339	-20	2
GI-20c	2579.10	2585.42	2612.23	2029.05			1190.50	1102.99	1897.70	76438	7	1
GI-21.1e	2687.35	2648.66	2676.28	2086.19			1294.13	1202.09	2010.15	84764	137	14
GI-21.2	2691.00	2650.68	2678.57	2088.10			1298.55	1206.20	2013.93	85050	-22	2
GI-22g	2746.60	2679.16	2704.38	2128.86			1358.68	1262.46	2071.10	90046	-2	0
GI-23.1	2891.50	2751.57	2749.11	2186.90			1497.29	1396.82	2189.92	104037	101	10
GI-23.2	2896.40	2752.93	2754.52	2188.05			1501.50	1401.42	2192.75	104501	-74	7
GI-24.1	2920.60			2195.13			1526.30	1423.36	2208.81	106760	-332	33
GI-24.2	2938.30			2203.94			1545.06	1441.85	2221.16	108292	184	18

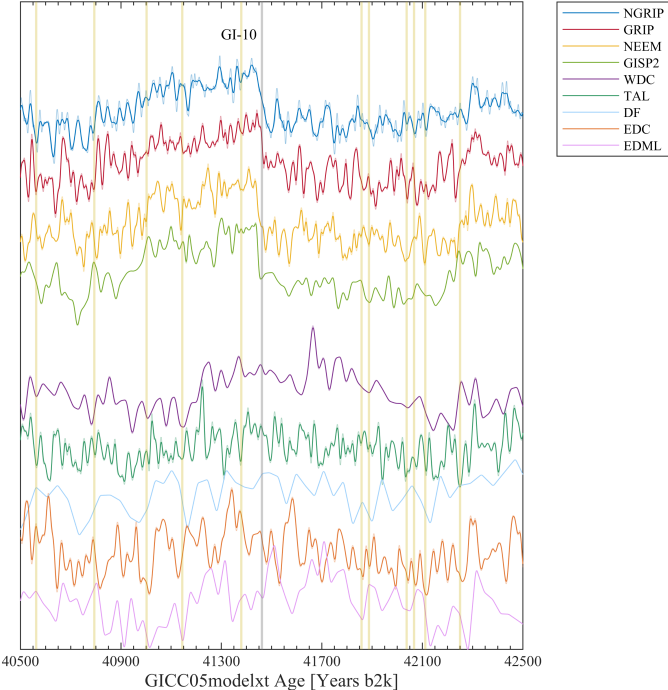
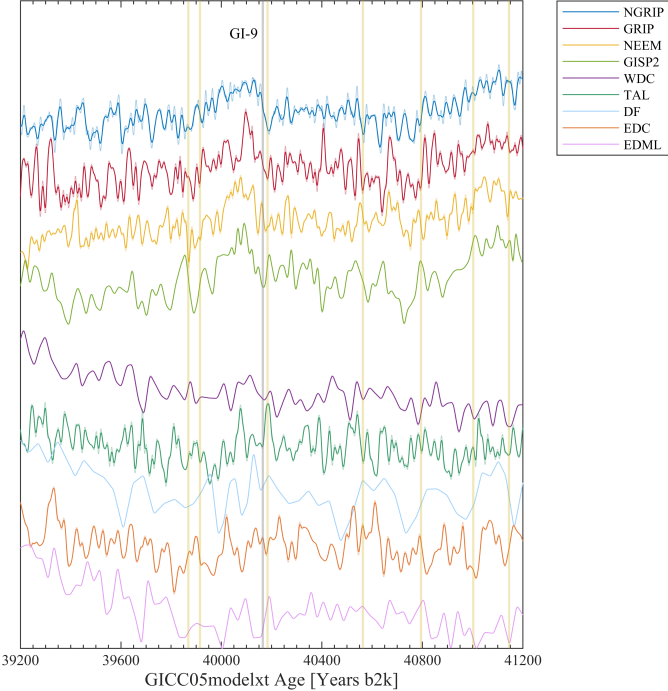


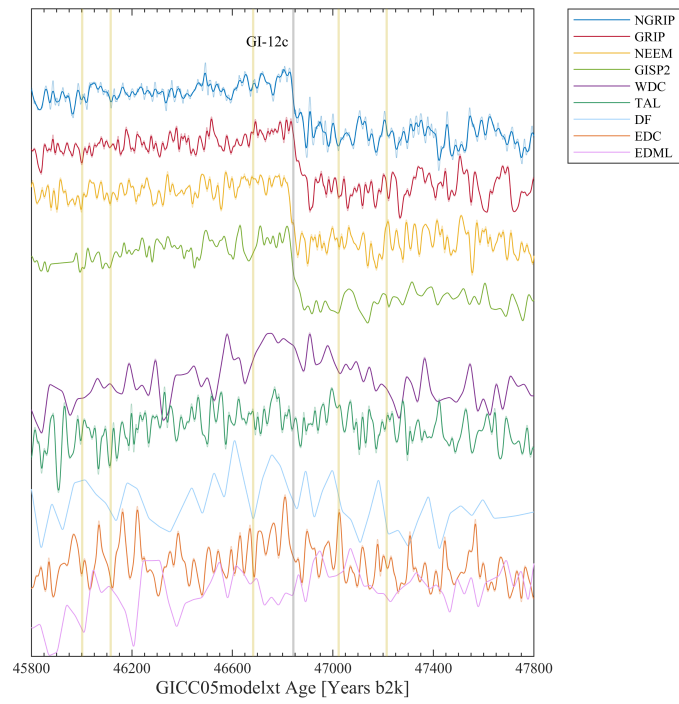
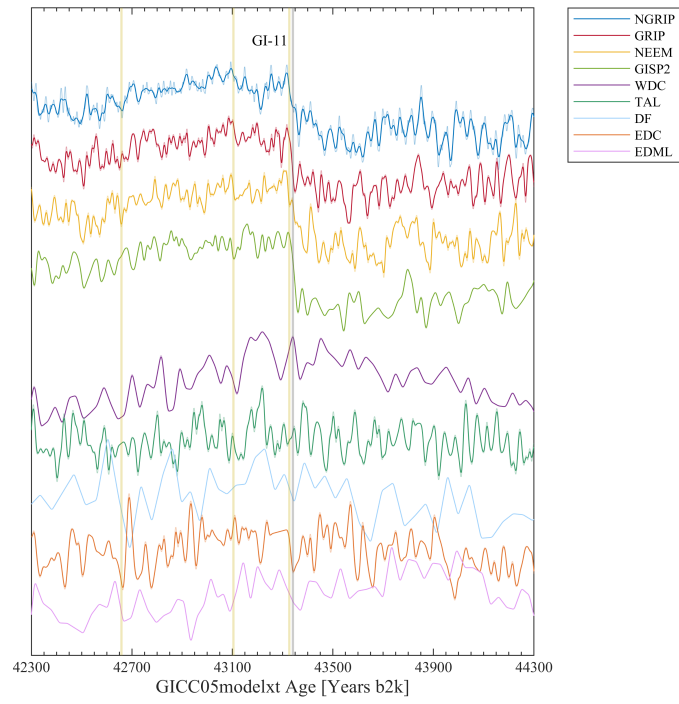


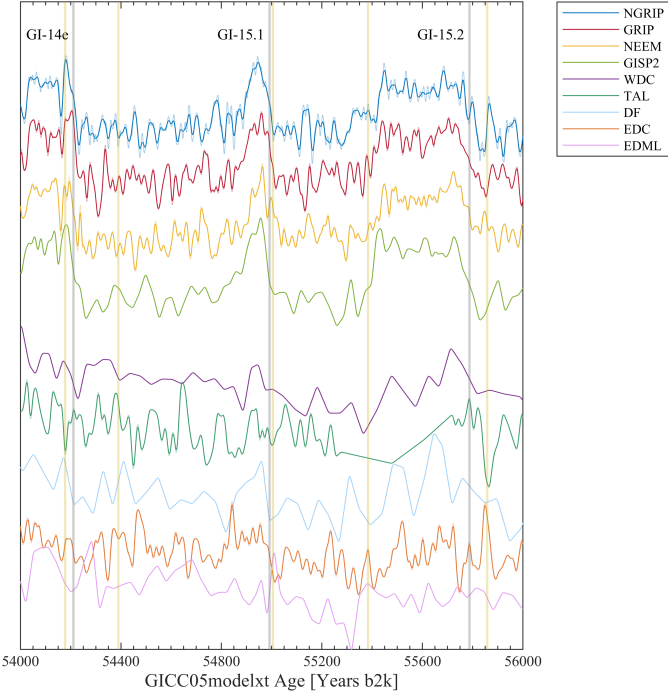
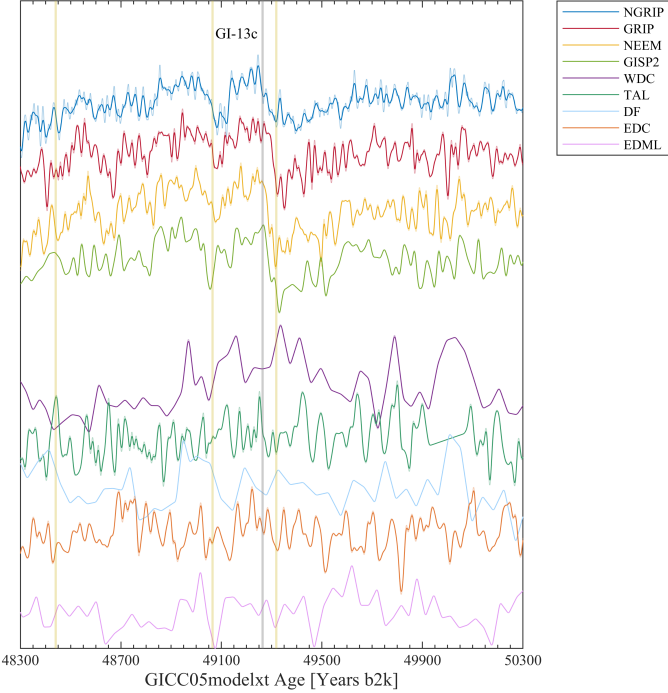


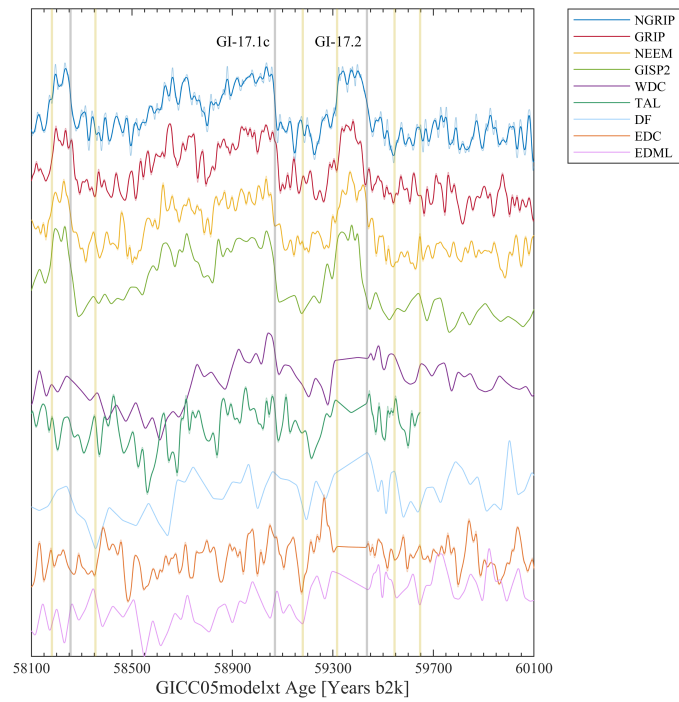
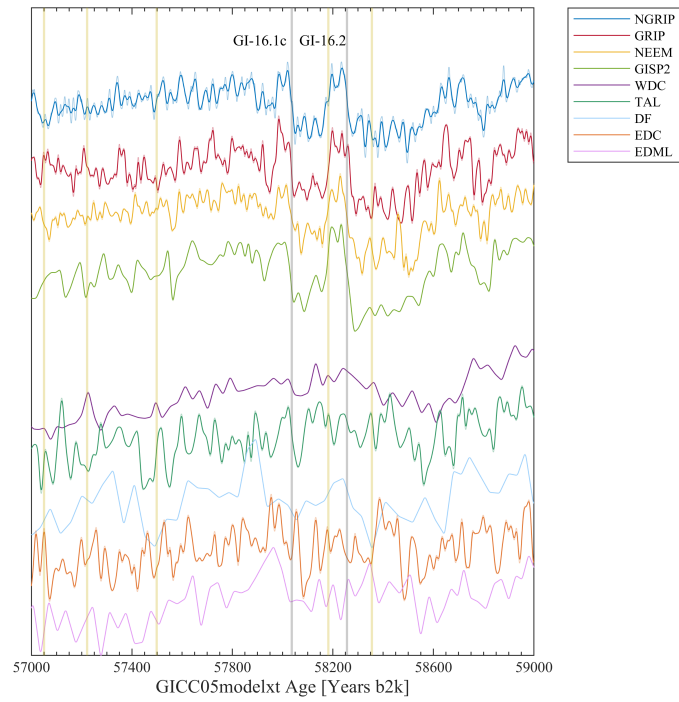


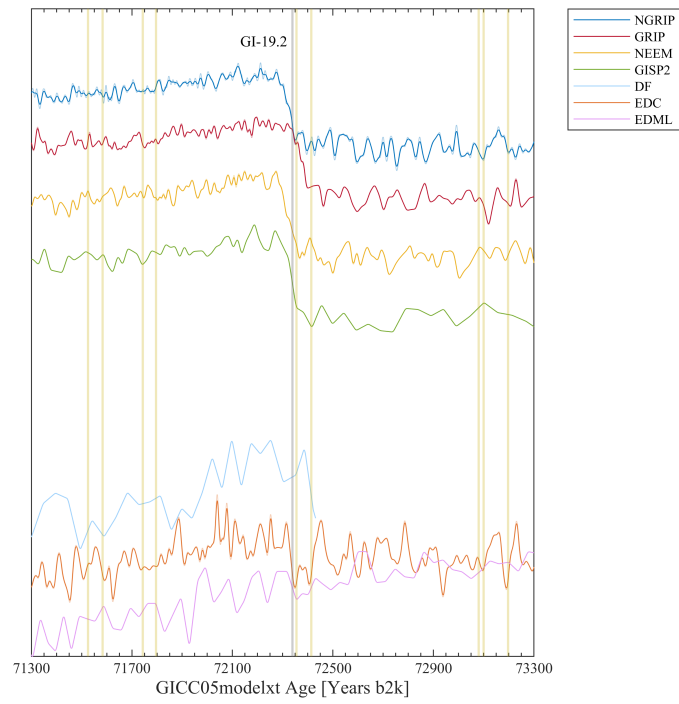
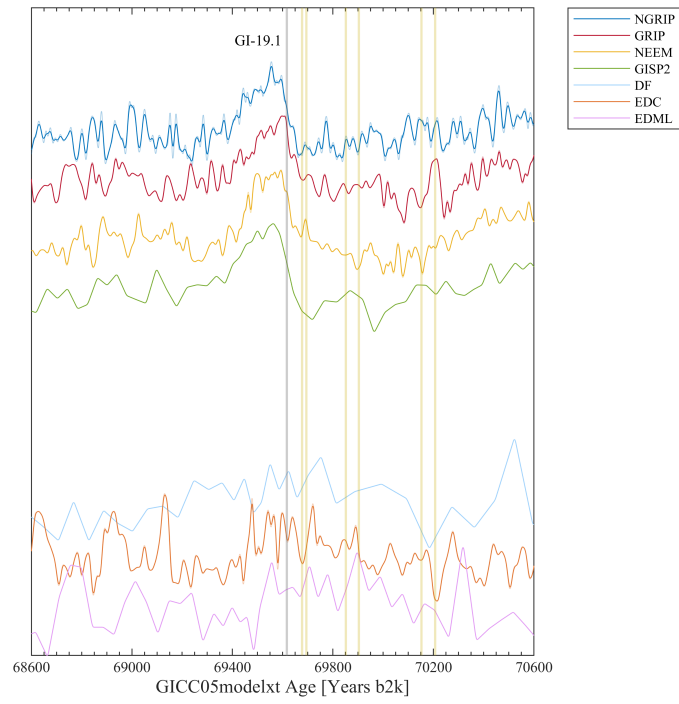


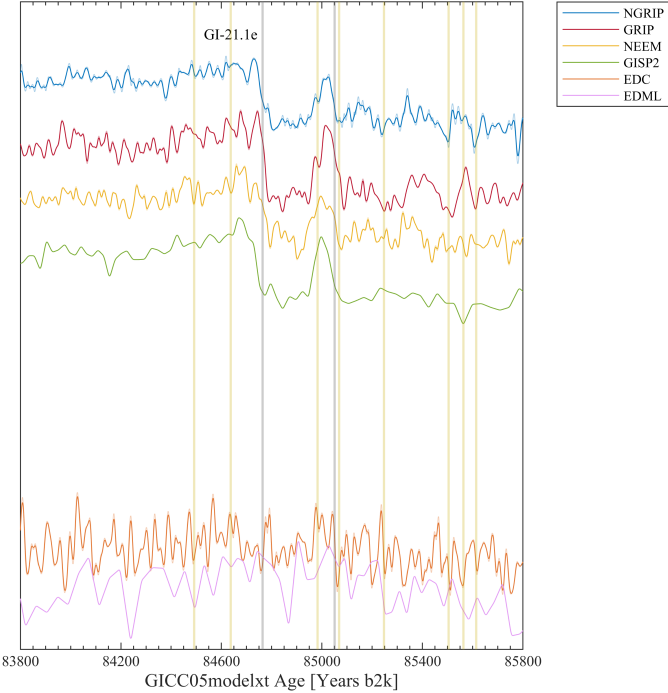
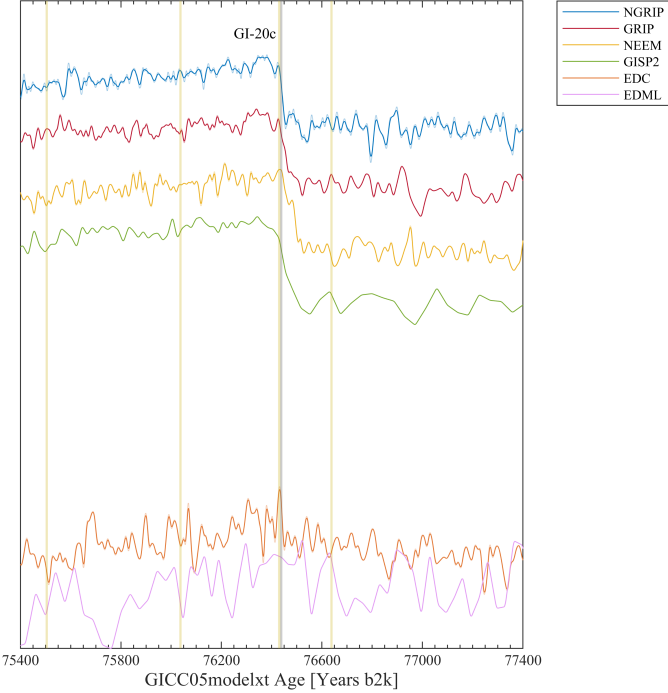


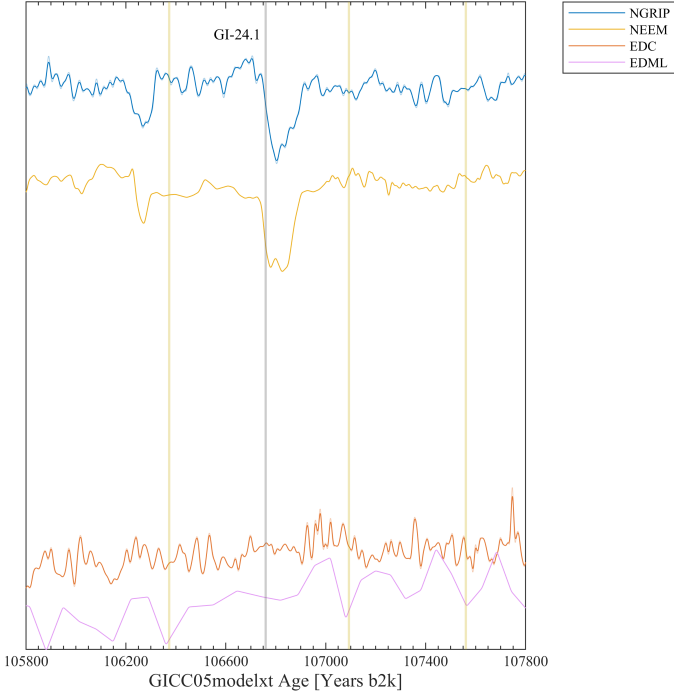
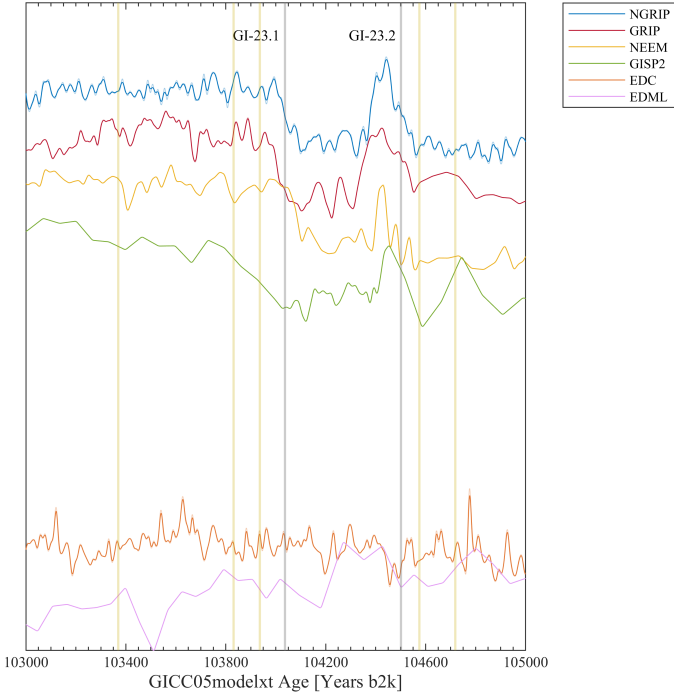












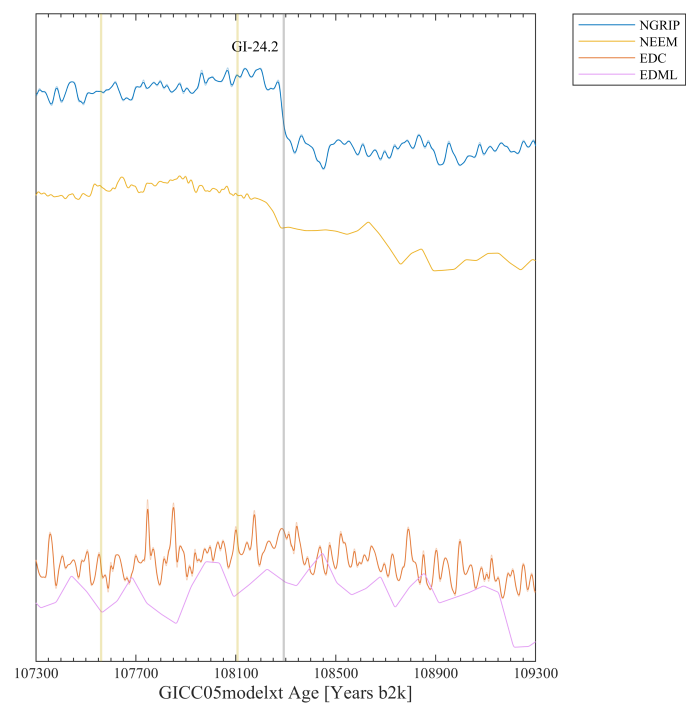


Figure E.1 | Interhemispherical climate signal across Dansgaard-Oeschger events. Normalised $\delta^{18}\text{O}$ records across the onsets of the Northern Hemisphere abrupt warming events (grey vertical lines) for the different Greenlandic and Antarctic ice cores aligned on the GICC05modelext timescale using bipolar volcanic synchronisation. 'DF' represents the ice core from Dome F. The applied bipolar volcanic matchpoints are marked as yellow vertical lines. Note that the record is plotted running backwards in time.

F. Bipolar Phasing Estimates

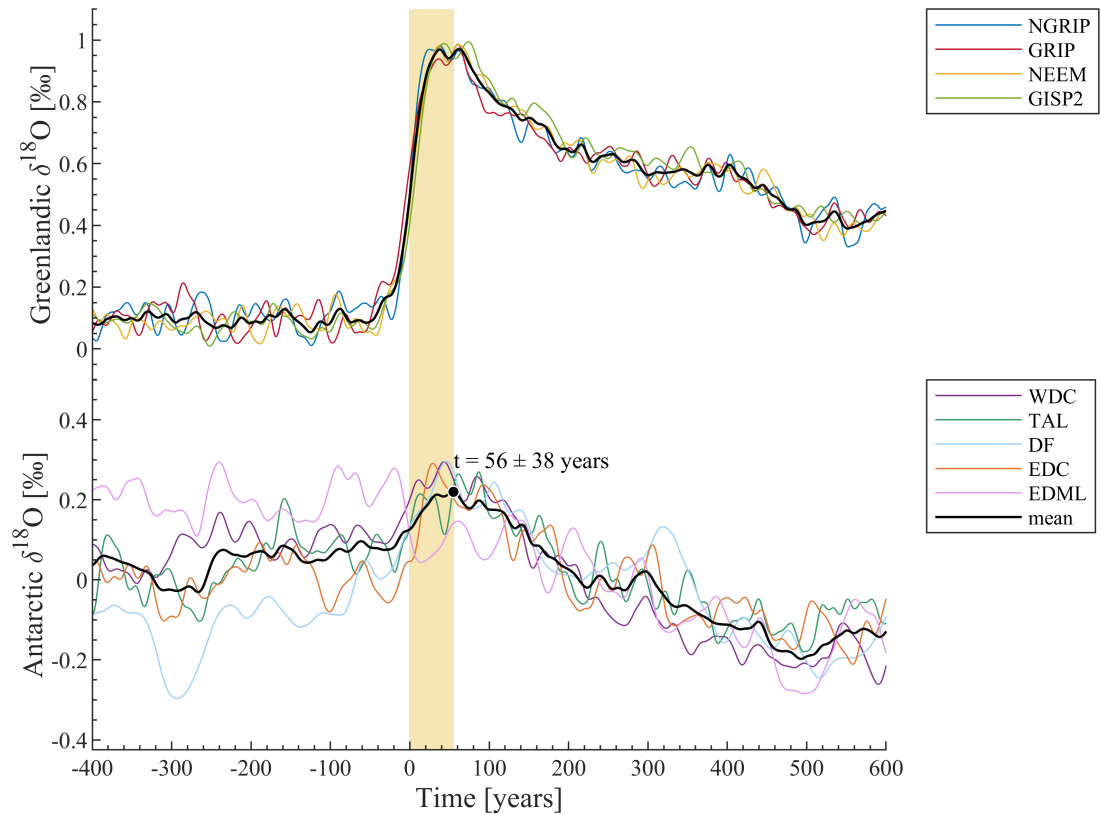


Figure F.1 | Bipolar phasing during the second half of the last ice age. Normalised stacks of the isotopic records across the Greenland interstadials YD-PB until and including GI-18, with $t = 0$ marking the onset determined in the NGRIP $\delta^{18}\text{O}$ profile as listed in Table 4.1. The breakpoint is defined as the maximum in the Antarctic three-core stack at $t = 56 \pm 38$ years and marks the temporal delay of the Antarctic cooling relative to Northern Hemisphere abrupt warming for the whole last glacial period. See Table 3.2 for the number of averaged DO events for Greenland and Antarctica, respectively.

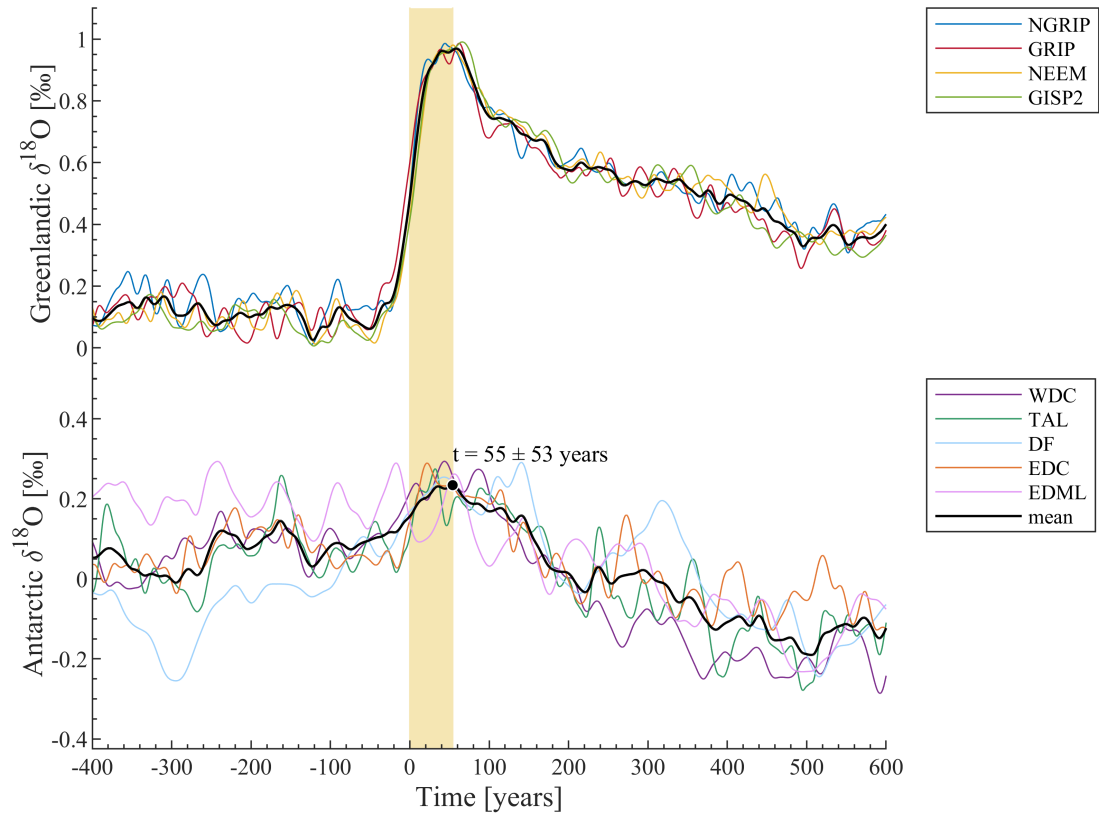


Figure F.2 | Bipolar phasing for minor Dansgaard-Oeschger events. Normalised stacks of the isotopic records across the smaller Greenland interstadials, with $t = 0$ marking the onset determined in the NGRIP $\delta^{18}\text{O}$ profile as listed in Table 4.1. The breakpoint is defined as the maximum in the Antarctic three-core stack at $t = 55 \pm 53$ years and marks the temporal delay of the Antarctic cooling relative to Northern Hemisphere abrupt warming for these smaller events. Note that the records from EDML and Dome F are offset for better vividness. The respective DO events included in the stacks can be seen in Table 3.2.

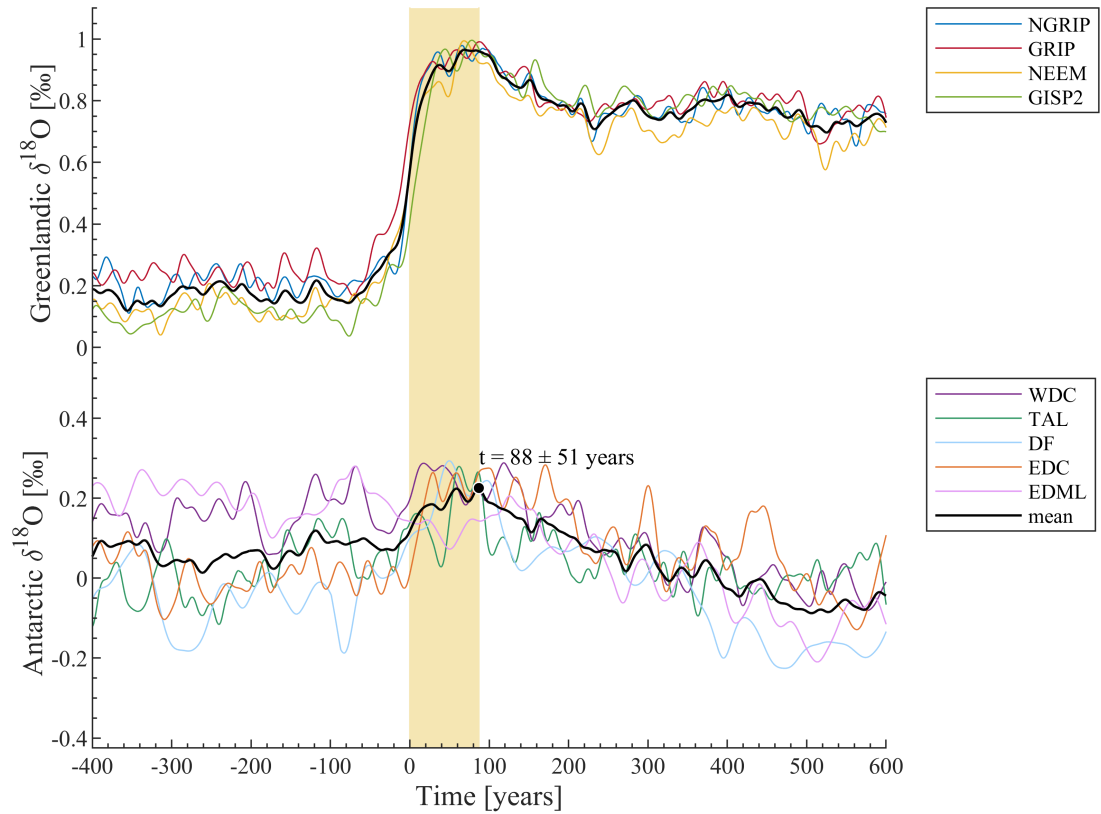


Figure F.3 | Bipolar phasing for major Dansgaard-Oeschger events. Normalised stacks of the isotopic records across the major Greenland interstadials following a Heinrich stadial, with $t = 0$ marking the onset determined in the NGRIP $\delta^{18}\text{O}$ profile as listed in Table 4.1. The breakpoint is defined as the maximum in the Antarctic three-core stack at $t = 88 \pm 51$ years and marks the temporal delay of the Antarctic cooling relative to Northern Hemisphere abrupt warming for these smaller events. Note that the records from EDML and Dome F are offset for better vividness. The respective DO events included in the stacks can be seen in Table 3.2

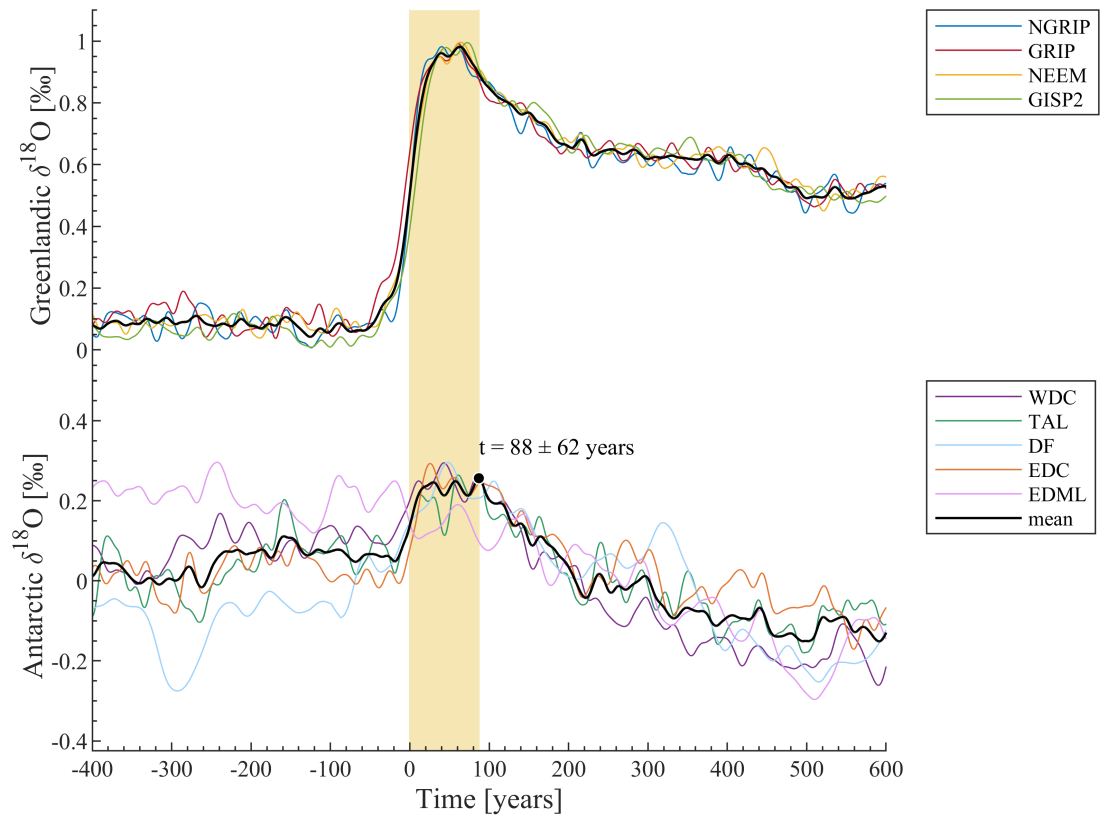
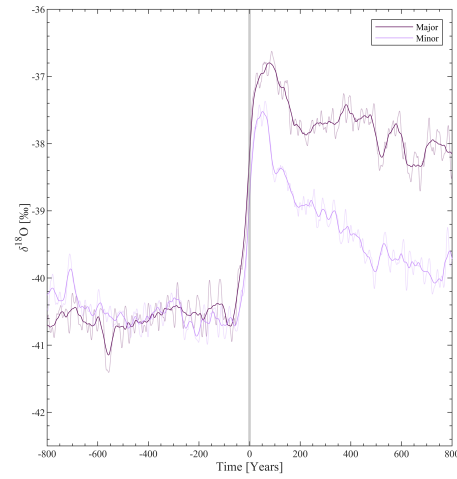
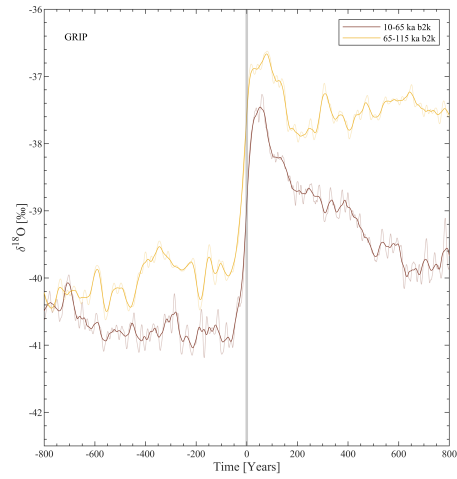
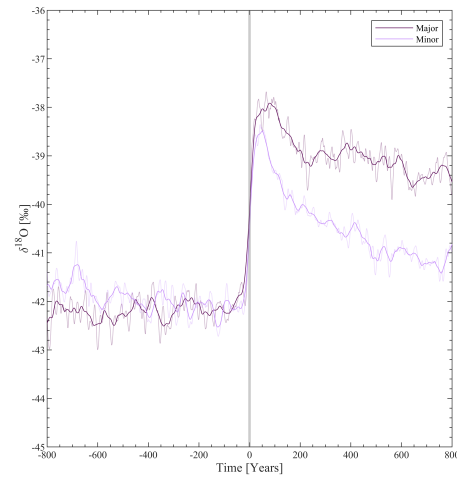
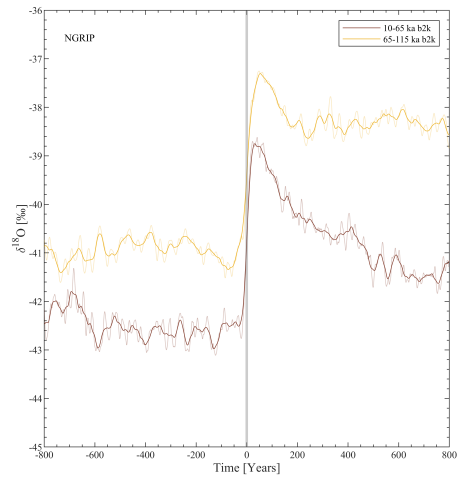
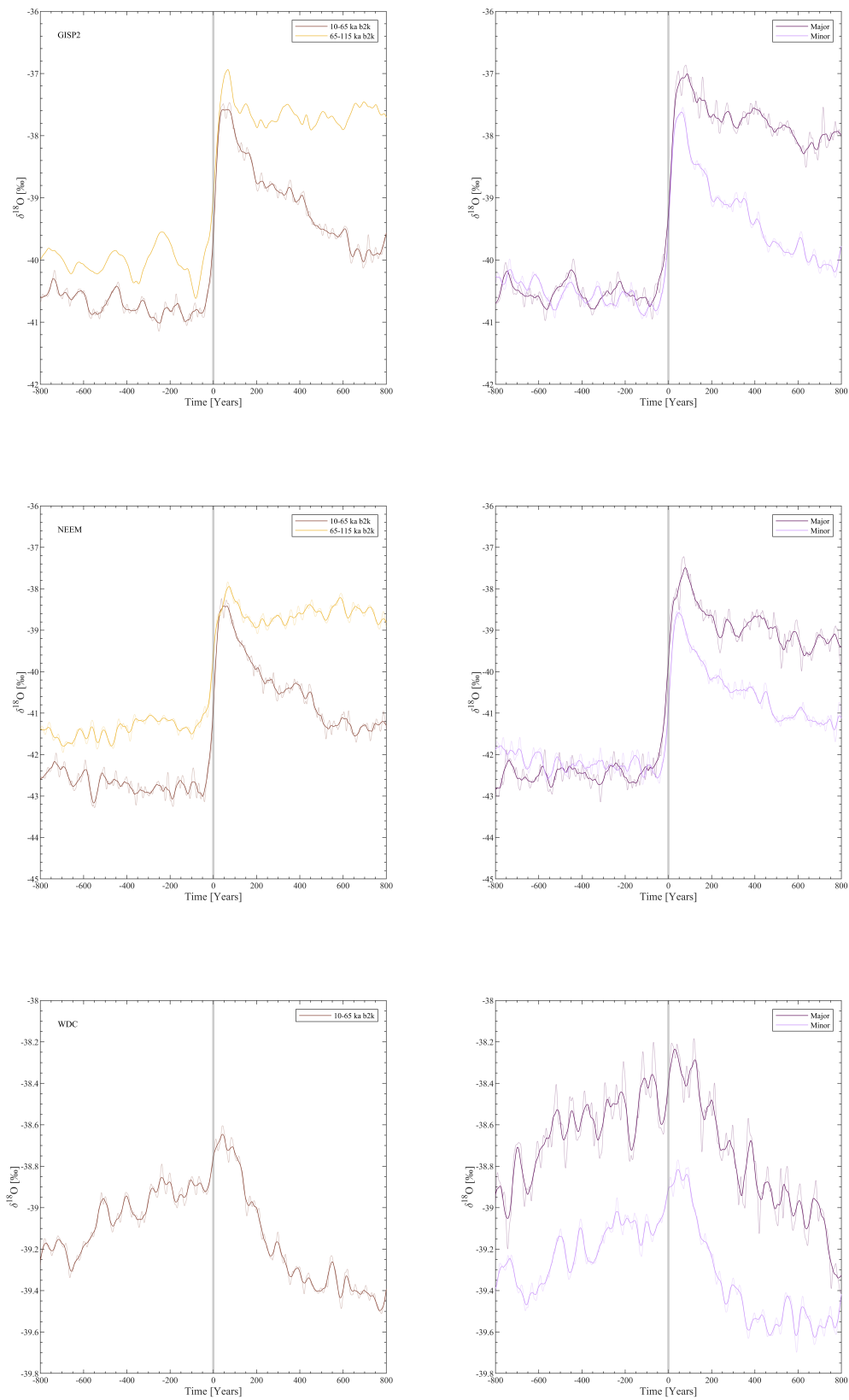


Figure F.4 | Bipolar phasing excluding EDML and Dome F. Normalised stacks of the isotopic records across the Greenland interstadials YD-PB until and including GI-24.2, with $t = 0$ marking the onset determined in the NGRIP $\delta^{18}\text{O}$ profile as listed in Table 4.1. The breakpoint is defined as the maximum in the Antarctic three-core stack at $t = 88 \pm 62$ years and marks the temporal delay of the Antarctic cooling relative to Northern Hemisphere abrupt warming for the whole last glacial period.

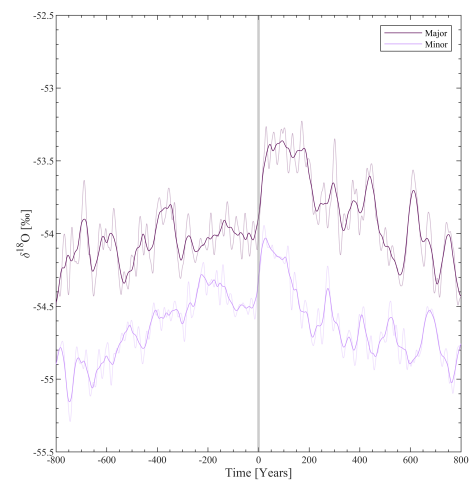
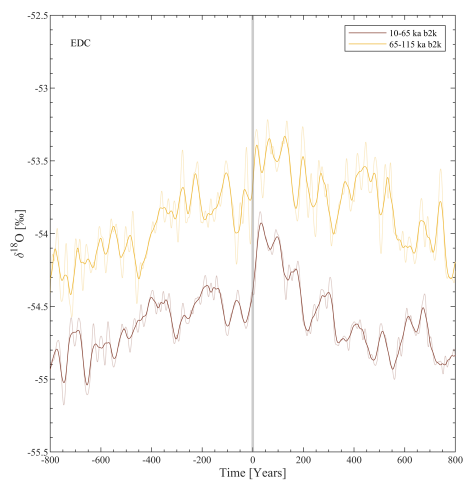
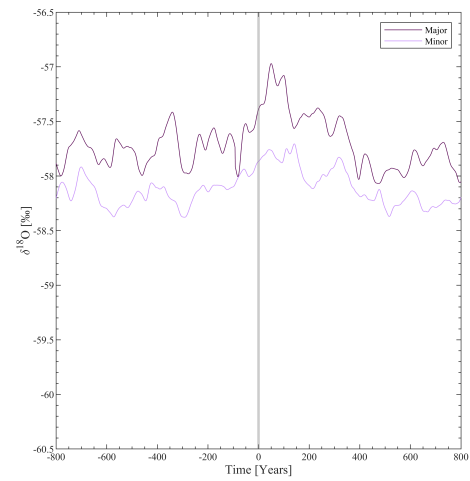
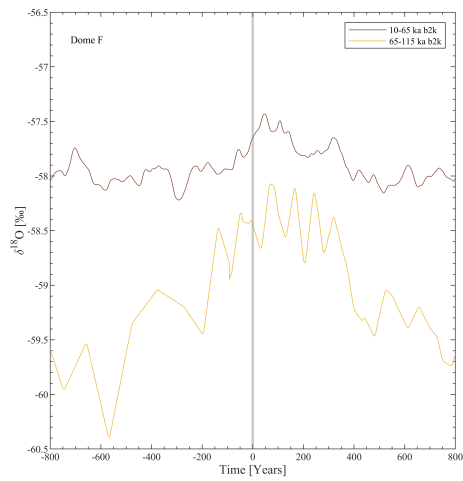
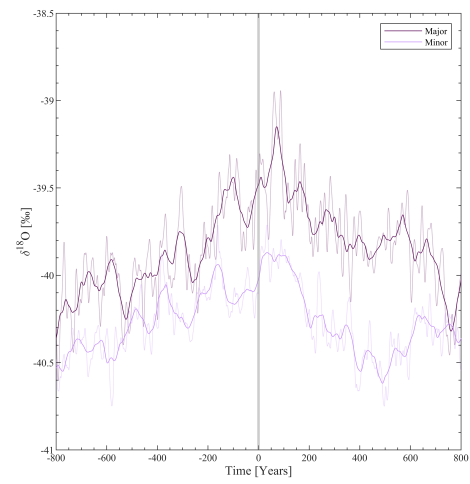
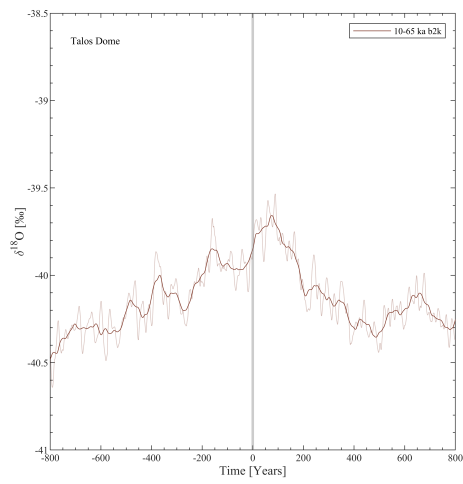
G. Class Comparison of DO Events



G. Class Comparison of DO Events



G. Class Comparison of DO Events



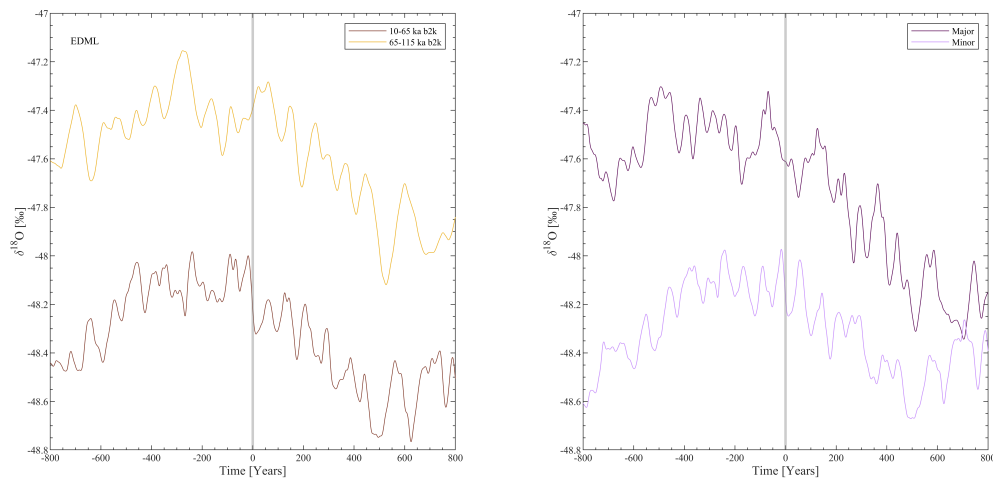


Figure G.4 | Comparing Dansgaard-Oeschger events of different classes. Stacked $\delta^{18}\text{O}$ records of different groups of events for the nine ice cores. The left panel compares transitions occurring in the first half of the last glacial (65-115 ka b2k), and the second half (10-65 ka b2k). The right panel shows the events grouped by size, where major events refer to interstadials with a preceding Heinrich event. See Table 3.2 for the events representing the different classifications.

H. Simulated Bipolar Phasing

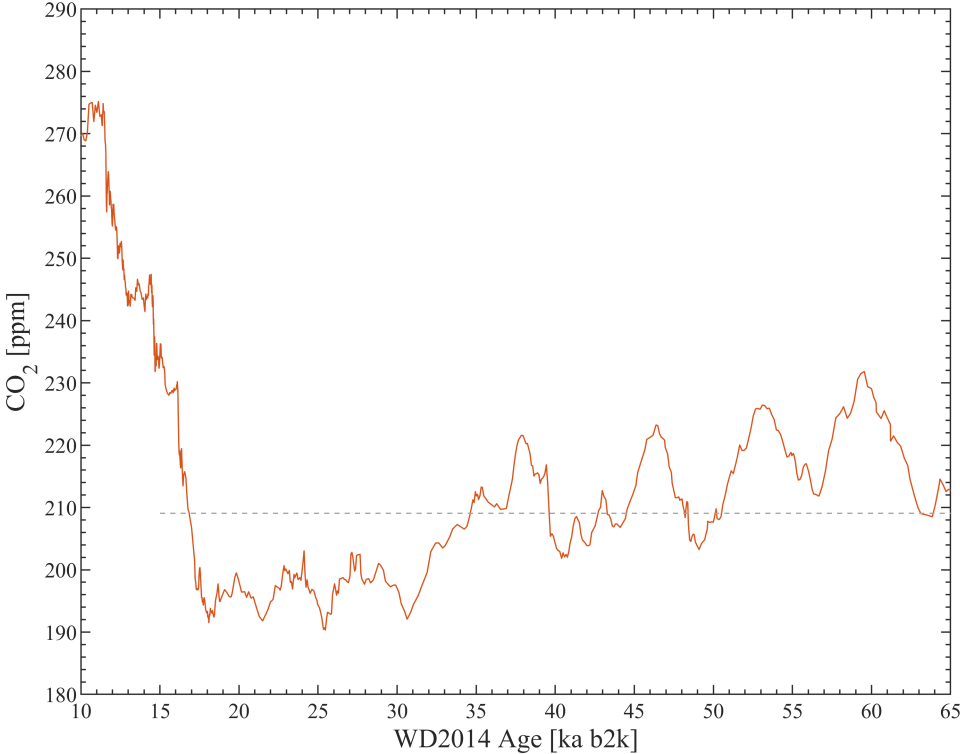
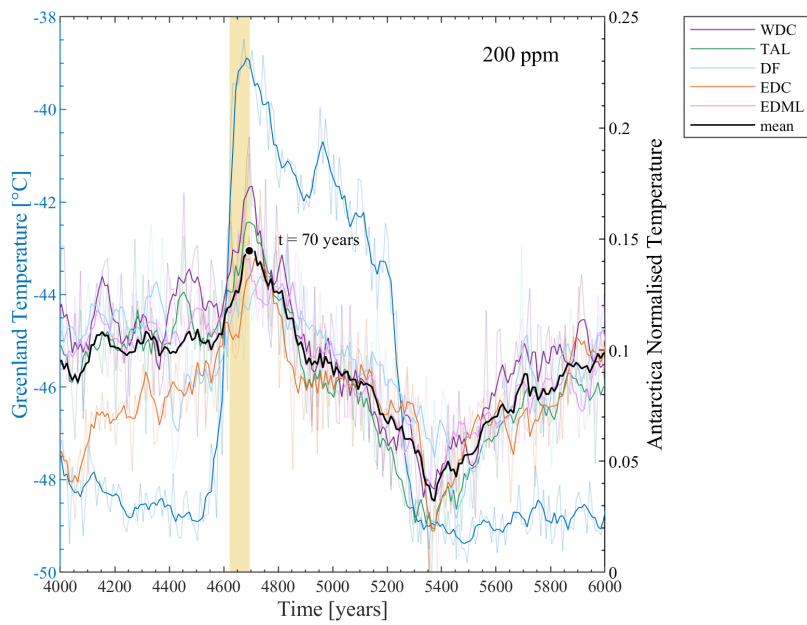
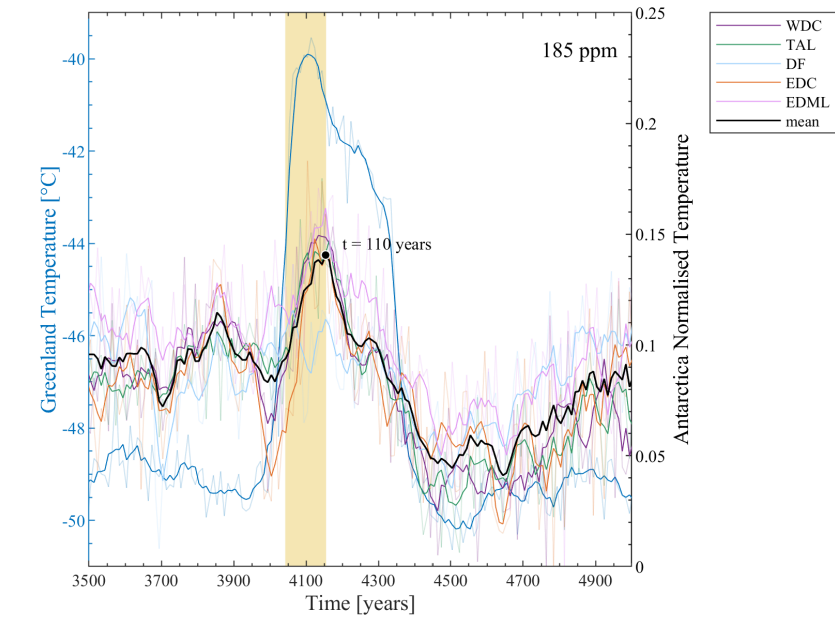
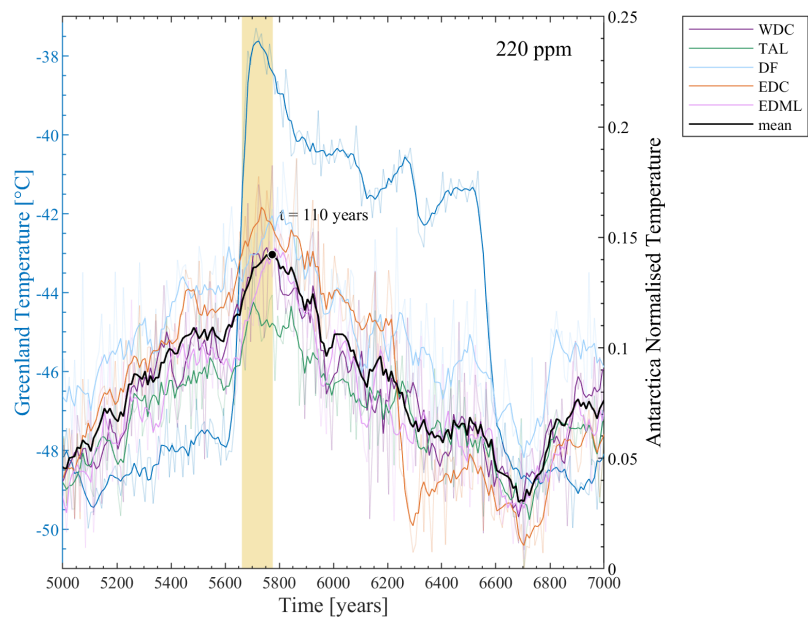
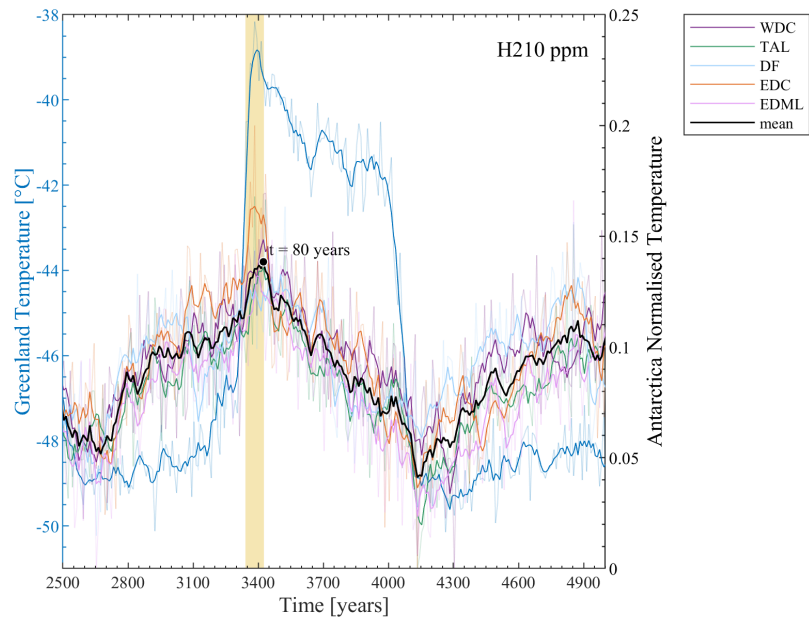


Figure H.1 | Atmospheric CO₂ Concentration between 15 ka and 65 ka b2k. Atmospheric CO₂ record measured from enclosed air in the WDC ice core dated on the WD2014 chronology (Data from Bauska et al. (2021)). Dashed grey line marks the average CO₂ concentration over the period 15-65 ka b2k of 209 ppm.

H. Simulated Bipolar Phasing



H. Simulated Bipolar Phasing



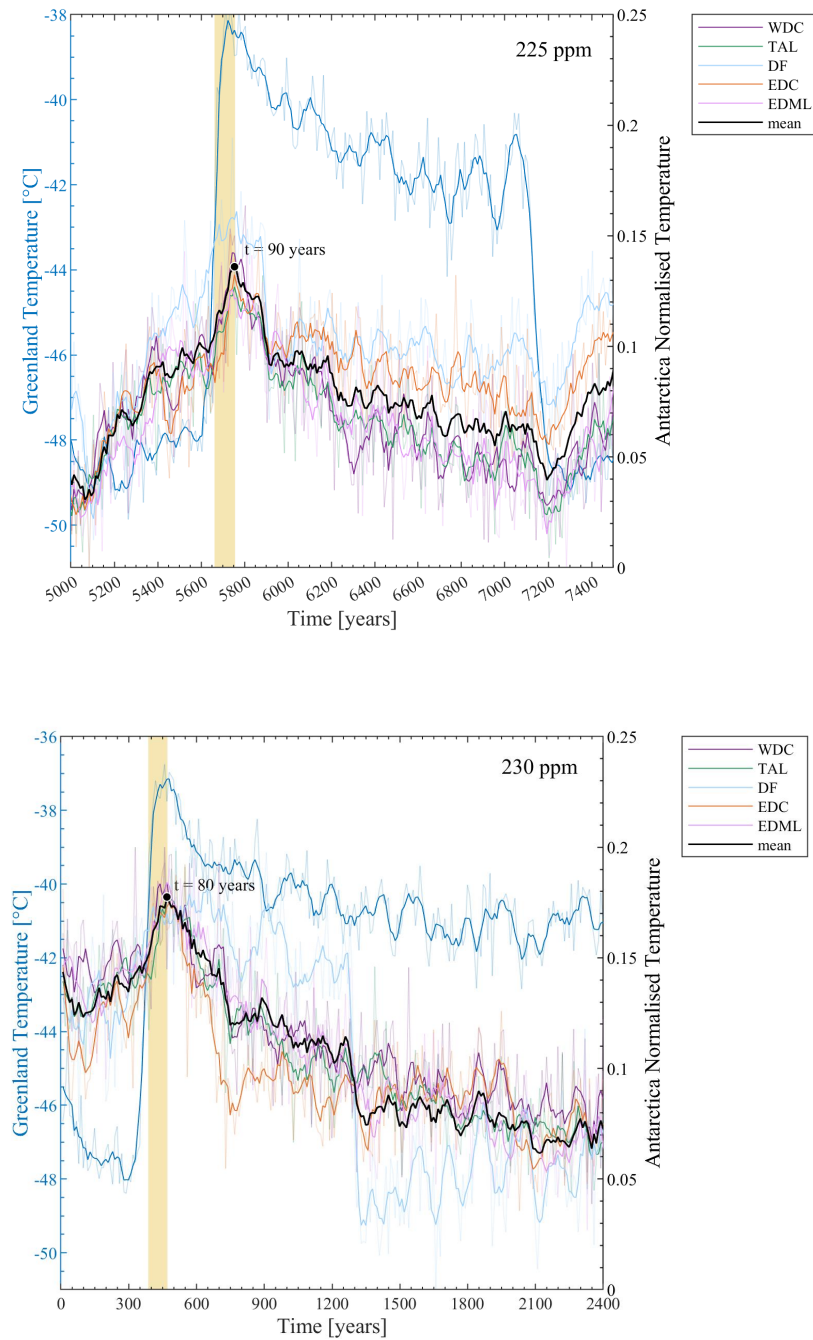


Figure H.4 | Bipolar phasing for simulated Dansgaard-Oeschger events. Mean Greenland and Antarctic temperature profiles from a CCSM4 model simulation (Vettoretti et al. (2022)) showing the Antarctic response time relative to Greenland abrupt warming for a single DO event under different atmospheric CO₂ forcing. The signal from Antarctica is normalised with respect to its extreme values and scaled for better visualisation and is not representative of the actual simulated temperature.

I. Code and Data Availability

In this work, no new data have been collected. The used data sets have been provided by Anders Svensson and are referenced in Table 3.1. The netCDF files including the global temperature produced by the CCSM4 model have been provided by Guido Vettoretti. The most representative MATLAB scripts produced during this project will be available in the following GitHub repository: <https://github.com/AnnaMKlussendorf/MastersThesis>